CHAPTER 4 RESULTS AND DISCUSSION

The main objective of this research was to synthesize and characterize ionic copper(II) mixed-carboxylates as metal-containing ionic liquids and metallomesogens. The former complexes were especially designed to function as solvent-cum-catalysts in the C-C bond-forming reaction of methyl ketones.

Ionic liquids (ILs) [1] are organic salts which melt at around 100^{o}C or below. These compounds are considered as environmental-friendly solvents as they are non-flammable, have no vapour pressure and can be reused or recycled.

The C-C bond-forming reaction, such as aldol condensation of carbonyls, are important in organic syntheses. The aldol-reaction normally uses strong bases, such as NaOH, though there were reports on the use of special and difficult to synthesize metal(II) complexes. However, it was accidentally discovered recently that copper(II) arylcarboxylate ($[Cu_2(XC_6H_4COO)_4]$; X = H, 4-NO_2, 4-OH, 4-Cl) reacted with acetone to form black solids, which were soluble in most organic solvents but insoluble in water, with physical characteristics tuned by the arylcarboxylates used, were redox active, and thus potential low band gap photonic materials and redox catalysts [2]. It was noted that one of the ligands in the black solid was formed from the C-C bond forming reaction of two acetone molecules. Hence, this reaction may be utilized to serve as a new and facile synthetic method for such industrially important organic products.

Copper(II) alkylcarboxylates $[Cu_2(RCOO)_4]$, where R is a long linear or branched hydrocarbon chain, such as $[Cu_2(CH_3(CH_2)_{14}COO)_4]$ and $[Cu_2(CH_3(CH_2)_7)_2CHCOO)_4]$, were thermotropic metallomesogens with melting temperatures 112^{o}C and below -20^{o}C respectively [3]. These carboxylates may be converted to ionic liquid precursors by substituting at least one of the alkylcarboxylates with an arylcarboxylate ligand containing ionisable functional groups, such as –OH or –NH_2. Examples are

$[Cu_2(p\text{-}HOC_6H_4COO)_a(RCOO)_{4-a}]$ and $[Cu_2(p\text{-}H_2NC_6H_4COO)_a(RCOO)_{4-a}]$, where a = 1 and 2.

The strategies that can be adopted to reduce the melting temperatures of these complexes to less than 100^oC, so as to meet the definition of ionic liquids, are use of: (a) long, preferably branched, alkylcarboxylate ions [3], (b) non-planar large counterions [4], and (c) mixed ligands (to reduce the molecular symmetry) [4].

Hence, the complexes studied in this research are anionic copper(II) complexes of general formula, $K_a[Cu_2(p\text{-}OC_6H_4COO)_a(CH_3(CH_2)_nCOO)_{4-a}]$, where a = 1, 2; n = 14, 10, 8, 6), and cationic copper(II) complexes of general formula, $[Cu_2(p\text{-}H_3NC_6H_4COO)_a(CH_3(CH_2)_nCOO)_{4-a}]X_a$, where a = 1, 2; n = 14; X = Cl, CH_3COO and CF_3SO_3.

The initial challenge of this research was to use the correct synthetic method to obtain the designed complexes. There are several methods reported in the literature for the synthesis of $[Cu_2(RCOO)_4]$. Examples are the reaction between a Cu(II) salt (chloride, sulphate, and nitrate) with RCOONa [6-10], metathesis reaction between $[Cu_2(RCOO)_4]$ and R'COOH [3,7,10-14], reaction between $CuCO_3$ and RCOOH [15-17], and reaction between $Cu(OH)_2$ and RCOOH [18]. However, a specific method for Cu(II) mixed-carboxylates was not found in the literature. Thus, this research began with method development to find the best method for these complexes. Suitable ionic complexes were then used in the C-C bond-forming reaction with 3,3-dimethyl-2-butanone, $(CH_3)_2CH\text{-}CO\text{-}CH_3$.

The instrumental techniques used in this project were mainly C,H elemental analyses, Fourier transform infrared spectroscopy, UV-vis spectroscopy, thermogravimetry, optical polarised microscopy, differential scanning calorimetry, magnetic susceptibility and cyclic voltammetry. In addition, gas chromatography-mass

spectroscopy was used for the determination of products from the C-C bond-forming reaction.

4.1 METHOD DEVELOPMENT

The three methods selected in an attempt to find the best method for the synthesis of the designed complexes were: one-pot, ligand-exchange, and carbonate-base-acid reactions. The complexes prepared were: (a) $K_2[Cu_2(p\text{-}OC_6H_4COO)_2(CH_3(CH_2)_{14}COO)_2]$, (one-pot reaction) and $[Cu_2(p\text{-}HOC_6H_4COO)_2(CH_3(CH_2)_{14}COO)_2]$, (ligand-exchange and carbonate-base-acid reactions); and (b) $[Cu_2(p\text{-}H_3NC_6H_4COO)_2(CH_3(CH_2)_{14}COO)_2]Cl_2$, (one-pot reaction) and $[Cu_2(p\text{-}H_2NC_6H_4COO)_2(CH_3(CH_2)_{14}COO)_2]$ (ligand-exchange and carbonate-base-acid reactions).

4.1.1 $K_2[Cu_2(p\text{-}OC_6H_4COO)_2(CH_3(CH_2)_{14}COO)_2]$

a) One-pot reaction

The one-pot reaction involved complete deprotonation of all of the acidic hydrogen using KOH, and reacting the anions formed with Cu(II) ion. The overall reaction was expected to occur according to **Scheme 4.1**.

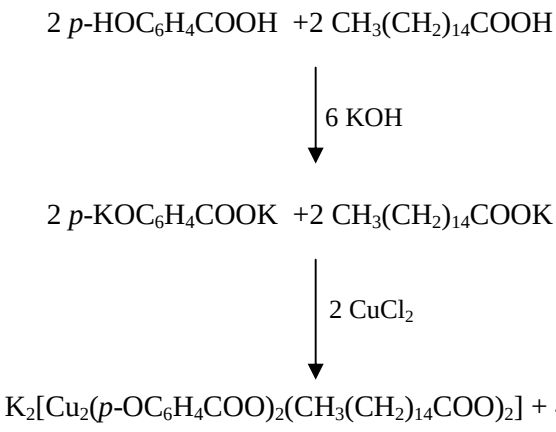

Scheme 4.1 One-pot synthesis of $K_2[Cu_2(p\text{-}OC_6H_4COO)_2(CH_3(CH_2)_{14}COO)_2]$

The product obtained was a dark brown powder (**Complex 1)**. It was soluble in a mixture of CH_3OH-CH_3COOH (95:5), but insoluble in water and almost all common organic solvents.

i) Structural elucidation

Based on the following analytical results, it is proposed that the structural formula of **Complex 1** is $K_2[Cu_2(p\text{-}OC_6H_4COO)_2(CH_3(CH_2)_{14}COO)_2(p\text{-}HOC_6H_4COOH)_2].2H_2O$ (formula mass, 1300.6 g mol^{-1}; **Figure 4.1)**. Thus, its yield was 47.0 %. The structure is known as paddle-wheel, and is similar to the structure of most other metal(II) carboxylates previously reported in the literature [3,12,16,17,19-22].

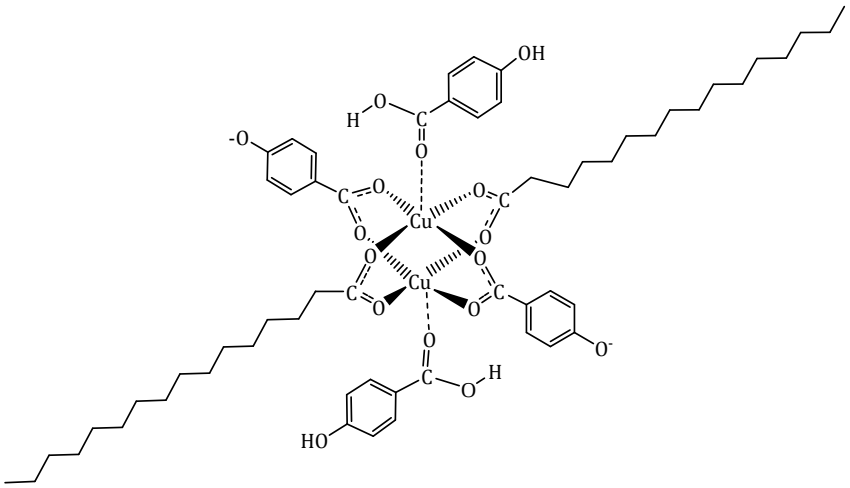

Figure 4.1 Proposed structure of **Complex 1** (K^+ ions and H_2O solvate molecules are not shown)

The results of the **elemental analyses** (C, 55.67%; H, 6.68%) are in good agreement with the calculated values for $KCuC_{30}H_{43}O_9$ (C, 55.41%; H, 6.66%; formula mass, 1300.6 g mol^{-1}).

The **FTIR** spectrum (**Figure 4.2)** is distinctly different from the reactants, $CH_3(CH_2)_{14}COOH$ (**Figure 4.3**) and p-HOC_6H_4COOH (**Figure 4.4)**, indicating a reaction occurred between the two materials.

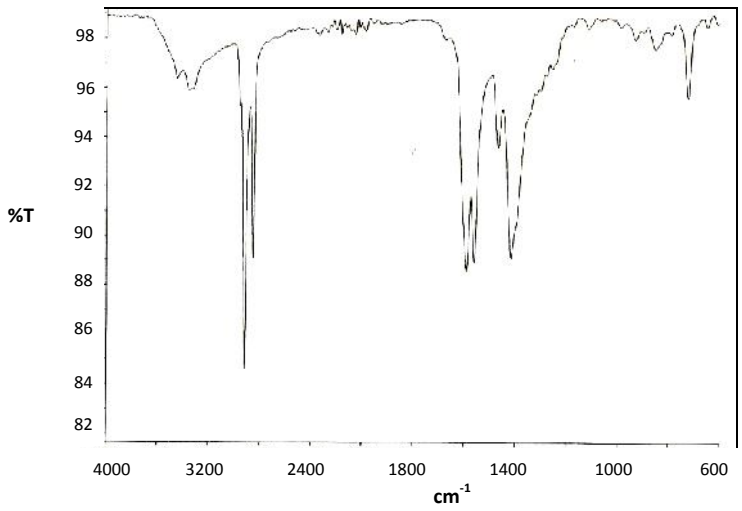

Figure 4.2 FTIR spectrum of **Complex 1**

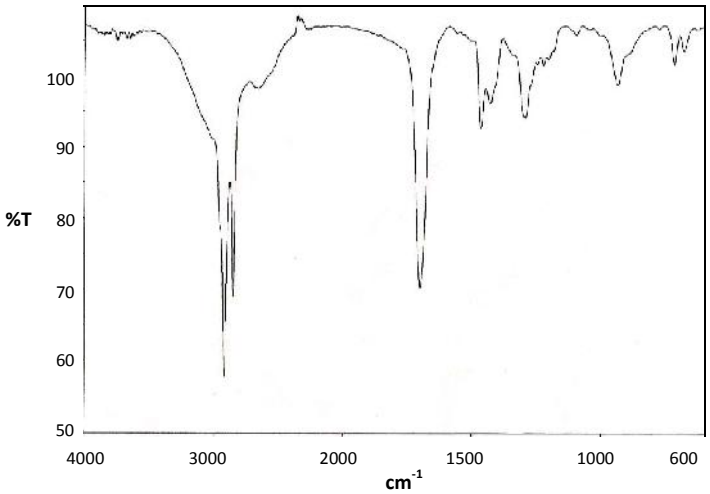

Figure 4.3 FTIR spectrum of $CH_3(CH_2)_{14}COOH$

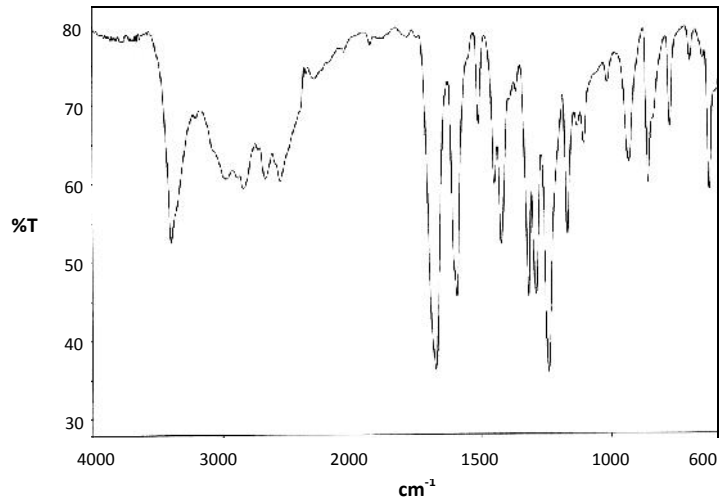

Figure 4.4 FTIR spectrum of *p*-HOC_6H_4COOH

The spectrum also shows the presence of the expected functional groups (**Table 4.1)**. It is noted that the peak at 1589 cm^{-1} for the aromatic ring vibration is strong and broaden, suggesting an overlap with the -C=O peak of *p*-HOC_6H_4COOH. It is also noted that the –C=O peak of this acid is shifted to lower frequency (by 88 cm^{-1}) compared to that of the free acid (1677 cm^{-1}), implying its coordination to Cu(II) centre through the oxygen atom of the –C=O group.

The Δ value ($\Delta = \nu_{asym} - \nu_{sym}$) is 145 cm^{-1}. This suggests bridging carboxylates [23], and hence a binuclear copper(II) complex. It is further noted that the spectrum for **Complex 1** is simple, suggesting a highly symmetrical geometry, and thus a *trans*-complex (as shown in the proposed structure).

Table 4.1 FTIR data and assignment for **Complex 1**

Wavenumber/cm^{-1}	**Assignment**
3445, 3353	-OH
2918	CH_2 (ν_{asym})
2849	CH_2 (ν_{sym})
1589	C=C (aromatic)
1559	-COO (ν_{asym})
1414	-COO (ν_{sym})
721	*para* substitution

The **UV-vis spectrum** of **Complex 1** in the solid state (**Figure 4.5)** shows a gradual continuously increasing absorption from 1000 nm to 300 nm, with shoulders at about 700 nm and 425 nm. This supports a binuclear complex with square pyramidal Cu(II) centres [24-26], and extensive electronic delocalisation, possibly due to resonance which leads to the formation of conjugated double bonds (**Figure 4.6)**.

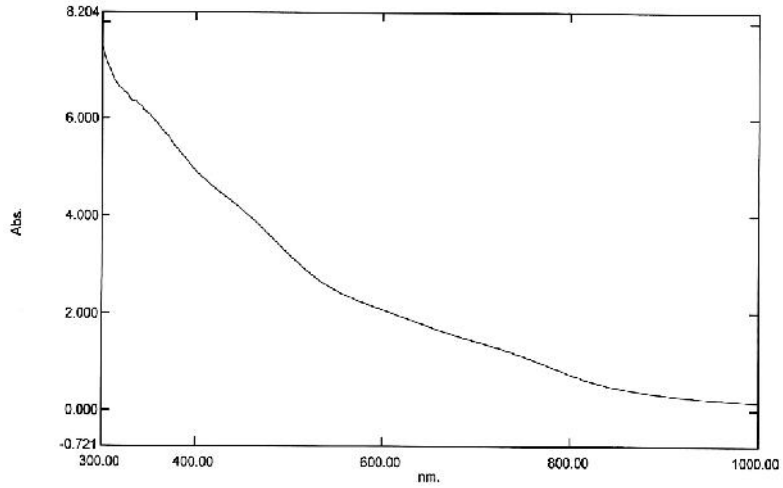

Figure 4.5 UV-vis spectrum of **Complex 1** (solid)

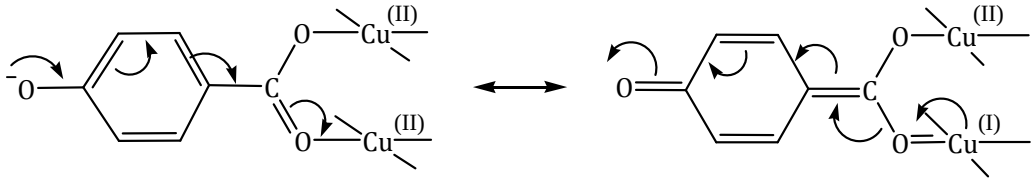

Figure 4.6 Resonance structure of **Complex 1** (only a partial structure is shown)

The UV-vis spectrum of **Complex 1** dissolved in CH_3OH-CH_3COOH (95:5) is similar to that of the solid sample (**Figure 4.7)**. This suggests that the complex maintained its binuclear square pyramidal geometry in this solvents mixture.

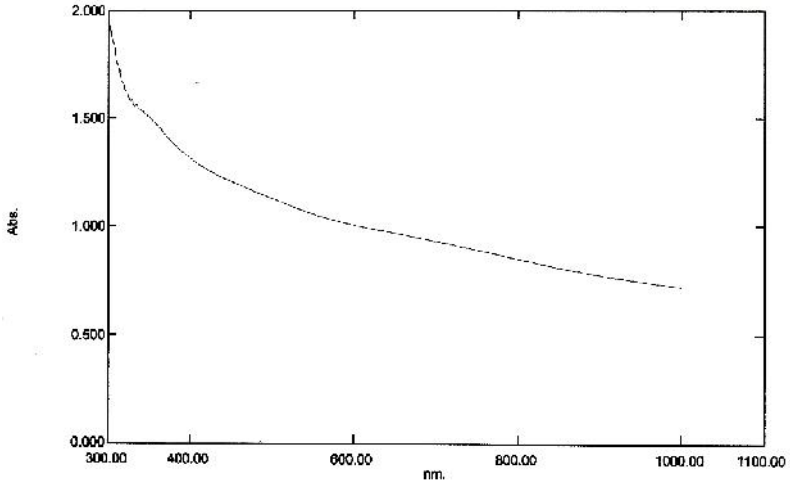

Figure 4.7 UV-vis spectrum of **Complex 1** (solution)

It is noted that the above spectrum differs markedly from copper(II) carboxylates published in the literature. The UV-vis spectra of copper(II) carboxylates, $[Cu_2(RCOO)_4]$ and their benzothiazole adducts $[Cu_2(RCOO)_4bt_2]$ (bt = benzothiazole, R = $CH_3(CH_2)_n$, n = 10, 12, 14, 16) show a broad *d-d* band in the range 672-700 nm, and a small shoulder at about 280-382 nm (characteristic of binuclear complexes) [27].

To summarise, the proposed structure for **Complex 1** is consistent with the empirical formula $KCuC_{30}H_{43}O_9$ as suggested by the elemental analyses, bridging carboxylate ligands as suggested from FTIR, and square pyramidal geometry at Cu(II) as suggested from UV-vis spectroscopy.

ii) Molar conductance

The molar conductance of **Complex 1** in CH_3OH-CH_3COOH (95:5) is 172 S cm^{-1} at 25^oC. This means that it is a 1:2 electrolyte [28], and suggests that in these solvents, it dissociated to one $[Cu_2(p\text{-}OC_6H_4COO)_2(CH_3(CH_2)_{14}COO)_2)(p\text{-}HOC_6H_4COOH)_2]^{2-}$ and two K^+ ions.

iii) Thermal and metallomesogenic properties

The thermogram (**Figure 4.8)** shows that **Complex 1** initially suffered a gradual initial weight loss of 2.2% at about 44^oC, assigned to the evaporation of two H_2O solvates (expected 2.8%). This is followed by another weight loss of 24.5% at 222^oC, which is assigned to the loss of two $p\text{-}HOC_6H_4COOH$ molecules coordinated to the axial positions (expected, 21.2%).

Further heating to temperatures above 424^oC to about 800^oC did not lead to any further weight loss. Hence, the decomposition temperature for the complex is about 424^oC. This is in contrast with most copper(II) alkylcarboxylates and copper(II) arylcarboxylates. As examples, the decomposition temperatures of

$[Cu_2(CH_3(CH_2)_{10}COO)_4]$ [29], $[Cu_2(CH_3(CH_2)_8COO)_4]$ [30] and $[Cu_2(C_6H_5COO)_4].2C_2H_5OH$ [31] are 250°C, 210°C and 230°C, respectively. The high thermal stability of **Complex 1** may be due to resonance, as suggested from the result of UV-vis spectrum (**Figure 4.6**).

The amount of residue at temperatures below 800°C is 71.3%. The expected amount, assuming that the complex decomposed completely to K_2O and CuO, is 19.5% **(Appendix 2)**. This suggests that the organic ligands of the complex did not decompose completely below this temperature. Further increased of the temperature to above 900°C was not possible due to the limitation of the instrument.

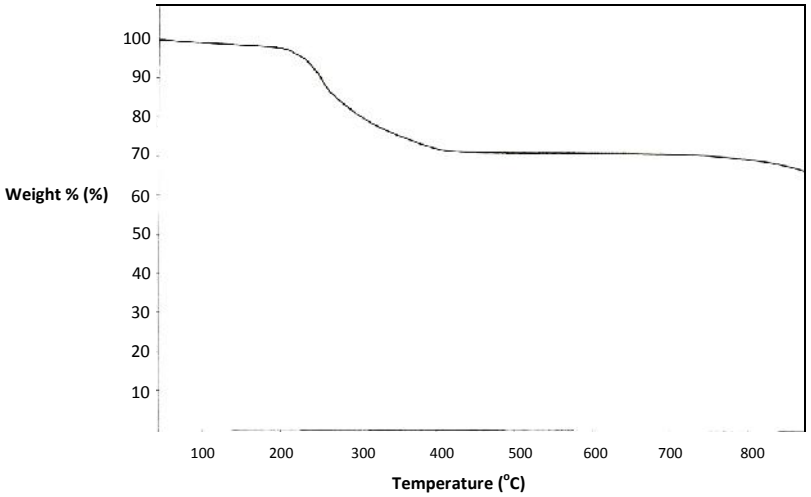

Figure 4.8 Thermogram of **Complex 1**

The DSC for **Complex 1** (**Figure 4.9**) shows two weak endotherms at 64°C (ΔH = +4 kJ mol^{-1}) and 91°C (ΔH = +1.4 kJ mol^{-1}), a sharp endotherm at 162°C (ΔH = +21 kJ mol^{-1}), and a broad endotherm at 210°C (ΔH = +49 kJ mol^{-1}). These endotherms may corresponds to the breaking of intramolecular H-bonds, intermolecular H-bonds between the –OH group of *p*-HOC_6H_4COOH with H_2O, and *p*-HOC_6H_4COOH-Cu axial bonds (**Figure 4.1**), respectively.

The calculated ΔH value for the intermolecular H-bonds is in good agreement with the theoretical value (10-40 kJ mol^{-1}) [32]. It is postulated that the freed axially-

coordinated *p*-HOC_6H_4COOH molecules melted (mp = 214-217^oC) and then decomposed at 223^oC. This is supported by a broad exotherm at peak temperature of 256^oC (ΔH = -21 kJ mol^{-1}), which is mostly likely due to the formation of CO_2 and other organic volatiles [31].

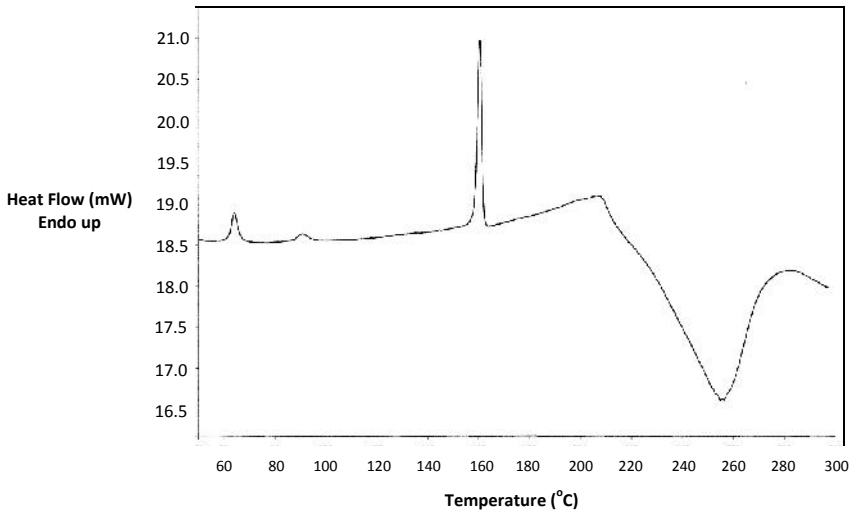

Figure 4.9 DSC curve of **Complex 1**

Thus, the DSC curve did not show peaks for the melting and clearing processes prior to decomposition. The result is further supported by OPM pictures, which did not show any observable changes from 25^oC to 206^oC(**Figure 4.10**).

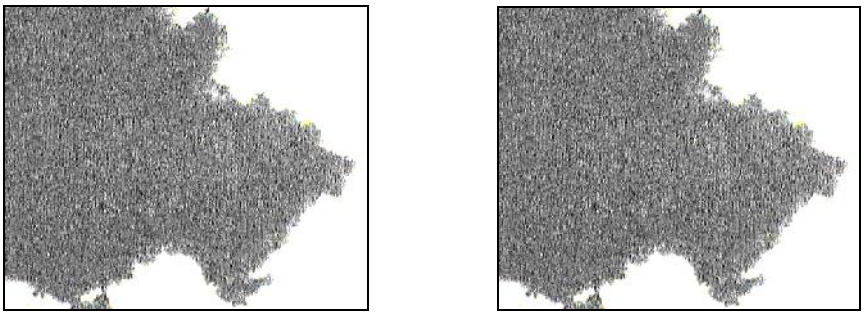

(a) (b)

Figure 4.10 OPM of **Complex 1** at: (a) 25^oC; (b) 206^oC

iv) Magnetic properties

The value of the effective magnetic moment, μ_{eff}, calculated using the values of χ_g, χ_m, χ_{dia} and χ_m^{corr} (**Table 4.2)** is 3.12 B.M. at 298K (**Appendix 3**). The singlet and triplet

energy level separation (or exchange integral, normally denoted as -2J), as a result of the electron spin interaction between the Cu(II) centres, is -60 cm^{-1}. The value is calculated using the Bleaney-Bower equation [33] **(Appendix 4).** From these, it may be suggested that there is a weak ferromagnetic interaction between the two Cu(II) centres.

Table 4.2 The χ values for **Complex 1** used for the calculation of μ_{eff}

χ	**Values**
χ_g	2.97 x $10^{-6}cm^3g^{-1}$
χ_m	386.28 x 10^{-5} cm^3mol^{-1}
χ_{dia}	-36.38 x 10^{-5} cm^3mol^{-1}
χ_m^{corr}	422.66 x 10^{-5} cm^3mol^{-1}

The magnetic properties of **Complex 1** contrasts with the antiferromagnetic interaction of most dinuclear Cu(II) carboxylates and its derivatives reported in the literature [34,35]. The magnetic interaction for these complexes were postulated to occur through the bridging carboxylate ligands (the superexchange pathway).

The contrasting behaviour for **Complex 1** suggests a more distorted geometry at Cu(II) centres, resulting in reduced overlap between the magnetic orbital of Cu(II) ($d_{x^2-y^2}$) with the oxygen p_x orbital of the ligand.

v) Redox properties

The cyclic voltammogram (CV) for **Complex 1** was recorded cathodically from 0 V within the potential window -1.0 V to +1.0 V (**Figure 4.11**).

The voltammogram showed three cathodic peaks at -0.07, -0.26 and -0.79 V, and a single broad anodic peak at +0.16 V. The first cathodic peak at -0.07 V is assigned to the reduction of [Cu(II)Cu(II)] to [Cu(II)Cu(I)]. The mixed-valence [Cu(II)Cu(I)] formed then underwent two processes: (a) reduction to [Cu(I)Cu(I)] at -0.79 V, and (b)

dissociation to [Cu(II)] and [Cu(I)] complexes. The mononuclear [Cu(II)] complex formed was then reduced to [Cu(I)] at -0.26 V.

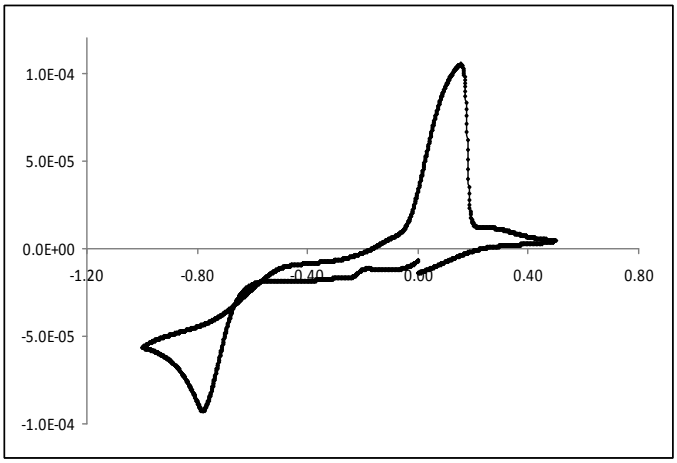

Figure 4.11 Cyclic voltamogram of **Complex 1**

The single broad oxidation peak observed on the other hand may be assigned to multiple close charge transfer oxidation processes with nearly similar potentials. These hindered the observation of separate current peaks for each anodic process [36]. The electrochemical processes are summarised in **Scheme 4.2.**

The large ΔE values for the three processes (230 mV, 950 mV and 420 mV) suggest quasireversible electrochemical reactions, due to extensive structural reorganisation upon reduction.

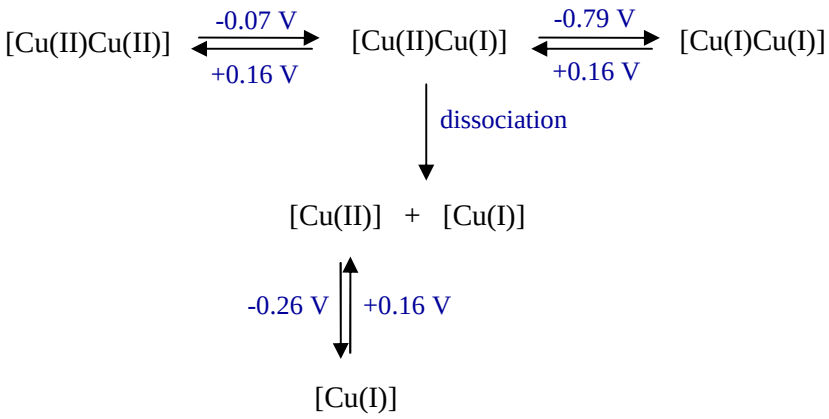

Scheme 4.2 Electrochemical processes for **Complex 1**

b) Ligand-exchange reaction

The ligand-exchange reaction [10] involved: (a) synthesis of the starting complexes ([Cu_2(*p*-$HOC_6H_4COO)_4$]and [$Cu_2(CH_3(CH_2)_{14}COO)_4$]); and (b) reacting the starting complexes in a 1:1 mole ratio to form the corresponding mixed-carboxylates complex with the expected chemical formula, [Cu_2(*p*-$HOC_6H_4COO)_2(CH_3(CH_2)_{14}COO)_2$]. These reactions were expected to proceed according to **Scheme 4.3**.

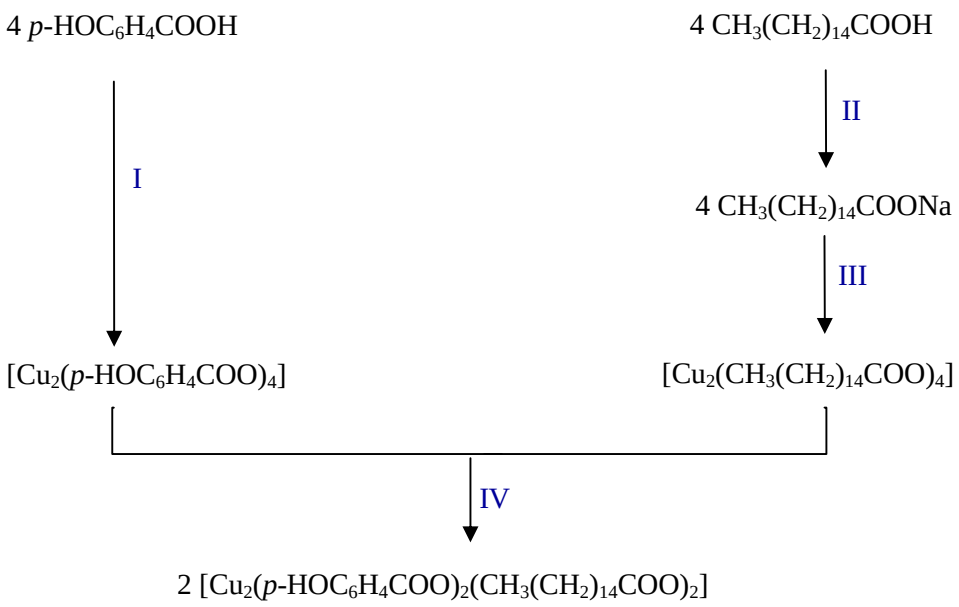

Scheme 4.3 Ligand-exchange reaction for the formation of [Cu_2(*p*-$HOC_6H_4COO)_2(CH_3(CH_2)_{14}COO)_2$]: (I) [$Cu_2(CH_3COO)_4$], EtOH, Δ; (II) Na_2CO_3, H_2O, Δ; (III) $CuCl_2$, EtOH, Δ; (IV) EtOH, pyridine, Δ

i) Structural elucidation [Cu_2(p-$HOC_6H_4COO)_4$]

The complex was obtained as a fine peacock-blue powder. Based on the following analytical results, it is proposed to have the structural formula ([Cu_2(*p*-$HOC_6H_4COO)_4$].$8H_2O$) (formula mass, 819.7 g mol^{-1}; **Figure 4.12**), which is as expected. Thus, its percentage yield was 70.8 %.

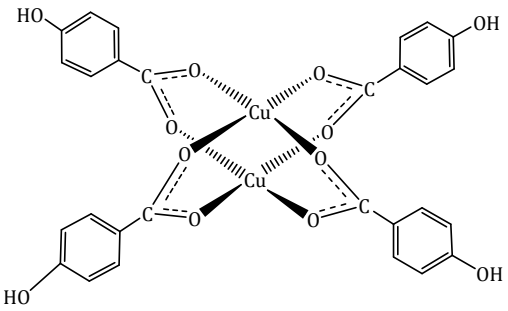

Figure 4.12 Proposed structural formula of $[Cu_2(p\text{-}HOC_6H_4COO)_4]$ (H_2O solvate molecules are not shown)

The results of **elemental analyses** (C, 40.70%; H, 3.73%) are in good agreement with the calculated values for $Cu_2C_{28}H_{36}O_{20}$ (C, 41.03%; H, 4.43%).

Its **FTIR spectrum** (**Figure 4.13)** shows the presence of all of the expected functional groups **(Table 4.3).** The Δ value is 176 cm^{-1}, in agreement with the presence of bridging carboxylate group [23], and thus a binuclear complex.

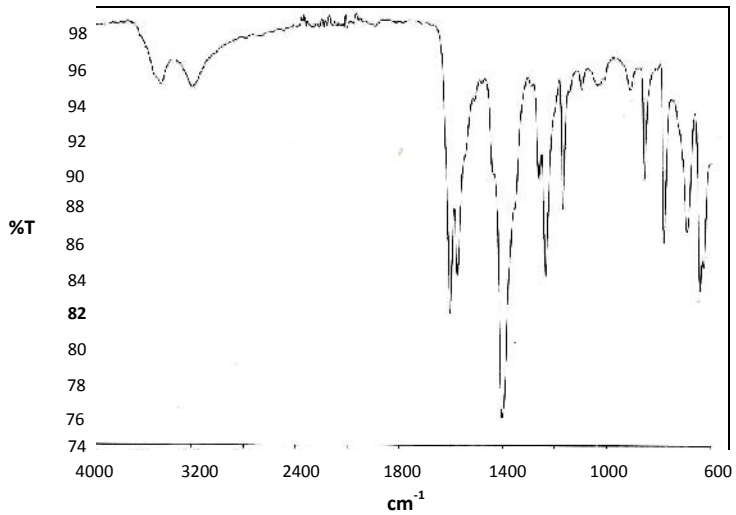

Figure 4.13 FTIR spectrum of $[Cu_2(HOC_6H_4COO)_4].8H_2O$

Table 4.3 FTIR data and assignment for $[Cu_2(p\text{-}HOC_6H_4COO)_4].8H_2O$

Wavenumber/cm^{-1}	**Assignment**
3445, 3203	-OH
1604	C=C (aromatic)
1578	-COO (ν_{asym})
1402	-COO (ν_{sym})

The **UV-vis spectrum** of the complex dissolved in CH_3COOH-CH_3OH (**Figure 4.14**) shows a broad band at 685 nm (ε_{max}= 220 M^{-1} cm^{-1}) and a distinct shoulder on the charge-transfer band at 362 nm (ε = 58 M^{-1} cm^{-1}). These support the proposed binuclear square pyramidal structure [24-26].

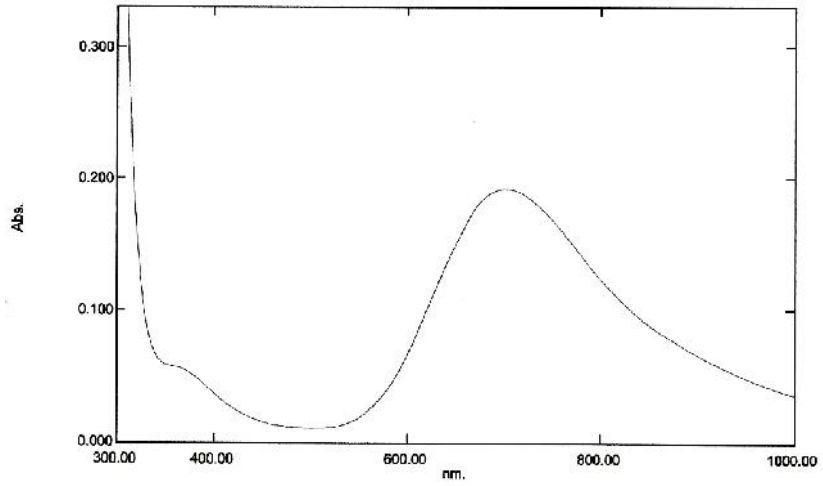

Figure 4.14 UV-vis spectrum of $[Cu_2(p\text{-}HOC_6H_4COO)_4].8H_2O$ (solution)

To summarise, the proposed structure is consistent with the empirical formula $CuC_{14}H_{18}O_{10}$ as suggested by the elemental analyses, bridging carboxylate ligands as suggested from FTIR, and binuclear square pyramidal geometry at Cu(II) as suggested from UV-vis spectroscopy.

ii) Structural elucidation of $[Cu_2(CH_3(CH_2)_{14}COO)_4]$

The complex was obtained as a greenish-blue fine powder. Based on the following analytical results, it is proposed to have the structural formula $[Cu_2(CH_3(CH_2)_{14}COO)_4]$ (formula mass 1148.8 g mol^{-1}; **Figure 4.15**), which is the expected product. Thus, its percentage yield is 71.2%.

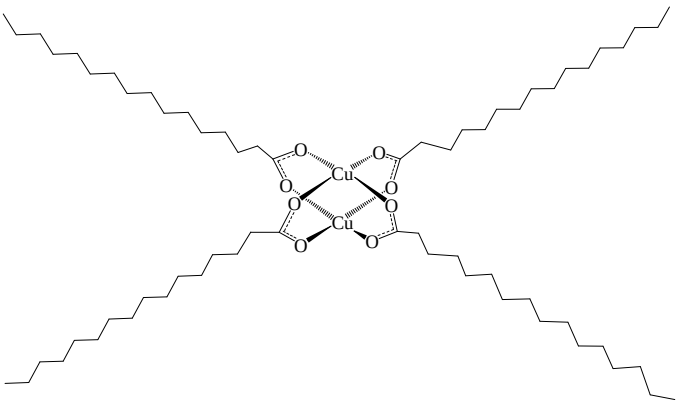

Figure 4.15 Proposed structural formula of $[Cu_2(CH_3(CH_2)_{14}COO)_4]$

The results of the **elemental analyses** (66.64% C; 11.63% H) are in good agreement with the calculated values for $Cu_2C_{64}H_{124}O_8$ (66.91% C; 10.88% H).

Its **FTIR spectrum** (**Figure 4.16)** shows the presence of all of the functional group expected to be present, as previously discussed. The value of Δ is 142 cm^{-1}, in agreement with the presence of bridging carboxylates group [23], and hence a dinuclear complex.

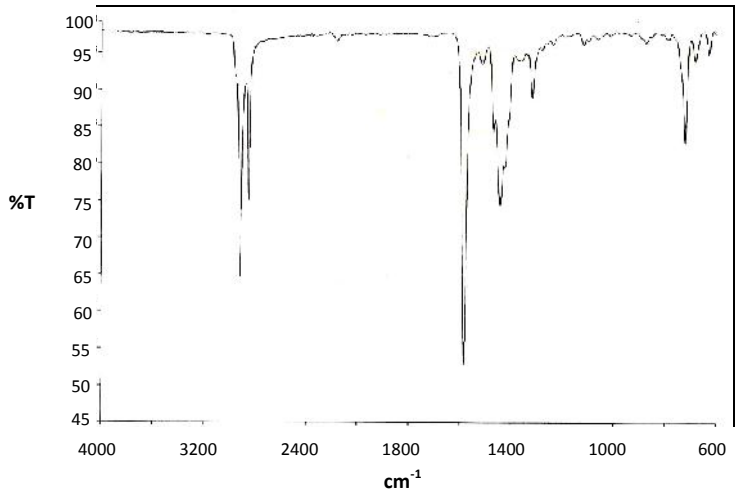

Figure 4.16 FTIR spectrum of $[Cu_2(CH_3(CH_2)_{14}COO)_4]$

The **UV-vis spectrum** of $[Cu_2(CH_3(CH_2)_{14}COO)_4]$ in CH_3OH-CH_3COOH (95:5) (**Figure 4.17)** shows a broad *d-d* band at 700 nm (ε_{max}= 229 M^{-1} cm^{-1}) and a distinct shoulder on the charge-transfer band at 365 nm (ε = 59 M^{-1} cm^{-1}). The results suggest a binuclear square pyramidal [24-26] complex in solution, indicating axial ligation of the solvent molecules.

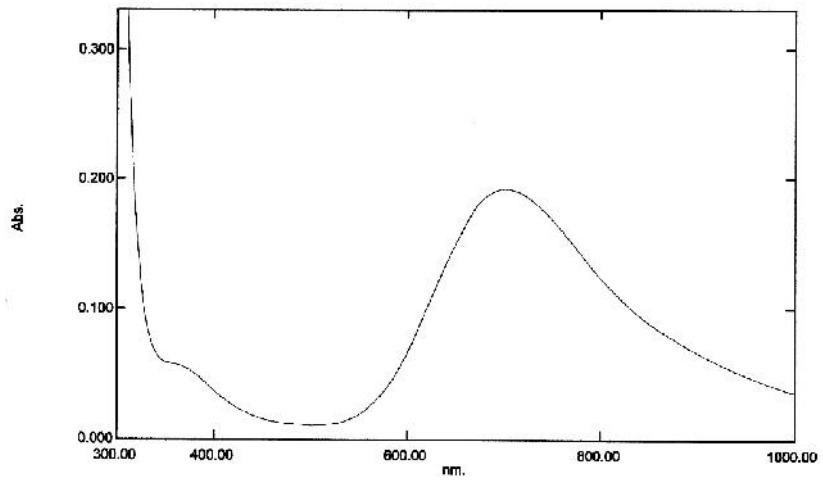

Figure 4.17 UV-vis spectrum of $[Cu_2(CH_3(CH_2)_{14}COO)_4]$ (solution)

To summarise, the proposed structure is consistent with the chemical formula $Cu_2C_{64}H_{124}O_8$ as suggested by the elemental analyses, bridging carboxylate ligands as suggested from FTIR, and binuclear square pyramidal geometry at Cu(II) as suggested from UV-vis spectroscopy.

iii) Structural elucidation of $[Cu_2(p\text{-}HOC_6H_4COO)_2(CH_3(CH_2)_{14}COO)_2]$

The ligand-exchange reaction between $[Cu_2(p\text{-}HOC_6H_4COO)_4]$ and $[Cu_2(CH_3(CH_2)_{14}COO)_4]$ formed a pale green fine powder (**Complex 2)**. It was soluble in CH_3OH-CH_3COOH (95:5), but insoluble in water and almost all common organic solvents.

Based on the following analytical results, its proposed structural formula is $[Cu_2(p\text{-}HOC_6H_4COO)_2(CH_3(CH_2)_{14}COO)_2(CH_3(CH_2)_{14}COOH)(H_2O)].CH_3CH_2OH$ (formula mass, 1232.6 g mol^{-1}; **Figure 4.18)**. Thus, its yield was 64.8%.

The results of the **elemental analyses** (62.69% C and 10.74% H) are in good agreement with the calculated values for $Cu_2C_{64}H_{112}O_{14}$ (62.36% C and 9.16% H).

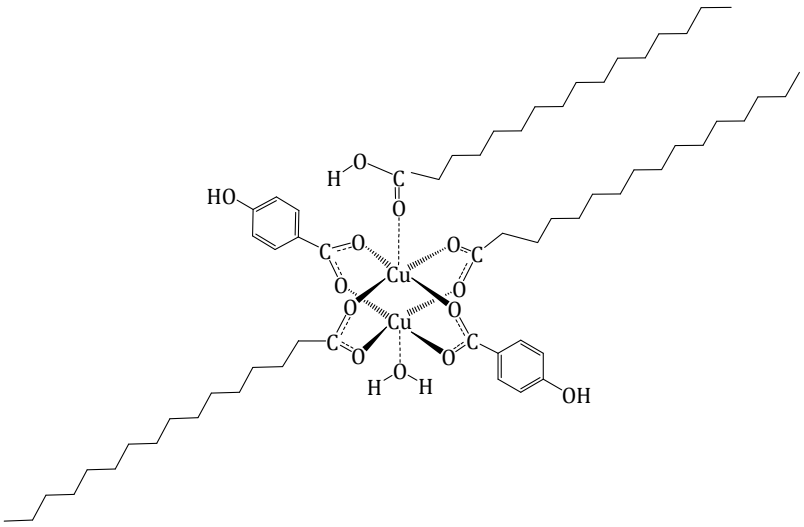

Figure 4.18 Proposed structural formula of **Complex 2** (CH_3CH_2OH solvate is not shown)

The **FTIR spectrum** (**Figure 4.19**) is distinctly different from its starting complexes (**Figure 4.13**) and (**Figure 4.15**), and shows the presence of all of the expected functional groups, as explained previously.

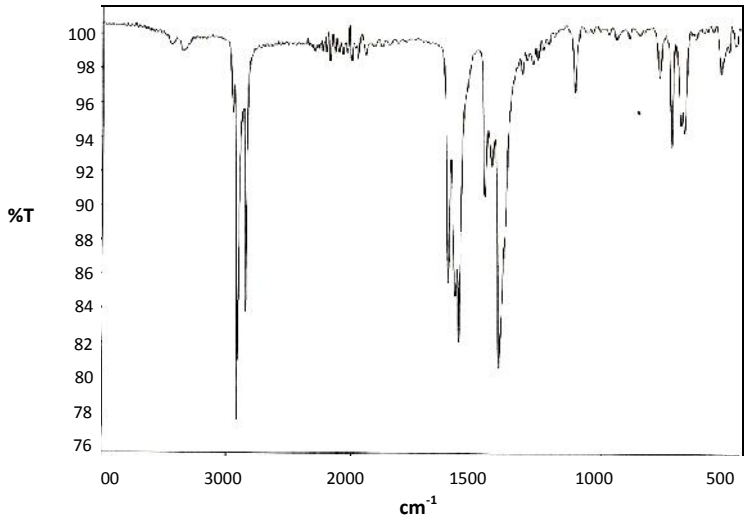

Figure 4.19 FTIR spectrum of **Complex 2**

As for **Complex 1**, the spectrum shows a strong and sharp peak at 1615 cm^{-1}, assigned to the -C=O peak of $CH_3(CH_2)_{14}COOH$. The Δ value is 162 cm^{-1}, in agreement with the proposed bridging carboxylate ligands [23].

The **UV-vis spectrum (Figure 4.20)** of **Complex 2,** dissolved in CH_3OH-CH_3COOH, shows a broad *d-d* band at 700 nm (ε_{max}= 229 M^{-1} cm^{-1}) and a distinct shoulder on the charge-transfer band at 362 nm (ε = 59 M^{-1} cm^{-1}). These gave support to a binuclear complex with square pyramidal Cu(II) centres [24-26], as discussed above.

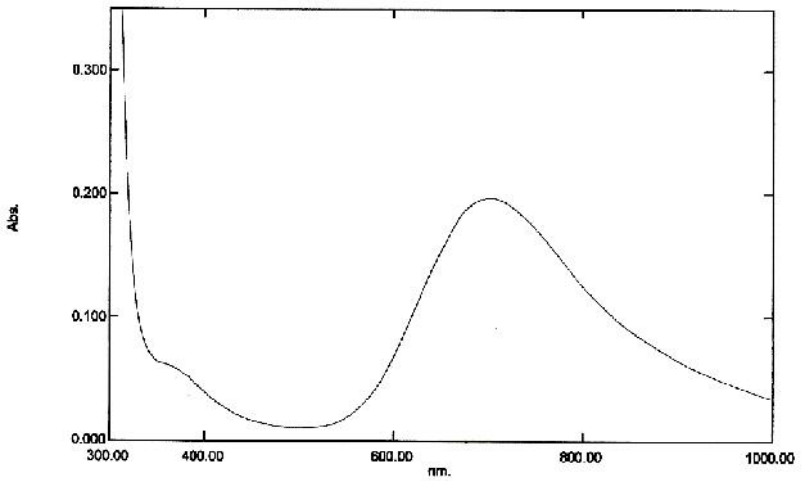

Figure 4.20 UV-vis spectrum of **Complex 2** (solution)

To summarise, the proposed structure is consistent with the chemical formula $Cu_2C_{64}H_{112}O_{14}$ as suggested by the elemental analyses, bridging carboxylate ligands as suggested from FTIR, and binuclear square pyramidal geometry at Cu(II) as suggested from UV-vis spectroscopy. It also shows a $CH_3(CH_2)_{14}COOH$ molecule and a H_2O molecule coordinated at the axial positions of copper(II) centres **(Figure 4.18).**

iv) Thermal and mesogenic properties of ***Complex 2***

The **TGA (Figure 4.21)** shows that **Complex 2** is thermally stable up to around 230^oC. The initial gradual weight loss of 5.7% from 78^oC to 230^oC is assigned to the evaporation of CH_3CH_2OH solvate and coordinated H_2O (expected 5.2%). The complex then decomposed by a multi-stage process with a total weight loss of 79.9%, assigned to the decomposition of axially-coordinated $CH_3(CH_2)_{14}COOH$ and the carboxylate ligands, to CO_2 and other volatiles [31] (expected, 84.5%).

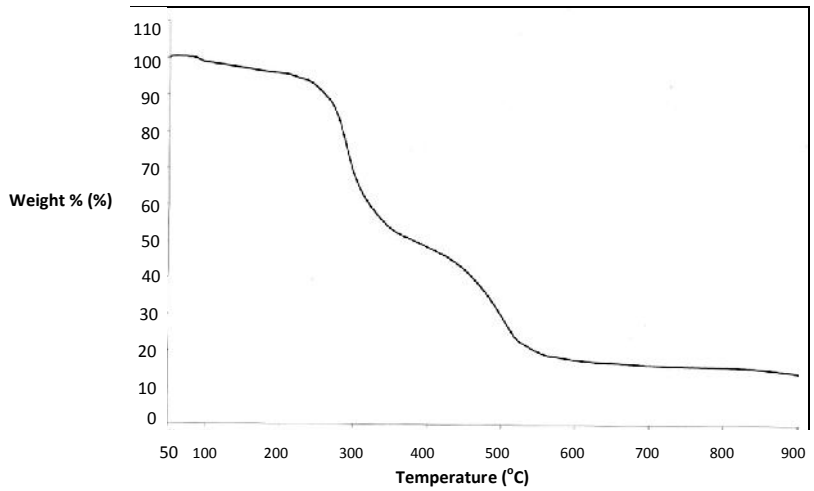

Figure 4.21 Thermogram of **Complex 2**

The amount of residue at temperatures above 900^{o}C is 14.3%. Assuming that it was CuO, as has been suggested for many copper(II) carboxylates [30,31], the estimated formula mass of the complex, calculated using the gravimetry concept (**Appendix 5)**, is 1111.1 g mol^{-1} (expected, 1232.6 g mol^{-1}). Thus, the results from TGA and elemental analyses are in fairly good agreement, and lend further support to the proposed structural formula

The development of optical structure of the complex on heating is illustrated by the sequence of **OPM** micrographs shown in **Figure 4.22 (a-d).** The pale green colour of the complex remained unchanged until it started to melt at around 140^{o}C, when its colour changed to pale blue. This may be due to structural change from square pyramidal to square planar due to the dissociation of the axially coordinated molecules. On further heating, the liquid became less viscous and then cleared to an isotropic liquid at 180^{o}C. On cooling from the isotropic liquid phase, birefringence was observed at 84^{o}C (**Figure 4.22 (d)**).

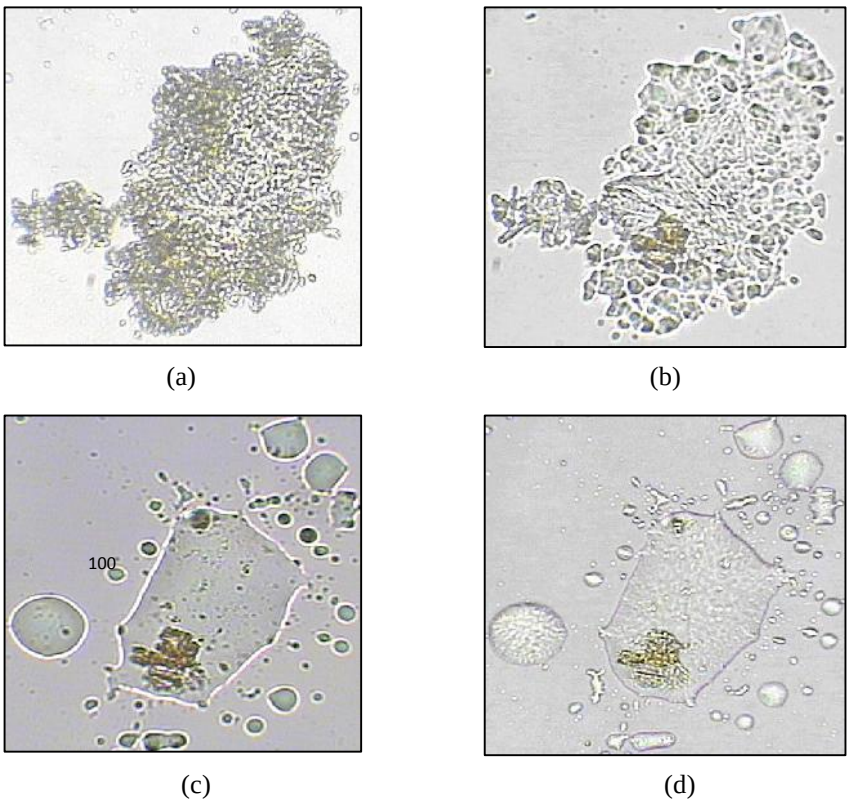

Figure 4.22 OPM micrographs of **Complex 2** on heating: (a) 25^{o}C; (b) 140^{o}C; (c) 180^{o}C; and (d) 84^{o}C

The **DSC curve** of the complex (**Figure 4.23**) shows several overlapping endotherms. The assignments of these endotherms are given in **Table 4.3.**

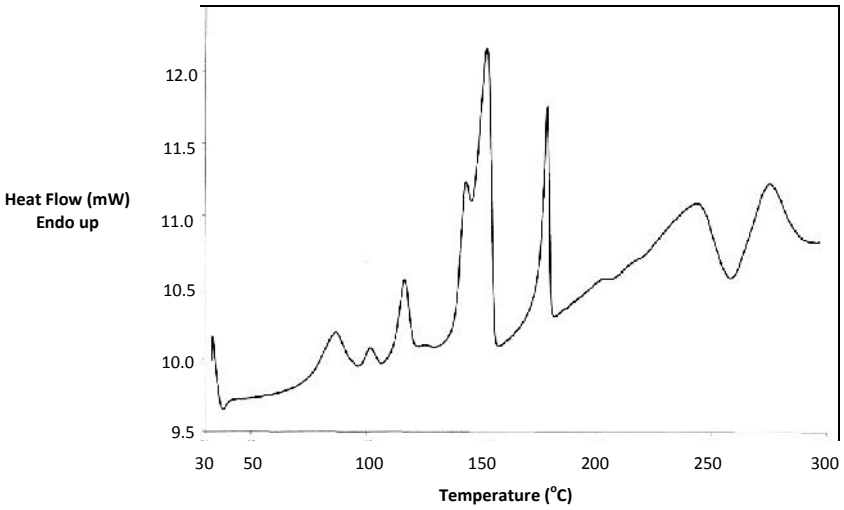

Figure 4.23 DSC curve of **Complex 2**

Table 4.4 DSC data and assignment for **Complex 2**

Peak Temperature (^oC)	**ΔH (kJ mol^{-1})**	**Assignment**
87	+11	Evaporation of solvated CH_3CH_2OH and coordinated H_2O
101	+3	
117	+11	
152	+77	Melting
179	+23	Dissociation of axially coordinated $CH_3(CH_2)_{14}COOH$ ligand and clearing of **Complex 2**
245	+35	Partial decomposition$^{\#}$ of $CH_3(CH_2)_{14}COOH$
275	+31	Decomposition of $CH_3(CH_2)_{14}COO$ and *p*-HOC_6H_4COO ligands

* T_{clear} = 180^{o}C (from OPM); and $^{\#}T_{decompose}$ = 230^{o}C ($CH_3(CH_2)_{14}COO$ ligand from TGA)

*v) Magnetic properties of **Complex 2***

The value of the effective magnetic moment, μ_{eff} at 298 K, calculated as before using the values tabulated in **Table 4.5**, is 2.54 B.M. at 298 K. The calculated value is slightly lower than the spin-only value for a dinuclear Cu(II) complex for two unpaired electrons (μ_{eff}= 2.83 B.M.). The corresponding -2J value is 80 cm^{-1}. The results indicate a weak antiferromagnetic interaction between the two Cu(II) centres. Most dinuclear Cu(II) carboxylates and its derivatives show antiferromagnetic interaction [34,35], postulated to occur through the bridging carboxylate ligands (the super-exchange pathway).

Table 4.5 The χ values for **Complex 2** used for the calculation of μ_{eff}

χ	**Values**
χ_g	0.18 x $10^{-6}cm^3g^{-1}$
χ_m	221.87 x 10^{-5} cm^3mol^{-1}
χ_{dia}	-62.58 x 10^{-5} cm^3mol^{-1}
χ_m^{corr}	284.45 x 10^{-5} cm^3mol^{-1}

It is noted that the magnetic properties of **Complex 2** (weak antiferromagnetism) contrasted with those of **Complex 1** (weak ferromagnetism). The main difference between the two complexes were the charge and the axial molecules. From this, it may be deduced that the geometry at Cu(II) for the former complex is more planar (less distorted) compared to that of the latter complex.

Table 4.6 shows the μ_{eff} value for **Complex 2** with those of its starting materials, namely $[Cu_2(p\text{-}HOC_6H_4COO)_4]$ and $[Cu_2(CH_3(CH_2)_{14}COO)_4]$. The results shows that the value of μ_{eff} for **Complex 2** is intermediate between that of $[Cu_2(p\text{-}HOC_6H_4COO)_4]$ (higher) and $[Cu_2(CH_3(CH_2)_{14}COO)_4]$ (lower). From this, it may be inferred that the electronic communication between two copper(II) centres is better through an alkylcarboxylate ligand compared to an arylcarboxylate ligand. This may be due to the fact that alkylcarboxylate ligands are stronger Lewis bases (better electron donors). As a result, the Cu(II) centres become less positive, which reduces the repulsion between the two centres.

Table 4.6 The μ_{eff} values (per Cu(II)) of **Complex 2** and its starting materials

Complex	**μ_{eff} / (B.M.)**
Complex 2	1.80
$[Cu(p\text{-}HOC_6H_4COO)_2].5H_2O$	2.03 [34]
$[Cu_2(CH_3(CH_2)_{14}COO)_4]$	1.45 [34]

*vi) Redox properties of **Complex 2***

The cyclic voltammogram for **Complex 2** was recorded cathodically from 0 V within the potential window -1.6 V to +1.0 V (**Figure 4.24**). It shows three cathodic peaks at -0.23, -0.47 and -1.25 V, and a single broad anodic peak at +0.43 V. The electrochemical processes (**Scheme 4.4;** ΔE = 900 mV, 1680 mV, 660 mV) are similar to those of **Complex 1**, and may be similarly explained.

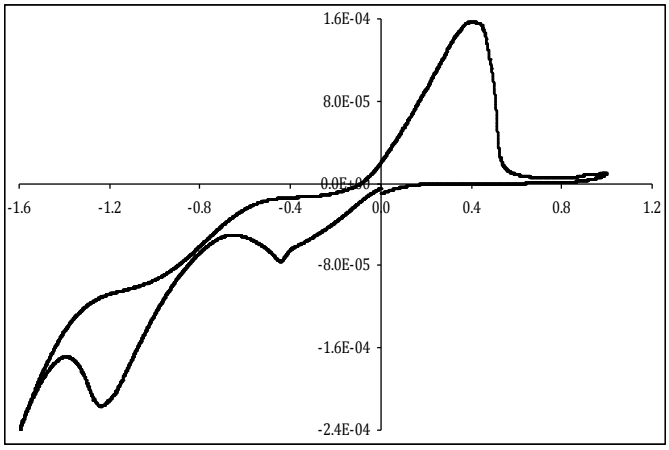

Figure 4.24 Cyclic voltamogram of **Complex 2**

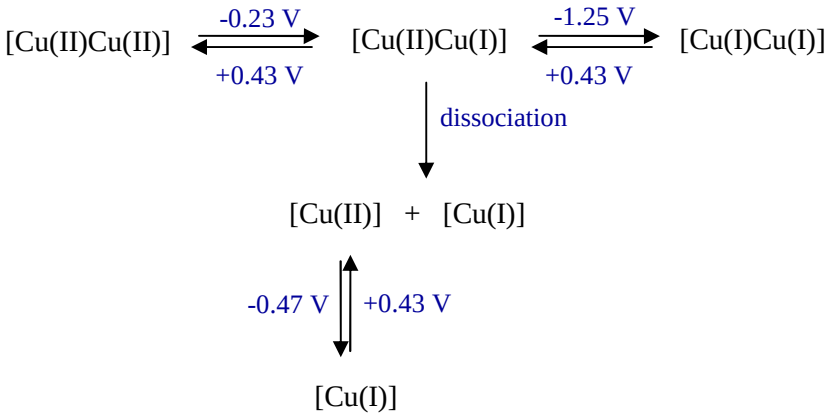

Scheme 4.4 Electrochemical processes for **Complex 2**

It is noted that the initial reduction of **Complex 2** occurs at a more negative potential (-0.23 V) as compared to that of **Complex 1** (-0.07 V). The easier reduction for the latter complex may be due to its negative charge.

c) Carbonate-base-acid reaction

The carbonate-base-acid reaction was done according to the literature for complexes with general formula $[M_2(RCOO)_4]$ [37,38]. This method was chosen as it is considered "clean" since the complex formed may be easily isolated from the by-products, which are CO_2 gas and H_2O.

In this method, a mixture of $CuCO_3.Cu(OH)_2$, *p*-HOC_6H_4COOH and $CH_3(CH_2)_{14}COOH$ (mole ratio = 1:2:2) was heated in methanol for about one week, to form complex with the expected chemical formula, $[Cu_2(p\text{-}HOC_6H_4COO)_2(CH_3(CH_2)_{14}COO)_2]$**.** These reactions were expected to proceed according to **Scheme 4.5**.

$$CuCO_3.Cu(OH)_2 + 2\ p\text{-}HOC_6H_4COOH + 2\ CH_3(CH_2)_{14}COOH$$

$$\downarrow \quad \begin{matrix} CH_3OH \\ 60^oC \\ 1\ week \end{matrix}$$

$$[Cu_2(p\text{-}HOC_6H_4COO)_2(CH_3(CH_2)_{14}COO)_2] + CO_2 + 3H_2O$$

Scheme 4.5 The carbonate-base-acid reaction for the formation of $Cu_2(p\text{-}OC_6H_4COO)_2(CH_3(CH_2)_{14}COO)_2]$

It must be stated that the reaction was very slow and did not go to completion even after reacting for one week.

i) Structural elucidation

The product isolated from the reaction was a greenish-blue powder. Based on the following analytical results, it was found that the expected complex, $[Cu_2(p\text{-}HOC_6H_4COO)_2(CH_3(CH_2)_{14}COO)_2]$ was not formed. Instead, the isolated product was $[Cu_2(CH_3(CH_2)_{14}COO)_4]$ (chemical formula, $Cu_2C_{64}H_{124}O_8$; formula mass 1148.8 g mol^{-1}), as discussed below.

The results of CHN elemental analyses (C, 66.64% and H, 11.63% H) are in good agreement with the calculated values (66.96% C and 10.81% H). Its FTIR (**Figure 4.25)**, UV-vis (**Figure 4.26)** spectra are similar to those of $[Cu_2(CH_3(CH_2)_{14}COO)_4]$ **(Figure 4.16, Figure 4.17)**.

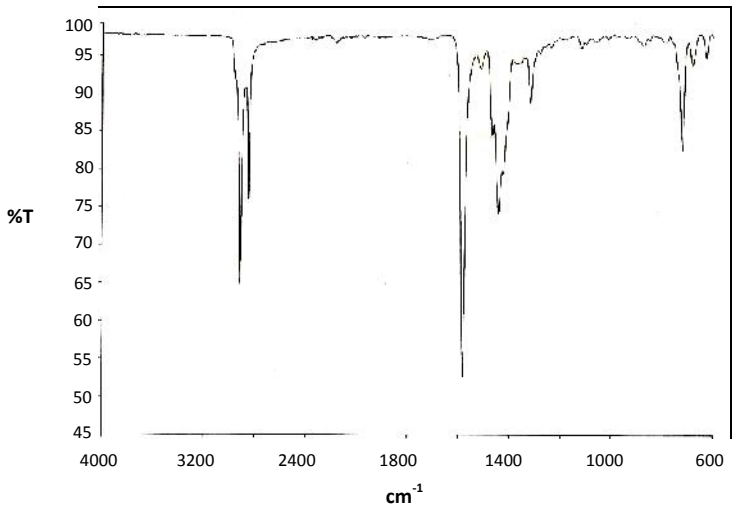

Figure 4.25 The FTIR spectrum of the product isolated from the carbonate-base-acid reaction

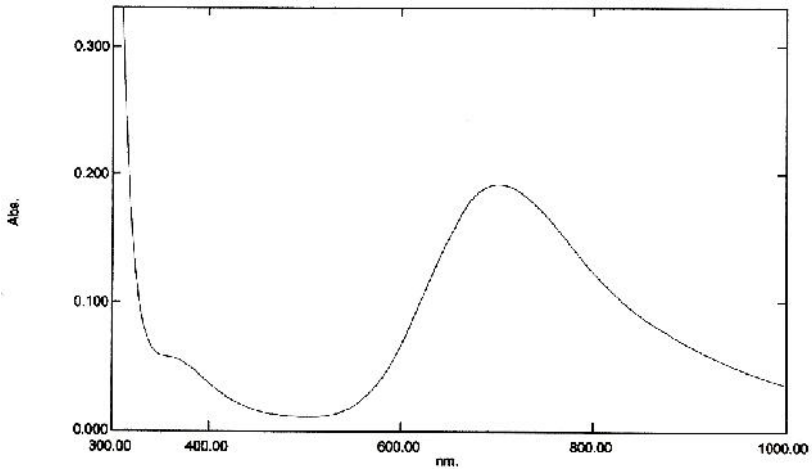

Figure 4.26 The UV-Vis spectrum of the product isolated from the carbonate-base-acid reaction

As a conclusion, the methods suitable for the preparation of copper(II) mixed carboxylates, namely $K_2[Cu_2(p\text{-}OC_6H_4COO)_2(CH_3(CH_2)_{14}COO)_2]$ and $[Cu_2(p\text{-}HOC_6H_4COO)_2(CH_3(CH_2)_{14}COO)_2]$ are the one-pot and ligand-exchange, but not the carbonate-base-acid. However, the one-pot method was preferred as it was more facile and the yield was higher than the ligand-exchange method.

4.1.2 $[Cu_2(p\text{-}H_3NC_6H_4COO)_2(CH_3(CH_2)_{14}COO)_2]Cl_2$

a) One-pot reaction

A facile one-pot reaction involving an equimolar ethanolic solution of $CuCl_2$, p-$H_2NC_6H_4COOH$ and $CH_3(CH_2)_{14}COOH$ was expected to proceed according to **Scheme 4.6.** The reaction involved self-assembly between Cu^{2+} ion with those of p-$H_2NC_6H_4COO^-$ and $CH_3(CH_2)_{14}COO^-$ ions generated *in-situ* by NH_3.

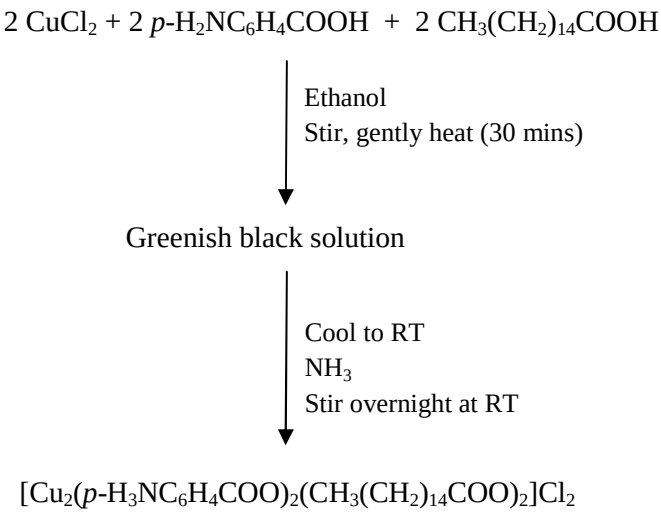

Scheme 4.6 One-pot synthesis of $[Cu_2(p\text{-}H_3NC_6H_4COO)_2(CH_3(CH_2)_{14}COO)_2]Cl_2$

The product obtained was a greenish blue powder (**Complex 3**), insoluble in water and in almost all common organic solvents, but completely soluble in a mixture of CH_3OH-CH_3COOH (95:5).

i) Structural elucidation

Based on the following analytical results, the proposed structural formula of the complex is $[Cu_2(p\text{-}H_2NC_6H_4COO)_2(CH_3(CH_2)_{14}COO)_2].2H_2O$ **(**formula mass 946.2 g mol^{-1}; **Figure 4.27).** Thus, its percentage yield is 73.2 %. Hence, it is **not** the expected ionic complex, $[Cu_2(p\text{-}H_3NC_6H_4COO)_2(CH_3(CH_2)_{14}COO)_2]Cl_2$.

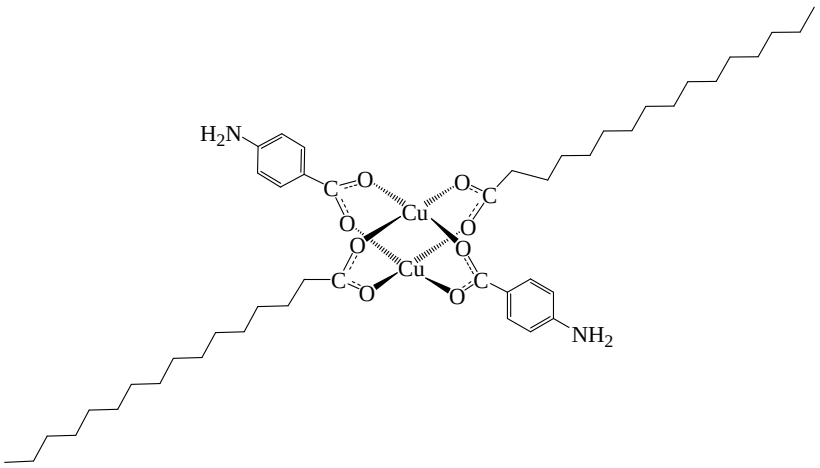

Figure 4.27 Proposed structure of **Complex 3** (H_2O solvate molecules are not shown)

The results of the **elemental analyses** of the complex (C, 58.79%; H, 10.5%; N, 2.77%) are in good agreement with the calculated values for $Cu_2C_{46}H_{78}N_2O_{10}$ (C, 58.39%; H, 9.61%; N, 2.96%).

Its **FTIR** spectrum (**Figure 4.28)** is distinctly different from its starting materials (**Figure 4.16) and** (**Figure 4.29).** It shows the presence of all of the expected functional groups as shown in **Table 4.7.** The Δ value is 127 cm^{-1}, suggesting bridging carboxylates, and thus a binuclear copper(II) complex.

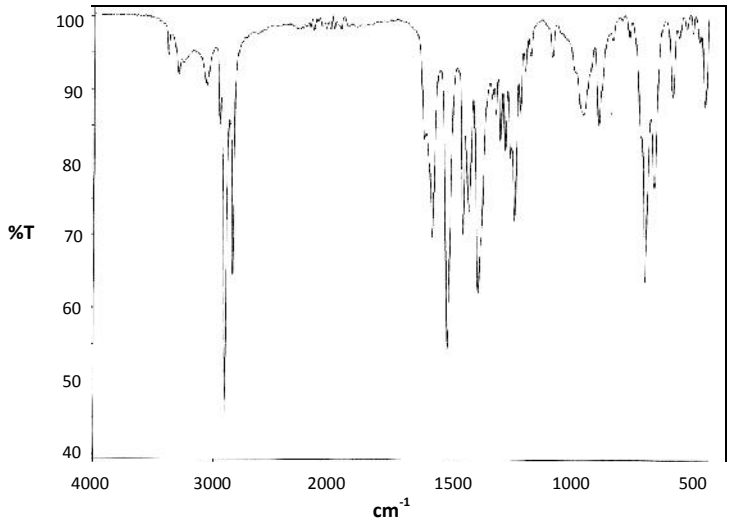

Figure 4.28 FTIR spectrum of **Complex 3**

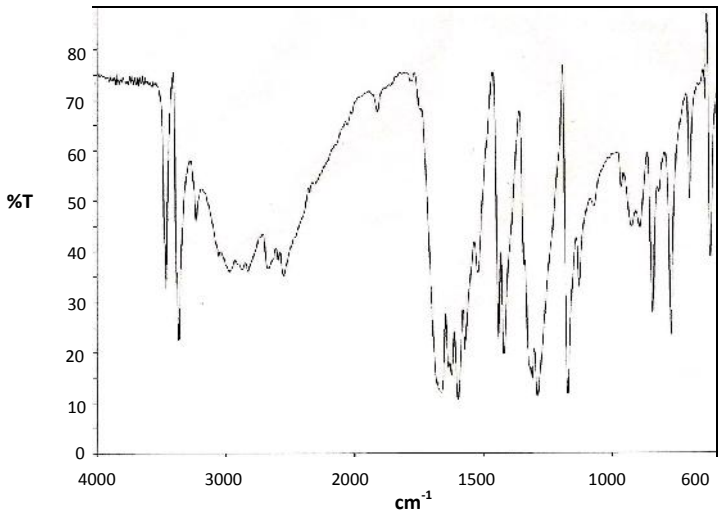

Figure 4.29 FTIR spectrum of *p*-$H_2NC_6H_4COOH$

Table 4.7 FTIR data and assignment for **Complex 3**

Wavenumber/cm^{-1}	**Assignment**
3385, 3301	NH_2
2913	CH_2 (ν_{asym})
2848	CH_2 (ν_{sym})
1597	C=C (aromatic)
1534	COO (ν_{asym})
1407	COO (ν_{sym})

The **UV-vis spectrum** of the complex in the solid state **(Figure 4.30)** shows a broad *d-d* band at 665 nm and a distinct shoulder on the charge-transfer band at 442 nm. These suggest a square planar binuclear Cu(II) complex.

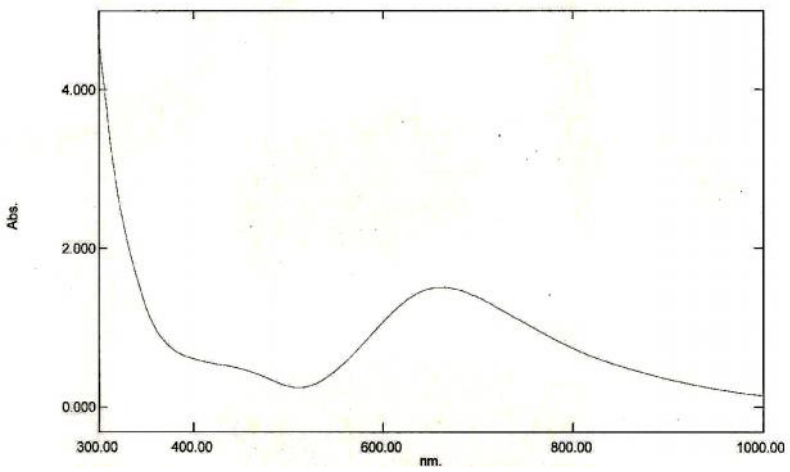

Figure 4.30 UV-vis spectrum of **Complex 3** (solid)

The **UV-vis spectrum** of the complex in solution (**Figure 4.31)** shows a broad *d-d* band at 693 nm (ε_{max}= 150 M^{-1} cm^{-1}) and a distinct shoulder on the charge-transfer band at 374 nm (ε = 30 M^{-1} cm^{-1}). The value support square pyramidal binuclear Cu(II) complex. The geometrical change may be due to the ligation of H_2O molecules at the axial position.

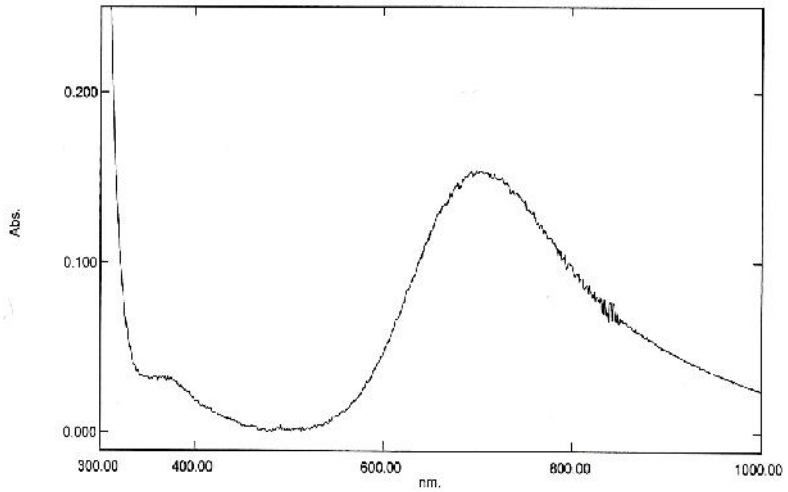

Figure 4.31 UV-visible spectrum of **Complex 3** (solution)

To summarise, the proposed structure is consistent with the chemical formula $Cu_2C_{46}H_{78}N_2O_{10}$ as suggested by the elemental analyses, bridging carboxylate ligands as suggested from FTIR, and square planar geometry at Cu(II) as suggested from UV-vis spectroscopy.

ii) Molar conductance

The molar conductance of the complex in CH_3OH-CH_3COOH (95:5) was 6 S cm^{-1} at 25^oC. Thus, it is a non-electrolyte, indicating that the dimeric structure remained intact in these solvents, as was also suggested from the UV-vis spectral result.

iii) Thermal and mesogenic properties

The thermogram of the complex (**Figure 4.32)** indicates that it is thermally stable up to around 250^oC before it decomposed by a two-stage process. The initial weight loss of

3.2% at around 100^{o}C is assigned to loss of two solvated H_2O molecules (expected, 3.8%). The total weight loss of 79.0% from 251^{o}C to 600^{o}C is assigned to the decomposition of the carboxylate ligands (expected, 82.8%) to CO_2 and other volatiles. The amount of residue at above 600^{o}C was 17.3%.

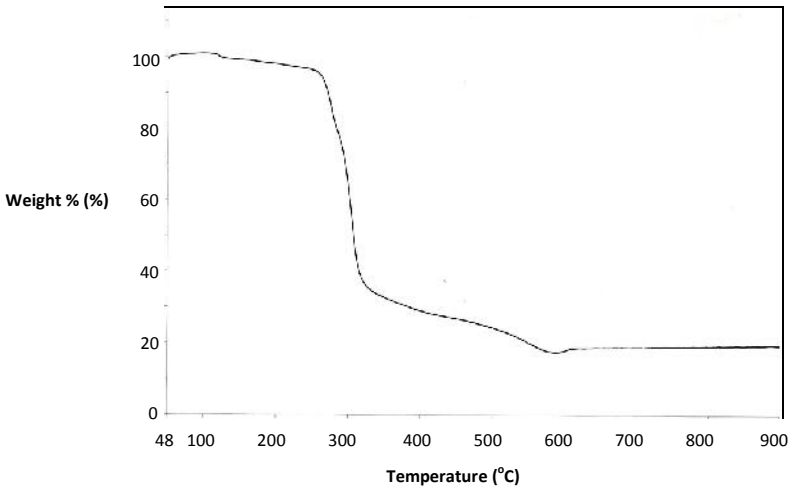

Figure 4.32 Thermogram of **Complex 3**

Assuming that the residue is CuO, the estimated formula mass of the complex, calculated using the gravimetric concept as previously done, is 920 g mol^{-1} (expected, 946.2 g mol^{-1}). Thus, the results from TGA and elemental analyses are in good agreement, and further support the proposed structural formula.

The **DSC curve** of the complex (**Figure 4.33**) shows several overlapping endotherms. The assignments of these endotherms are given in **Table 4.8.**

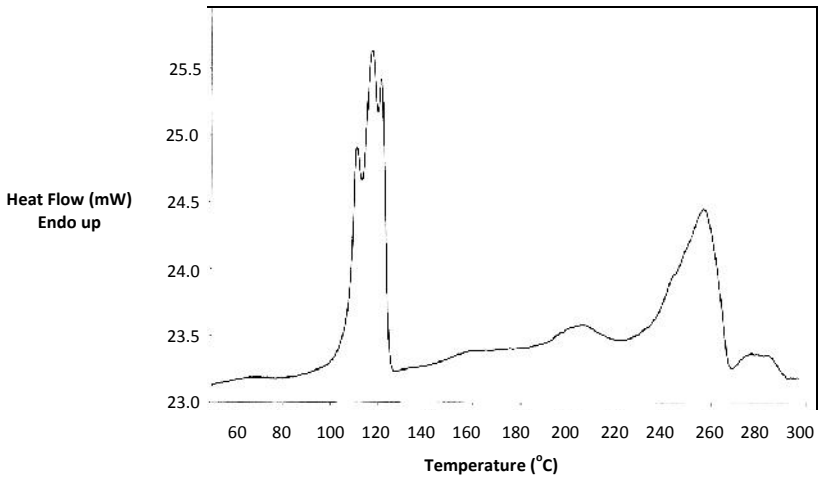

Figure 4.33 DSC curve of **Complex 3**

Table 4.8 DSC data and assignment for **Complex 3**

Temperature (^oC)	**ΔH (kJ mol^{-1})**	**Assignment**
110 117 121	+ 138	Evaporation of solvated H_2O molecules Melting of **Complex 3** (breaking of the van der Waals forces between the hexadecanoate ligands and breaking of hydrogen bonds between the $–NH_2$ groups of *p*-aminobenzoate ligands on adjacent dimer)
158	+16	Clearing of **Complex 3**
257	+103	Decomposition of $CH_3(CH_2)_{14}COO$ ligand[#]
284	+9	Further decomposition of $CH_3(CH_2)_{14}COO$ ligand

iii) Magnetic properties

The value of μ_{eff}, calculated as previously discussed using the values in **Table 4.9**, is 2.57 B.M. at 298 K, and the corresponding -2J value is 66 cm^{-1}.

Table 4.9 The χ values for **Complex 3** used for the calculation of μ_{eff}

χ	**Values**
χ_g	2.63 x $10^{-6}cm^3\ g^{-1}$
χ_m	248.54 x 10^{-5} $cm^3\ mol^{-1}$
χ_{dia}	-42.02 x 10^{-5} $cm^3\ mol^{-1}$
χ_m^{corr}	290.56 x 10^{-5} $cm^3\ mol^{-1}$

The μ_{eff} and -2J values of **Complex 3** is similar to those of **Complex 2** (μ_{eff} = 2.54 B.M, -2J = 80 cm^{-1}). This may be due to the similarity in their structures. The results suggest that the functional groups –OH and $-NH_2$ do not have a significant effect on the magnetic properties of these complexes.

iv) Electrochemical properties

The CV for **Complex 3** was recorded cathodically from 0 V within the potential window -1.5 V to +1.5 V (**Figure 4.34**). It shows two cathodic peaks at -0.30 and -1.02

V, and four anodic peaks at -0.07, 0.10, 0.14 and 0.82 V. The large ΔE values for the two processes (1120 mV and 1160 mV) suggest quasi-reversible electrochemical reactions, due to extensive structural reorganisation upon reduction.

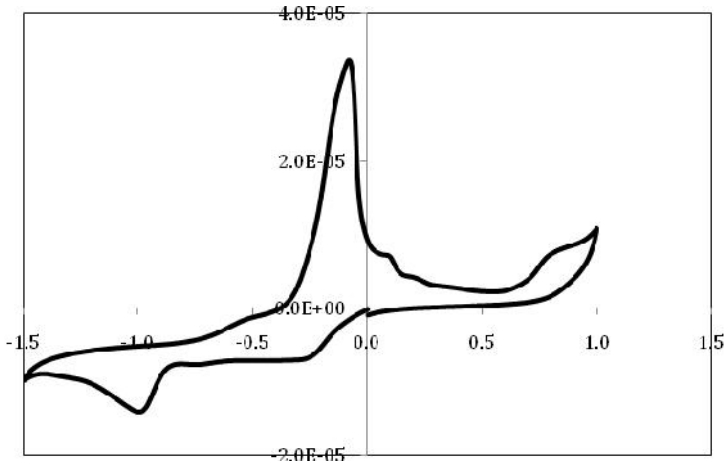

Figure 4.34 Cyclic voltammogram of **Complex 3**

The sharp anodic peak at -0.07 V provides evidence for Cu^0 deposit on the surface of the working electrode, while a small shoulder at around +0.2 V (normally observed in the CV of the Cu^{2+} salts at +0.1 V) [39], indicates the presence of Cu^{2+} ions in solution. Both Cu metal and Cu^{2+} ion result from disproportionation of [Cu(I)Cu(I)]. The redox reactions are summarised in **Scheme 4.7.**

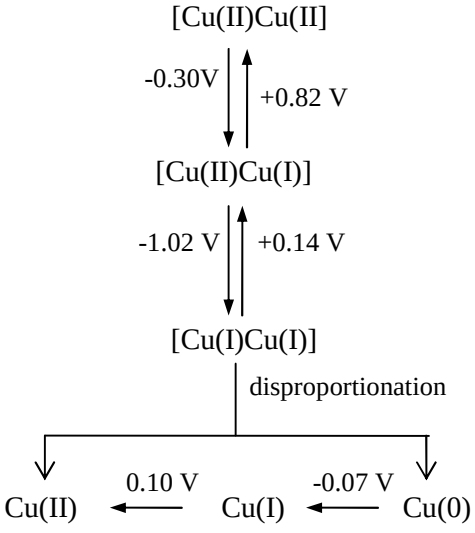

Scheme 4.7 Electrochemical processes for **Complex 3**

b) Ligand-exchange reaction

As discussed above, the ligand-exchange reaction involved several steps. The first step was the synthesis of $[Cu_2(CH_3(CH_2)_{14}COO)_4]$ and $[Cu_2(p\text{-}H_2NC_6H_4COO)_4]$, and then reacting the two complexes (1:1 mole ratio) to form complex with the expected formula,$[Cu_2(p\text{-}H_2NC_6H_4COO)_2(CH_3(CH_2)_{14}COO)_2]$**.** These reactions were expected to proceed according to **Scheme 4.8**.

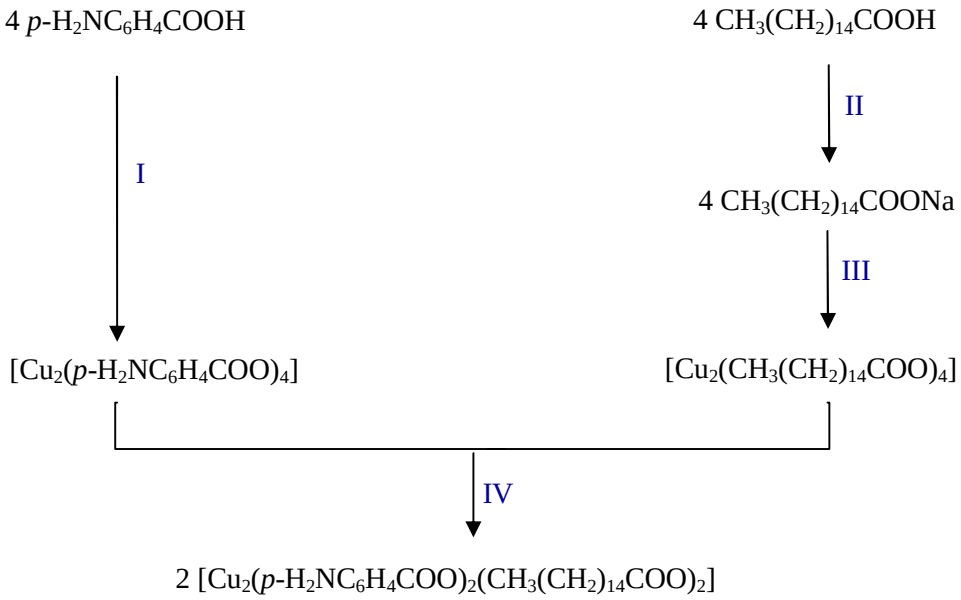

Scheme 4.8 The ligand-exchange reaction expected to form $Cu_2(p\text{-}H_2NC_6H_4COO)_2(CH_3(CH_2)_{14}COO)_2]$ (I) $[Cu_2(CH_3COO)_4]$, EtOH, Δ; (II)Na_2CO_3, H_2O, Δ; (III) $CuCl_2$, EtOH, Δ; (IV) EtOH, pyridine, Δ

The complex was obtained as a greenish blue powder. Based on the following analytical data, its proposed structural formula is $[Cu_2(CH_3(CH_2)_{14}COO)_4]$. Hence, the expected $[Cu_2(p\text{-}H_2NC_6H_4COO)_2(CH_3(CH_2)_{14}COO)_2]$ was not obtained from the reaction.

The results of CHN elemental analyses (C, 66.64% and H, 11.63% H) are in good agreement with the calculated values for $Cu_2C_{64}H_{124}O_8$ (66.96% C and 10.81% H). Its FTIR and UV-vis spectra (**Figure 4.35** and **Figure 4.36)** are also very similar to $[Cu_2(CH_3(CH_2)_{14}COO)_4]$ **(Figure 4.16** and **Figure 4.17**, respectively). As such, this complex was not further analysed as it was not the intended product.

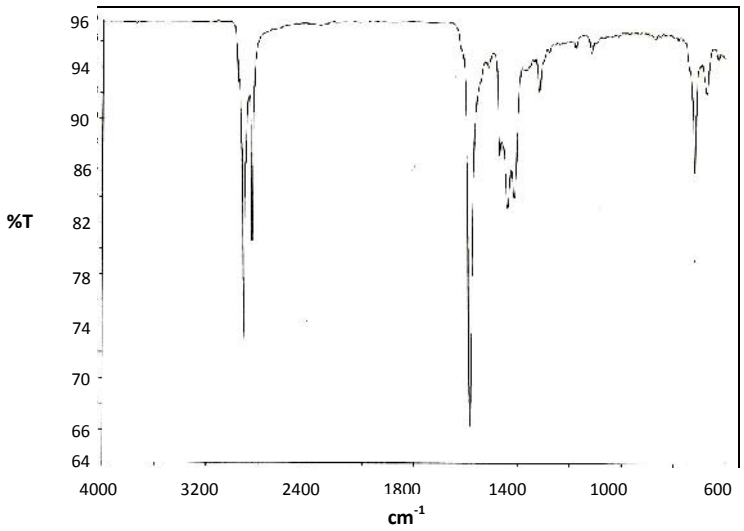

Figure 4.35 The FTIR spectrum of the product isolated from the ligand-exchange reaction

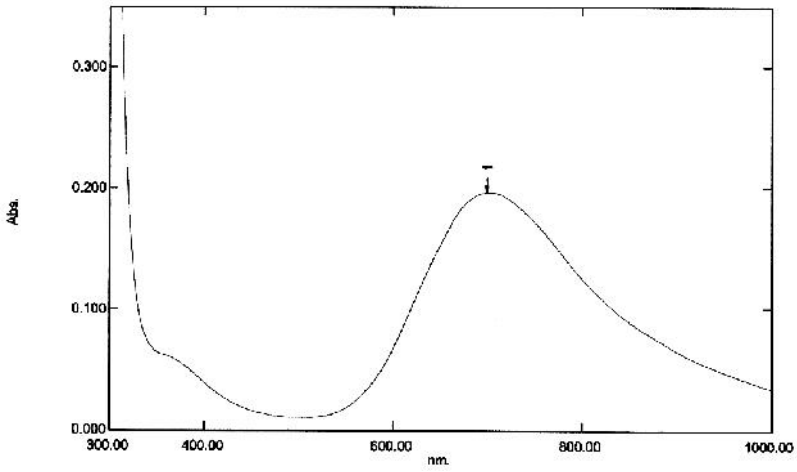

Figure 4.36 The UV-vis spectrum of the product isolated from the ligand-exchange reaction

c) Carbonate-acid-base reaction

As before, the carbonate-acid-base reaction involving a mixture of $CuCO_3.Cu(OH)_2$, *p*-$H_2NC_6H_4COOH$ and $CH_3(CH_2)_{14}COOH$ (mole ratio = 1:2:2) was expected to form, $[Cu_2(p\text{-}H_2NC_6H_4COO)_2(CH_3(CH_2)_{14}COO)_2]$. These reactions were expected to proceed according to **Scheme 4.9.**

$$CuCO_3.Cu(OH)_2 + 2\ p\text{-}H_2NC_6H_4COOH + 2\ CH_3(CH_2)_{14}COOH$$

$$\downarrow \begin{matrix} CH_3OH \\ 60^oC \\ 1\ week \end{matrix}$$

$$[Cu_2(p\text{-}H_2NC_6H_4COO)_2(CH_3(CH_2)_{14}COO)_2] + CO_2 + 3H_2O$$

Scheme 4.9 The carbonate-acid-base reaction for the formation of $[Cu_2(p\text{-}H_2NC_6H_4COO)_2(CH_3(CH_2)_{14}COO)_2]$

The product isolated from the reaction was a greenish blue powder. Based on the following analytical results, its proposed chemical formula is $[Cu_2(CH_3(CH_2)_{14}COO)_4]$, and not the expected complex, $[Cu_2(p\text{-}H_2NC_6H_4COO)_2(CH_3(CH_2)_{14}COO)_2]$.

The results of CHN elemental analyses of the intermediate complex (C, 66.64% and H, 11.63% H) are in good agreement with the calculated values for $Cu_2C_{64}H_{124}O_8$ (66.96% C and 10.81% H). Its FTIR and UV-Vis spectra (**Figure 4.37** and **Figure 4.38)** are also similar to $[Cu_2(CH_3(CH_2)_{14}COO)_4]$ **(Figure 4.16** and **Figure 4.17** respectively). As such, this complex was not further analysed as it was not the intended product.

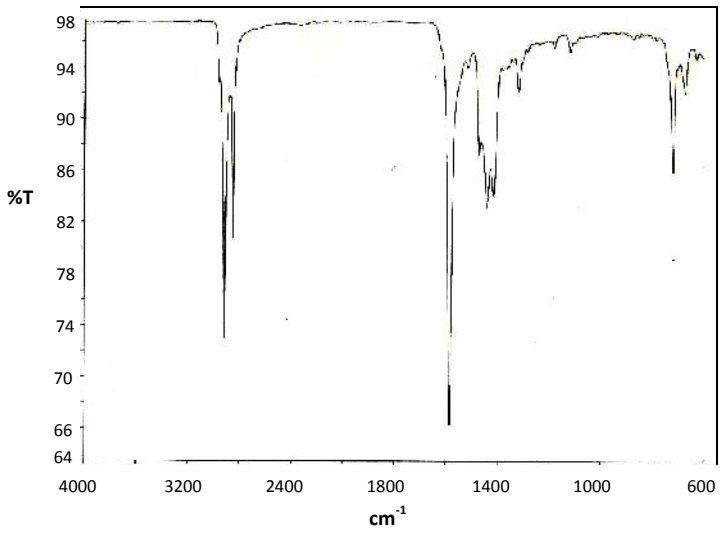

Figure 4.37 The FTIR spectrum of the product isolated from the carbonate-base-acid reaction

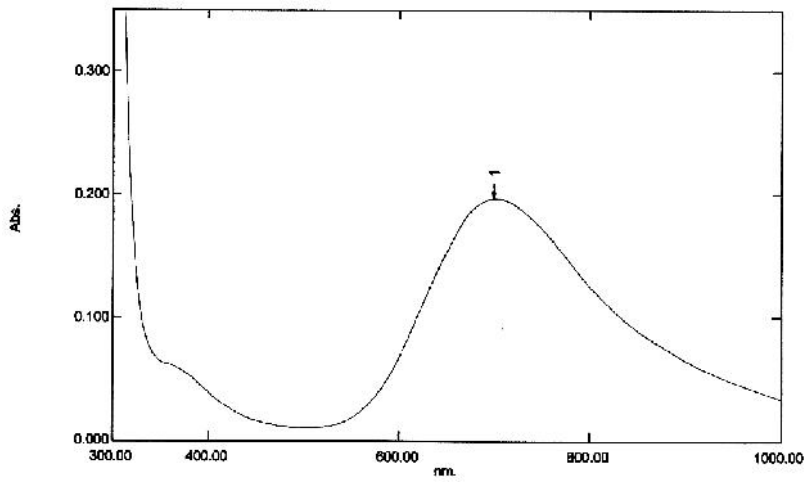

Figure 4.38 The UV-Vis spectrum of the product isolated from the carbonate-base-acid reaction

To summarise, the one-pot reaction is suitable for the preparation of the mixed carboxylate, $[Cu_2(p\text{-}H_2NC_6H_4COO)_2(CH_3(CH_2)_{14}COO)_2]$, but not the corresponding ionic complex, $[Cu_2(p\text{-}H_3NC_6H_4COO)_2(CH_3(CH_2)_{14}COO)_2]Cl_2$. On the other hand, both the ligand-exchange and carbonate-base-acid reactions were not suitable methods for the preparation of the complex.

4.2 COPPER(II) MIXED CARBOXYLATES OF LOWER SYMMETRY

As stated earlier, the strategies that may be adopted to reduce the melting temperatures of ionic complexes to less than 100^oC, so as to meet the definition of ionic liquids, are use of: (a) carboxylate ions with long, preferably branched, hydrocarbon chain,(b) non-planar large counterions, and (c) mixed ligands to reduce the molecular symmetry.

Thus, the next phase of this research was to prepare and characterise lower symmetry anionic copper(II) complex ($K[Cu_2(p\text{-}OC_6H_4COO)(CH_3(CH_2)_{14}COO)_3]$), $[Cu_2(p\text{-}HOC_6H_4COO)(CH_3(CH_2)_{14}COO)_3]$, and cationic copper(II) complex ($[Cu_2(p\text{-}H_3NC_6H_4COO)(CH_3(CH_2)_{14}COO)_3]Cl$).

4.2.1 K[Cu_2(*p*-OC_6H_4COO)($CH_3(CH_2)_{14}COO)_3$]

a) One-pot synthesis

The reaction between [$Cu(CH_3COO)_2$], *p*-HOC_6H_4COOH and $CH_3(CH_2)_{14}COOH$ (mole ratio = 2:1:3) was fast, facile, and proceeded as expected according to **Scheme 4.1**. The product was a fine turquoise blue powder, soluble in a mixture of CH_3OH-CH_3COOH (95:5), but insoluble in water and almost all other common organic solvents.

i. Structural elucidation

Based on the following analytical results, it is proposed that the structural formula of the product is K[Cu_2(*p*-OC_6H_4COO)($CH_3(CH_2)_{14}COO)_3$] (**Complex 4** ; formula mass, 1068.5 g mol^{-1}; **Figure 4.39)**. Thus, its yield was 66.9 %.

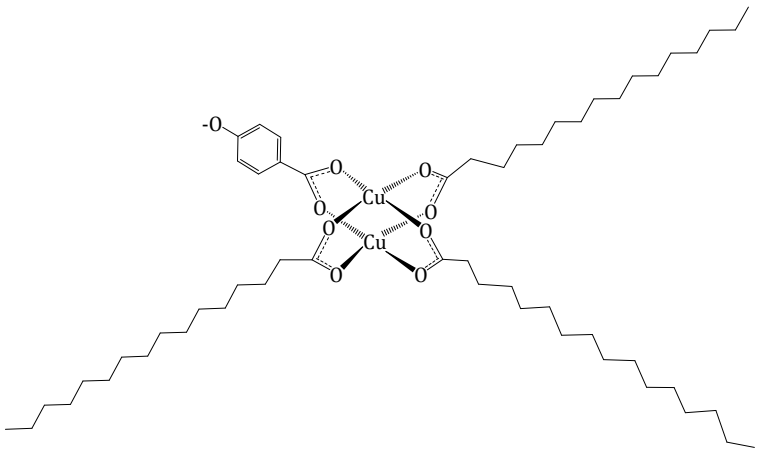

Figure 4.39 Proposed structure of **Complex 4** (K^+ ion is not shown)

The results of **elemental analyses** (C, 61.42%; H, 10.37%) are in good agreement with the calculated values for $KCu_2C_{55}H_{97}O_9$ (C, 61.86%; H, 9.09%).

The **FTIR** spectrum (**Figure 4.40)** is distinctly different from the reactants, $CH_3(CH_2)_{14}COOH$ (**Figure 4.3**) and *p*-HOC_6H_4COOH (**Figure 4.4**), indicating a reaction occurred between the two materials. It also shows the presence of the expected functional groups as previously discussed. The Δ value of 174 cm^{-1} is in agreement with bridging carboxylate groups.

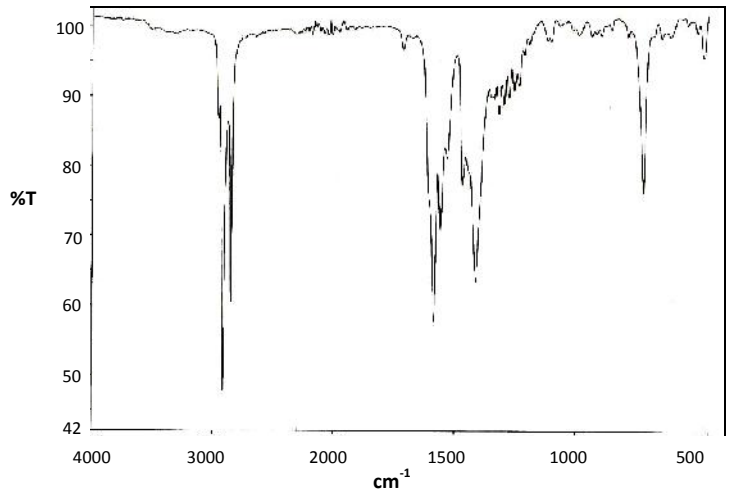

Figure 4.40 FTIR spectrum of **Complex 4**

The UV-vis spectrum of **Complex 4** in the solid state **(Figure 4.41)** shows a broad *d-d* band at 664 nm and a distinct shoulder on the charge-transfer band at 495 nm. This suggests a square planar binuclear Cu(II) complex.

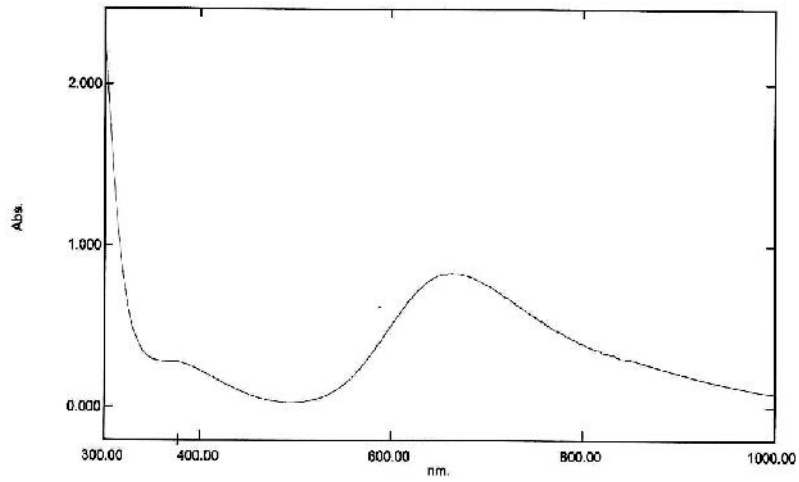

Figure 4.41 UV-vis spectrum of **Complex 4** (solid)

The UV-vis spectrum of the complex dissolved in CH_3OH-CH_3COOH (95:5) (**Figure 4.42)** shows a broad *d-d* band at 700 nm (ε_{max} = 229 M^{-1} cm^{-1}) and a distinct shoulder on the charge-transfer band at 362 nm (ε = 59 M^{-1} cm^{-1}). The values support square pyramidal binuclear Cu(II) complex. The geometrical change may be due to the ligation of solvent molecule at the axial position.

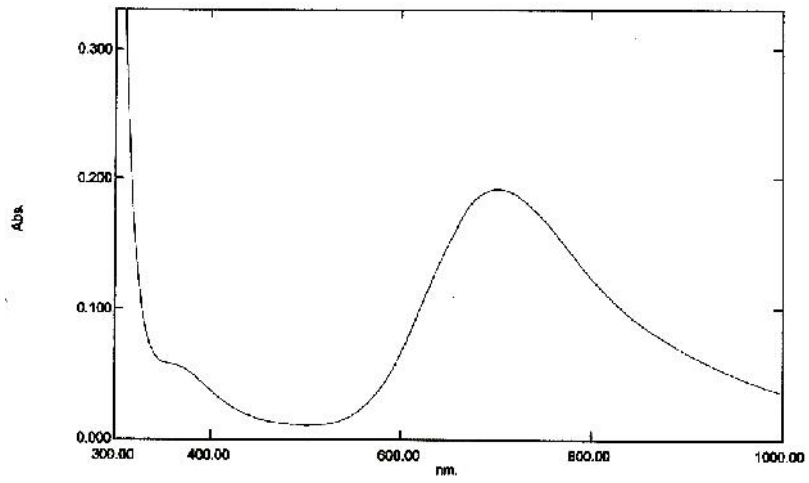

Figure 4.42 UV-vis spectrum of **Complex 4** (solution)

To summarise, the proposed structure for **Complex 4** is consistent with the chemical formula $KCu_2C_{55}H_{97}O_9$ as suggested by the elemental analyses, bridging carboxylate ligands as suggested from FTIR, and binuclear square planar geometry at Cu(II) as suggested from UV-vis spectroscopy **(Figure 4.39).**

ii. Thermal and mesogenic properties

The thermogram of **Complex 4** (**Figure 4.43)** shows that it is thermally stable up to around 244^{o}C. Thus, it is significantly less thermally stable than **Complex 1** ($K_2[Cu_2(p\text{-}OC_6H_4COO)_2(CH_3(CH_2)_{14}COO)_2]$). This is expected since **Complex 4** has a less symmetrical structure and does not have the resonance effect as **Complex 1.**

The complex then decomposed by a two-stage process with total weight loss of 82.0% (expected 84.4%). The amount of residue at temperatures above 550^{o}C to 900^{o}C is 18.0%. Assuming that it is K_2O and CuO, the estimated formula mass of **Complex 4**, calculated, using the gravimetry concept **(Appendix 6)**, is 1111.1 g mol^{-1} (expected 1067.0 g mol^{-1}). Thus, the results from TGA and elemental analyses are in good agreement, and lend further support for the proposed structural formula.

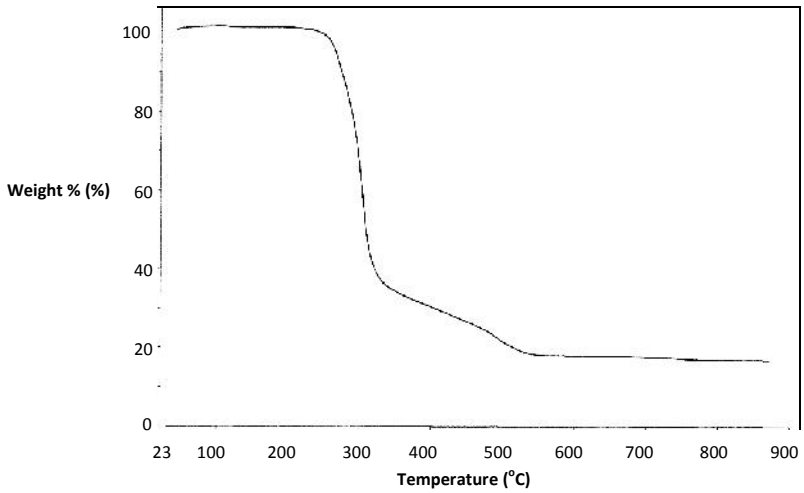

Figure 4.43 TGA of **Complex 4**

The DSC curve of **Complex 4** (**Figure 4.44)** shows several overlapping endotherms. The assignments of these endotherms are given in **Table 4.10.**

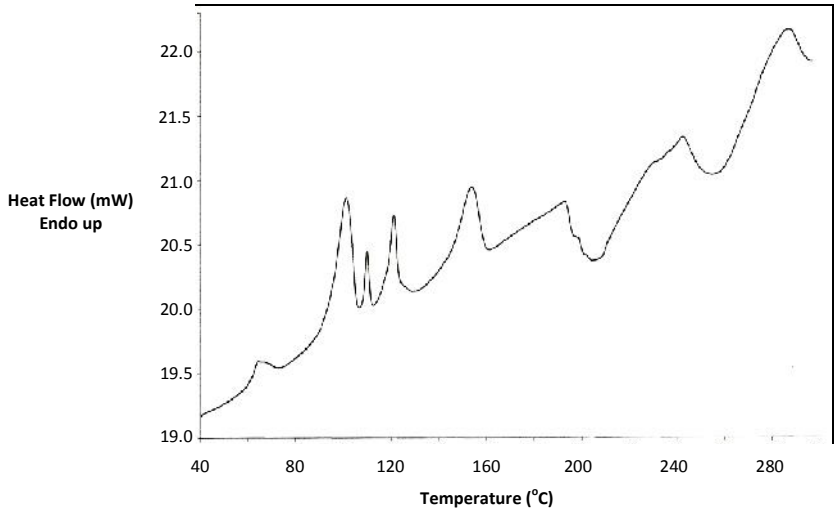

Figure 4.44 DSC of **Complex 4**

Thus as expected, the melting and clearing temperatures for **Complex 4,** ($K[Cu_2(p\text{-}OC_6H_4COO)(CH_3(CH_2)_{14}COO)_3]$) (145°C; 167°C respectively), are significantly lower than **Complex 1** ($K_2[Cu_2(p\text{-}OC_6H_4COO)_2(CH_3(CH_2)_{14}COO)_2]$, which did not melt or clear upon decomposition (T_{dec} = 424°C).

Table 4.10 DSC data and assignment for **Complex 4**

Temperature (^{o}C)		**ΔH*/ kJ mol^{-1}**	**Assignment**
onset	**peak**		
61	64	+ 9	Melting of "freed" $CH_3(CH_2)_{14}COOH$ (mp = 64^{o}C)
94	101	+65	Crystal-to-crystal transition
108	110	+8	Breaking of intramolecular H-bonds
118	121	+27	Crystal-to-crystal transition
145	154	+46	Melting of **Complex 4**
167	193	+80	Clearing of **Complex 4**
209	242	+128	Evaporation of "freed" $CH_3(CH_2)_{14}COOH$ (bp = 214-217^{o}C)
267	285	+85	Decomposition of **Complex 4**

*The ΔH value for each endotherm cannot be accurately computed due to overlapping peaks

iii. Magnetic properties

The μ_{eff} value, calculated as before using data in **Table 4.11**, is 2.38 B.M. at 298 K, and the corresponding -2J value is 156 cm^{-1}. The results indicate strong antiferromagnetic interactions between the two Cu(II) centres.

Table 4.11 The χ values for **Complex 4** used for the calculation of μ_{eff}

χ	**Values**
χ_g	1.81 x 10^{-6}cm^{3}g^{-1}
χ_m	193.13 x 10^{-5} cm^{3}mol^{-1}
χ_{dia}	-56.75 x 10^{-5} cm^{3}mol^{-1}
χ_m^{corr}	249.88 x 10^{-5} cm^{3}mol^{-1}

The result is due to the presence of more alkylcarboxylate ligands in **Complex 4**, consistent with the above deduction that an alkylcarboxylate ligand is a better superexchange pathway compared to an arylcarboxylate ligand.

iv. Redox properties

The cyclic voltammogram for **Complex 4** was recorded cathodically from 0 V within the potential window -1.5 V to +1.0 V (**Figure 4.45)**. It shows three cathodic peaks at -0.18 V,-0.29 V and -1.0 V, and a broad overlapping anodic peak at +0.22 V and +0.42 V.The electrochemical processes (**Scheme 4.10;** ΔE = 600 mV, 1200 mV, 510 mV) are similar to those of previous complexes, and may be similarly explained.

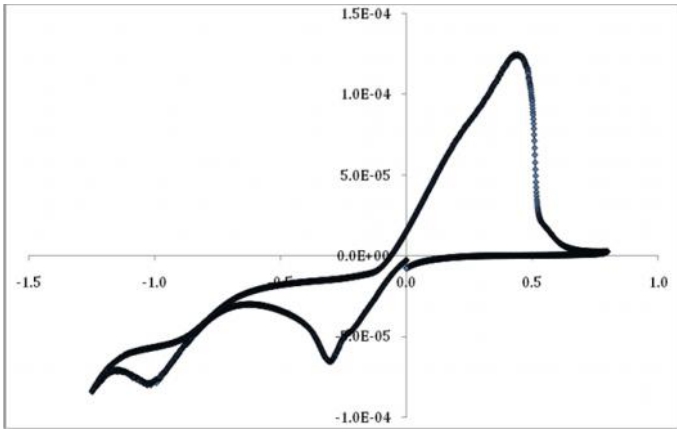

Figure 4.45 Cyclic voltammogram of **Complex 4**

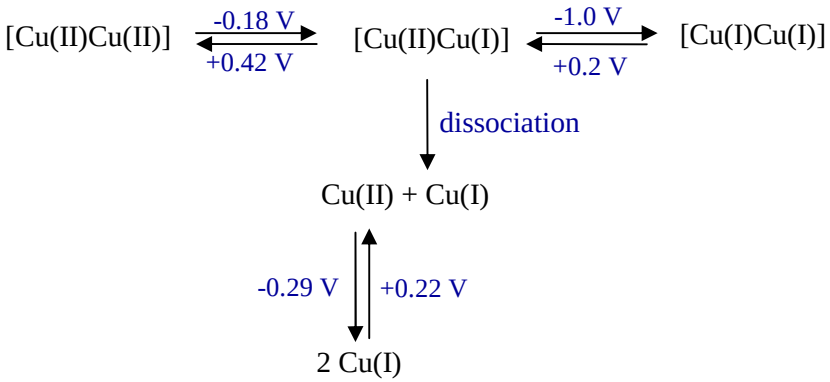

Scheme 4.10 Electrochemical processes of **Complex 4**

b) Ligand-exchange reaction

The ligand-exchange reaction involved reacting $[Cu_2(p\text{-}HOC_6H_4COO)_4]$ with $[Cu_2(CH_3(CH_2)_{14}COO)_4]$ in a 1:3 mole ratio, to form complex with the expected chemical formula, $[Cu_2(p\text{-}HOC_6H_4COO)(CH_3(CH_2)_{14}COO)_3]$**.**

It is envisioned that during the reaction, the dinuclear homocarboxylates dissociated, and then reassembled to form the desired mixed carboxylates. The reaction was facilitated by pyridine molecules, which formed strong coordinate bond with Cu(II) at the axial positions of these complexes, and hence weaken the equatorial coordinate bonds.

The product (**Complex 5**) was obtained as a greenish blue powder, soluble in a mixture of CH_3OH-CH_3COOH (95:5), but insoluble in water and almost all other common organic solvents.

i) Structural elucidation

Based on the following analytical results, it is proposed that the structural formula of the greenish-blue powder is $[Cu_2(p\text{-}HOC_6H_4COO)(CH_3(CH_2)_{14}COO)_3(CH_3CH_2OH)_2]$ (**Complex 5;** formula mass, 1122.6 g mol^{-1}; **Figure 4.46)**. Thus, its yield was 80.5 %.

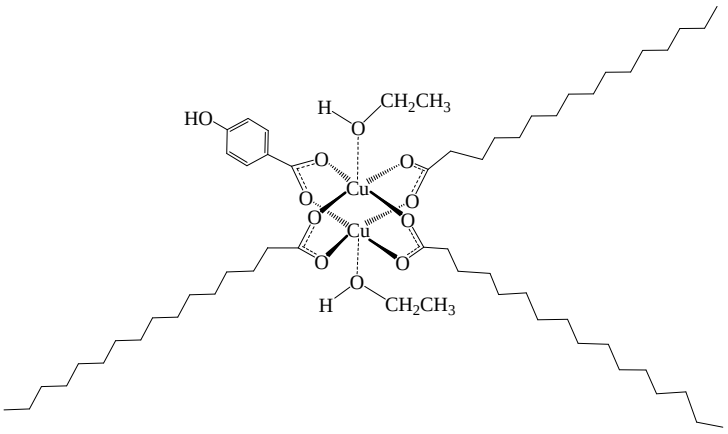

Figure 4.46 Proposed structure of **Complex 5**

The results of the **elemental analyses** (C, 63.53%; H, 10.50%) are in good agreement with the calculated values for $Cu_2C_{59}H_{110}O_{11}$ (C, 63.15%%; H, 9.88%).

The **FTIR** spectrum (**Figure 4.47)** is distinctly different from the reactants, $[Cu_2(p\text{-}HOC_6H_4COO)_4]$ and $[Cu_2(CH_3(CH_2)_{14}COO)_4]$ (**Figure 4.13 and 4.16 respectively**), indicating a reaction occurred between the two materials. It also shows the presence of the expected functional groups as previously discussed. The Δ_{OCO} value

of 171 cm^{-1} is in agreement with the presence of carboxylate group bridging the two copper(II) ions, and hence a binuclear complex.

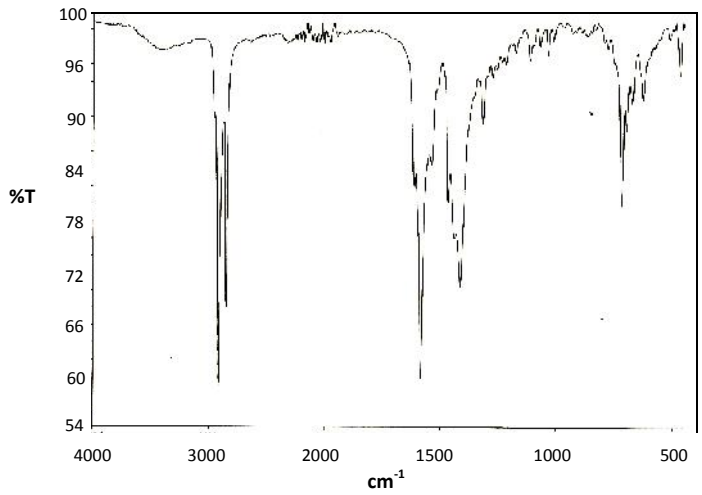

Figure 4.47 FTIR spectrum of **Complex 5**

The UV-vis spectrum of **Complex 5** in the solid state **(Figure 4.48)** shows a broad *d-d* band at 691 nm and a distinct shoulder on the charge-transfer band at 377 nm. This suggests a square pyramidal binuclear Cu(II) complex. This is in good agreement with the ligation of ethanol molecules at the axial positions.

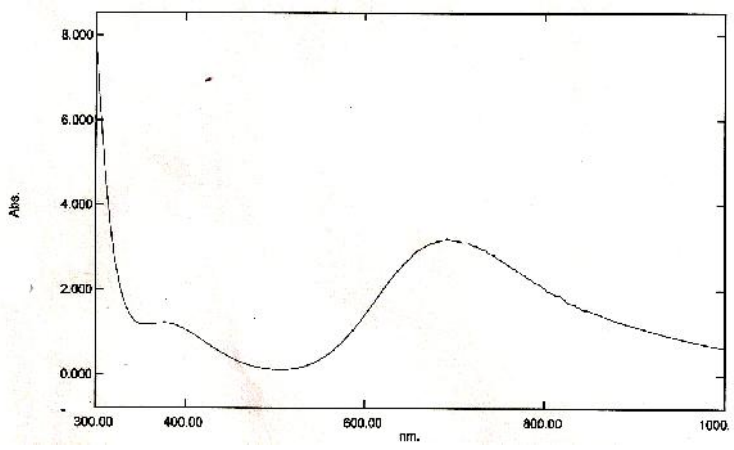

Figure 4.48 UV-vis spectrum of **Complex 5** (solid)

The UV-vis spectrum of the complex dissolved in CH_3OH-CH_3COOH (95:5) (**Figure 4.49)** shows a broad *d-d* band at 706 nm (ε_{max} = 203 M^{-1} cm^{-1}) and a distinct shoulder on the strong charge-transfer band at 367 nm (ε = 55 M^{-1} cm^{-1}). The result suggests that the geometry of the complex remained intact in these solvents.

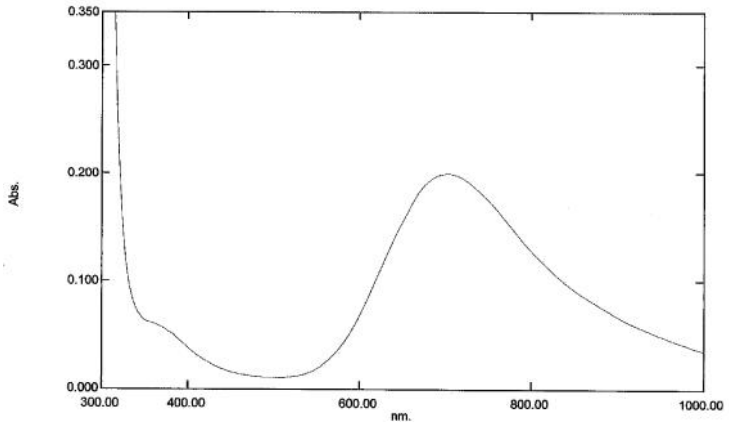

Figure 4.49 UV-vis spectrum of **Complex 5** (solution)

To summarise, the proposed structure for **Complex 5 (Figure 4.46)** is consistent with the chemical formula $Cu_2C_{59}H_{110}O_{11}$as suggested by the elemental analyses, bridging carboxylate ligands as suggested from FTIR, and binuclear square pyramidal geometry at Cu(II) as suggested from UV-vis spectroscopy**.** It also shows two CH_3CH_2OH molecules coordinated at the axial positions of the copper(II) centres.

ii) Thermal and mesogenic properties

The thermogram of **Complex 5** (**Figure 4.50)** shows that it is thermally stable up to around 241^oC. Thus, its thermal stability was slightly higher than other copper(II) homocarboxylates reported in the literature. Most copper(II) carboxylates were reported to be thermally stable up to about 220^oC.

The thermogram also shows an initial weight loss of 8.5% at 84^oC, assigned to the evaporation of two CH_3CH_2OH molecules (expected 8.2%). The complex then decomposed by a two-stage process with total weight loss of 77.0%, assigned to the decomposition of the carboxylate ligands to CO_2 and other volatiles (expected 80.5%).

The amount of residue at temperatures above 850^oC was 14.2%. Assuming that it was CuO, the estimated formula mass of **Complex 5,** calculated as previously done using the gravimetry concept, is 1124 g mol^{-1} (expected 1121 g mol^{-1}). Thus, the results from TGA and elemental analyses are in good agreement, and lend further support for the proposed structural formula

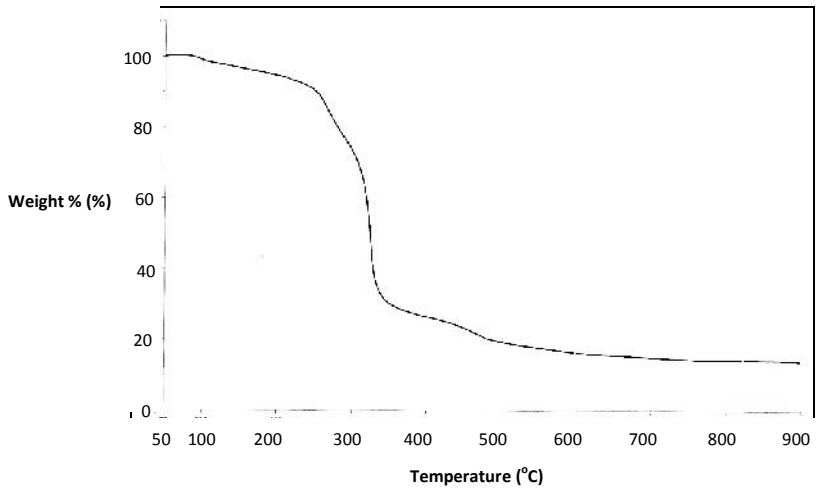

Figure 4.50 Thermogram of **Complex 5**

The development of optical structure of **Complex 5** on heating is illustrated by the sequence of OPM photographs as shown in **Figure 4.51 (a-f).** The complex was a greenish-blue powder before heating, and the colour remained the same when it started to melt at about 94^{o}C. On further heating, the complex cleared at 147^{o}C to an isotropic liquid. On further heating to 217^{o}C, which is below its decomposition temperature (241^{o}C from the TGA), the liquid became less viscous and the colour changed to paler blue. Thus, the isotropic temperature range is 70^{o}C, which is surprisingly large, and contrasts with other copper(II) carboxylates, reported to either have lower decomposition temperatures than the clearing temperatures [Godquin], or immediately decomposed upon clearing.

On cooling from an isotropic liquid phase to room temperature, it was observed that a mesophase began to developed at 195^{o}C **(Figure 4.52(a)).** From the optical texture, the mesophase of the complex may be said to be smectic. On further cooling to 98^{o}C, it developed into a more ordered columnar hexagonal mesophase, which accounts for the brighter birefringence **(Figure 4.52(b)).** This mesophase remain unchanged on further cooling to room temperature.

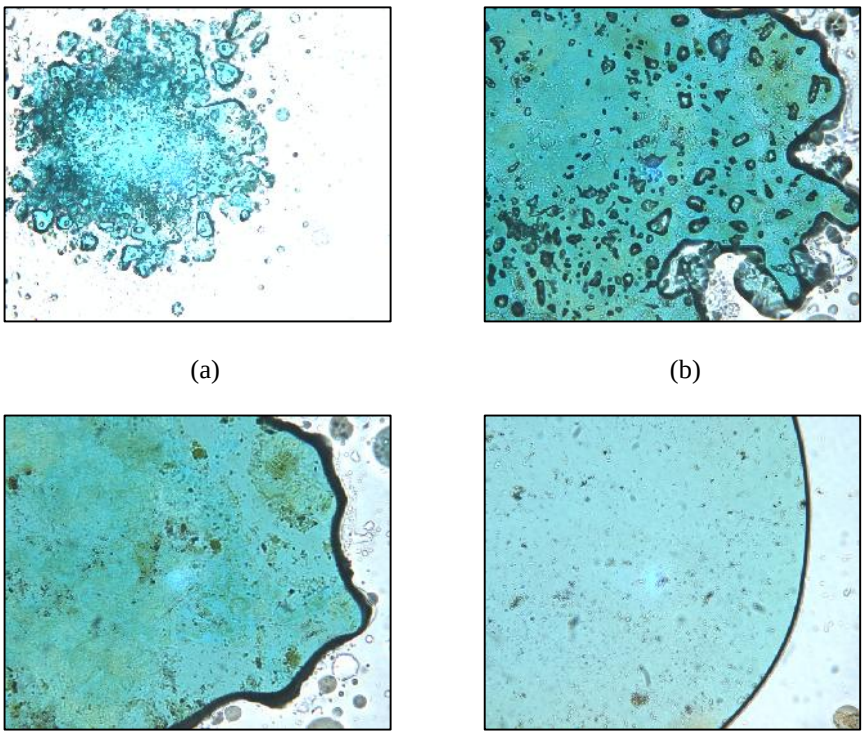

(a) (b)

(c) (d)

Figure 4.51 OPM of **Complex 5** on heating: (a) 147^{o}C; (b) 161C; (c) 208^{o}C; and (d) 217^{o}C

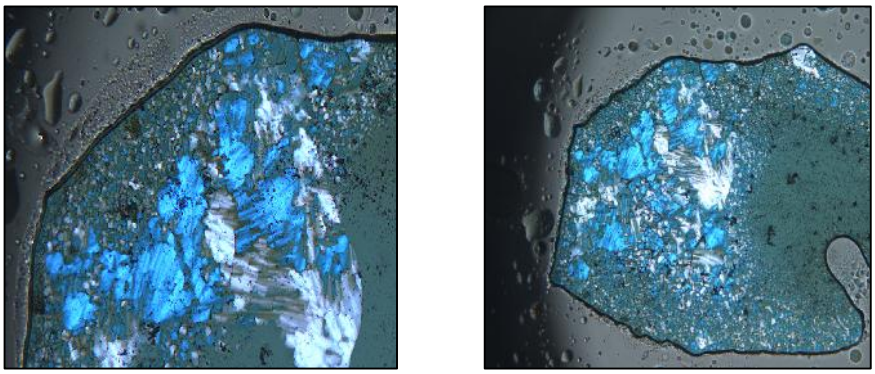

(a) (b)

Figure 4.52 OPM of **Complex 5** on cooling from the isotropic liquid phase: (a) 195^{o}C; (b) 98^{o}C

The DSC curve of **Complex 5** (**Figure 4.53**) shows several overlapping endotherms. The assignments of these endotherms are given in **Table 4.12.**

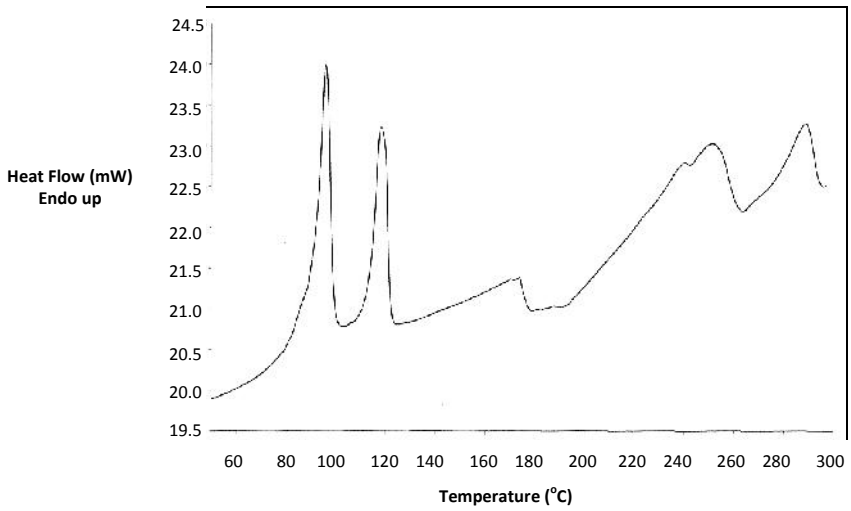

Figure 4.53 DSC curve of **Complex 5**

From the result, the melting temperature of **Complex 5** is lower than **Complex 2** ($[Cu_2(p\text{-}HOC_6H_4COO)_2(CH_3(CH_2)_{14}COO)_2)(CH_3(CH_2)_{14}COOH)(H_2O)].CH_3CH_2OH$); $T_{melting}$ = 139°C). This is as expected as **Complex 5** is less symmetrical, and thus less efficient packing in the solid state.

Table 4.12 DSC data and assignment for **Complex 5**

Temperature (°C)		**ΔH (kJ mol^{-1})**	**Assignment**
onset	**peak**		
91	96	+ 77	Concurrent evaporation of two CH_3CH_2OH molecules (from TGA) and melting (from OPM).
113	118	+55	Breaking of interdimeric H-bond involving *p*-HOC_6H_4OO ligands, and van der Waals involving $CH_3(CH_2)_{14}COO$ ligands.
140	174	+36	T_{clear} = 147°C (from OPM)
215	250	+138	**Complex 5** fully cleared; and decomposition of $CH_3(CH_2)_{14}COO$ ligands (241°C from TGA).
276	289	+40	Further decomposition of $CH_3(CH_2)_{14}COO$ ligands.

iii) Magnetic properties

The μ_{eff} value, calculated as before using the data in **Table 4.13**, is 1.87 B.M. at 298 K, and the corresponding -2J value is 346 cm^{-1}. The results indicate a very strong antiferromagnetic interactions between the two Cu(II) centres.

Table 4.13 The χ values for Complex 5 used for the calculation of μ_{eff}

χ	value
χ_g	8.30×10^{-7} cm^3 g^{-1}
χ_m	93.18×10^{-5} cm^3 mol^{-1}
χ_{dia}	-65.28×10^{-5} cm^3 mol^{-1}
χ_m^{corr}	158.46×10^{-5} cm^3 mol^{-1}

It is noted that the magnetic interaction is significantly stronger than the corresponding ionic complex, **Complex 4** ($K[Cu_2(p\text{-}OC_6H_4COO)(CH_3(CH_2)_{14}COO)_3]$; μ_{eff} = 2.38 B.M.; 2J = 156 cm^{-1}). From this, it may be deduced that magnetic interaction is stronger in neutral copper(II) mixed-carboxylates complexes compared to charged complexes. This is consistent with earlier observations (refer to **Complex 1**).

iv. Redox properties

The CV for **Complex 5** was recorded cathodically from 0 V within the potential window -1.5 V to +1.0 V (**Figure 4.54)**. It shows three reduction peaks at -0.26 V, -0.42 V and -1.22 V, and two overlapping anodic peaks at +0.40 V, and +0.47 V. The electrochemical processes (**Scheme 4.11;** ΔE = 890 mV, 1620 mV and 660 mV) are similar to those of previous complexes, and may be similarly explained.

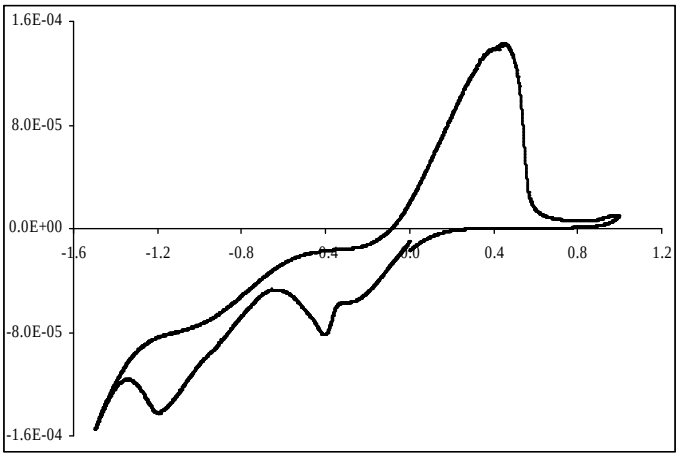

Figure 4.54 Cylic voltammogram of **Complex 5**

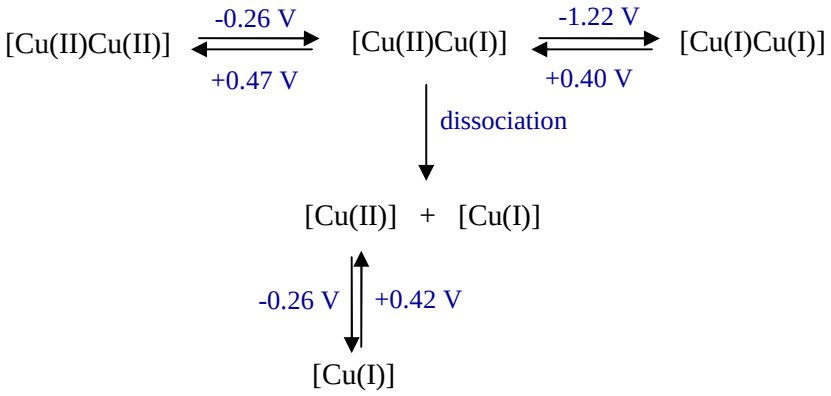

Scheme 4.11 Electrochemical processes for **Complex 5**

4.2.2 One-pot synthesis of $[Cu_2(p\text{-}H_3NC_6H_4COO)(CH_3(CH_2)_{14}COO)_3]Cl$

The reaction between $CuCl_2$, p-$H_2NC_6H_4COOH$ and $CH_3(CH_2)_{14}COOH$ (mole ratio = 2:1:3) was fast, facile, and proceeded as expected according to **Scheme 4.6**. Similarly, the reaction involved self-assembly between Cu^{2+} ion with those of p-$H_2NC_6H_4COO^-$ and $CH_3(CH_2)_{14}COO^-$ ions generated *in-situ* by NH_3. The product obtained was a fine light blue powder, soluble in a mixture of CH_3OH-CH_3COOH (95:5), but insoluble in water and almost all other common organic solvents.

i. Structural elucidation

Based on the following analytical results, the proposed structural formula of the complex formed is $[Cu_2(p\text{-}H_2NC_6H_4COO)_2(CH_3(CH_2)_{14}COO)_2(CH_3CH_2OH)(H_2O)]$. The complex formed is very similar to **Complex 3** $[Cu_2(p\text{-}H_2NC_6H_4COO)_2(CH_3(CH_2)_{14}COO)_2(H_2O)_2]$ **(Section 4.1.2.a),** the only difference being only in the solvate molecules..

The results of **elemental analyses** (C, 59.70%; H, 9.69%; N, 2.53%) are in good agreement with the calculated values for $Cu_2C_{46}H_{78}N_2O_8$ (C, 59.17%; H, 8.48%; N, 2.88%). Its **FTIR** (**Figure 4.55)** and UV-vis spectrum (solution) (**Figure 4.56)** and are

very similar to that of $[Cu_2(p\text{-}H_2NC_6H_4COO)_2(CH_3(CH_2)_{14}COO)_2(H_2O)_2]$, **Complex 3 (Figure 4.28 and 4.31)** respectively.

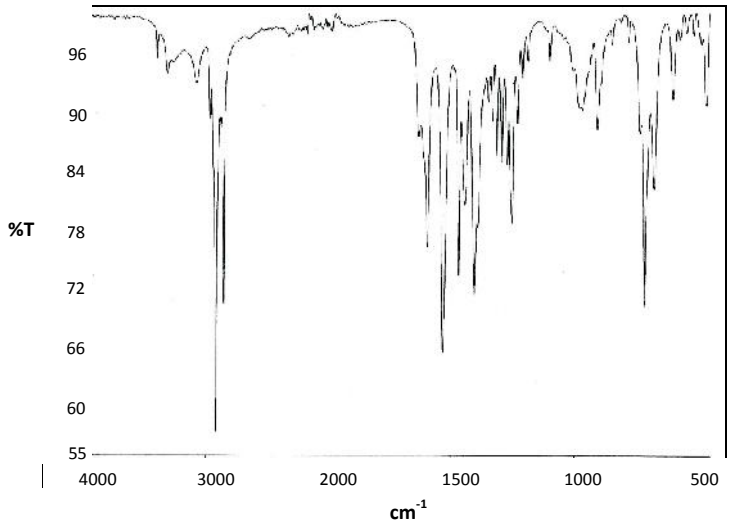

Figure 4.55 The FTIR spectrum

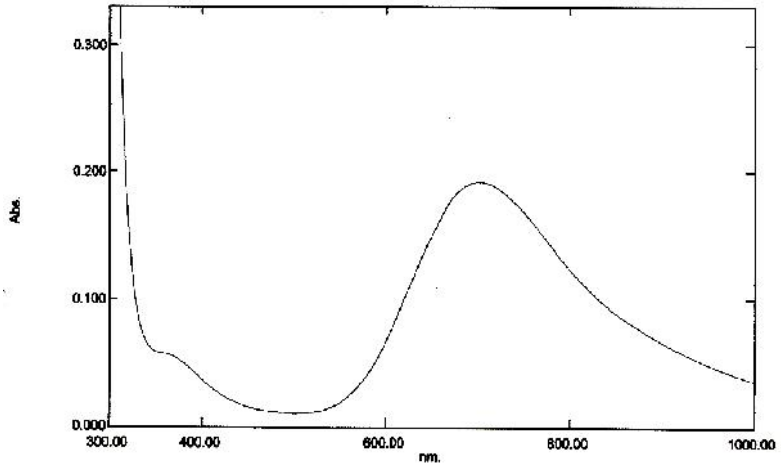

Figure 4.56 The UV-vis spectrum (solution)

To summarise, $K[Cu_2(p\text{-}OC_6H_4COO)(CH_3(CH_2)_{14}COO)_3]$ (anionic copper(II) mixed carboxylates) and $[Cu_2(p\text{-}HOC_6H_4COO)(CH_3(CH_2)_{14}COO)_3]$ were successfully prepared using the one-pot and ligand-exchange reactions, respectively. However, $[Cu_2(p\text{-}H_3NC_6H_4COO)(CH_3(CH_2)_{14}COO)_3]Cl$ (cationic copper(II) mixed carboxylates) was unsuccessfully prepared using the one-pot reaction.

4.3 LOW SYMMETRY COPPER(II) MIXED CARBOXYLATES WITH SHORTER ALKYL CHAINS

The main objective of this part of the research was to prepare complexes with melting points lower than $[Cu_2(p\text{-}HOC_6H_4COO)(CH_3(CH_2)_{14}COO)_3]$ (**Section 4.2**). The complexes chosen have the general formula $[Cu_2(p\text{-}HOC_6H_4COO)(CH_3(CH_2)_nCOO)_3]$ (n = 10, 8, 6), and the synthetic method used was ligand exchange. The reactions were expected to proceed according to **Scheme 4.3,** where the ratio of aromatic to aliphatic ligands was changed from 2:2 to 1:3. All complexes were analysed as previously discussed.

4.3.1 $[Cu_2(p\text{-}HOC_6H_4COO)(CH_3(CH_2)_{10}COO)_3]$

a) Synthesis and structural elucidation

The ligand-exchange reaction involved reacting $[Cu_2(p\text{-}HOC_6H_4COO)_4]$ (**Section 4.1.1)** with $[Cu_2(CH_3(CH_2)_{10}COO)_4]$. The latter complex was obtained as a greenish blue powder from the reaction of $CuCl_2$ with $CH_3(CH_2)_{10}COONa$. The results of the **elemental analyses** (C, 58.93%; H, 9.88%) are in good agreement with the calculated values for $Cu_2C_{48}H_{98}O_{11}$ (C, 58.93%; H, 10.10%).

Its **FTIR spectrum** (**Figure 4.57)** shows the presence of all of the functional groups expected to be present, as previously discussed. The Δ_{OCO} value of 144 cm^{-1} suggests a bridging carboxylate group.

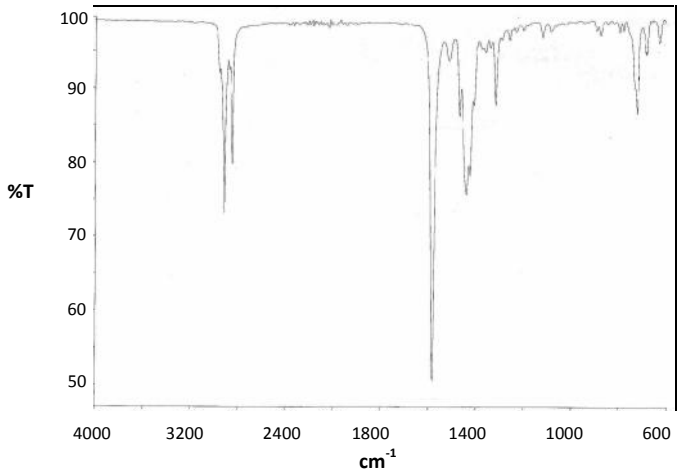

Figure 4.57 FTIR spectrum of $[Cu_2(CH_3(CH_2)_{10}COO_4]$

Its **UV-vis spectrum** in the solid state (**Figure 4.58)** shows a broad *d-d* band at 708 nm and a distinct shoulder on the charge-transfer band at 383 nm. These suggest a square pyramidal binuclear Cu(II) complex.

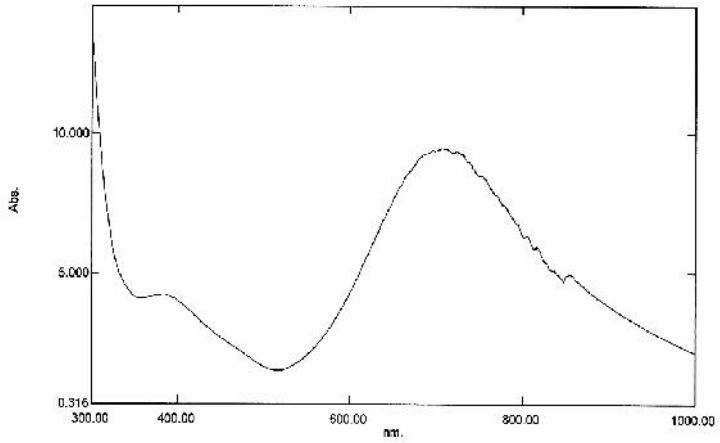

Figure 4.58 UV-visible spectrum of $[Cu_2(CH_3(CH_2)_{10}COO)_4]$ (solid)

Hence, the proposed structural formula of the complex is $[Cu_2(CH_3(CH_2)_{10}COO)_4].3H_2O$; (formula mass, 978.4 g mol^{-1}) which is similar to that proposed for $[Cu_2(CH_3(CH_2)_{14}COO)_4]$ (**Figure 4.15; Section 4.1.1).** Thus, its percentage yield is 90.8 %.

The product obtained from the above reaction was a greenish blue powder (**Complex 6**), soluble in a mixture of CH_3OH-CH_3COOH (95:5) and CH_3OH-THF (1:1), but insoluble in H_2O and almost all other common organic solvents.

Based on the following analytical results, its proposed structural formula is $[Cu_2(p\text{-}HOC_6H_4COO)(CH_3(CH_2)_{10}COO)_3].H_2O$ (formula mass, 880.1 g mol^{-1}). This is similar to that proposed for $[Cu_2(p\text{-}HOC_6H_4COO)(CH_3(CH_2)_{14}COO)_3(CH_3CH_2OH)_2]$ (**Complex 5**; n = 14; **Figure 4.46**; **Section 4.2.1**). Thus, its yield was 82.0 %.

The results of the **elemental analyses** (C, 58.78 % and H, 9.28%) are in good agreement with the calculated values for $Cu_2C_{43}H_{76}O_{10}$ (C, 58.68% and H, 8.70%).

Its **FTIR spectrum** (**Figure 4.59)** is distinctly different from its starting complexes (**Figure 4.13) and** (**Figure 4.57**), and shows the presence of all of the

expected functional groups, as discussed previously. The Δ_{OCO} value of 160 cm^{-1} suggests bridging carboxylate groups.

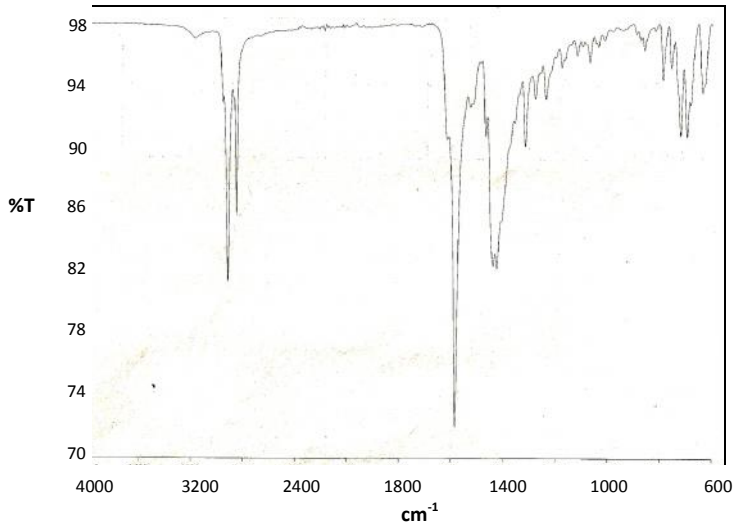

Figure 4.59 FTIR spectrum of **Complex 6**

Its **UV-vis spectrum** in the solid state **(Figure 4.60)** shows a broad *d-d* band at 676 nm and a distinct shoulder on the charge-transfer band at 380 nm. These suggest a square planar binuclear Cu(II) complex

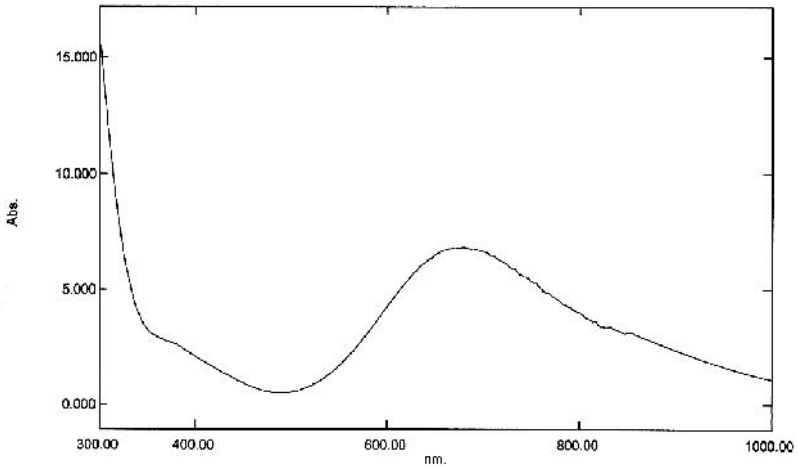

Figure 4.60 UV-vis spectrum of **Complex 6** (solid)

The **UV-vis spectrum** in solution (**Figure 4.61)** shows a broad *d-d* band at 701 nm (ε_{max} = 213 $M^{-1}cm^{-1}$) and a distinct shoulder on the charge-transfer band at 365 nm (ε = 56 $M^{-1}cm^{-1}$). These indicate that its binuclear square planar structure was maintained in solution.

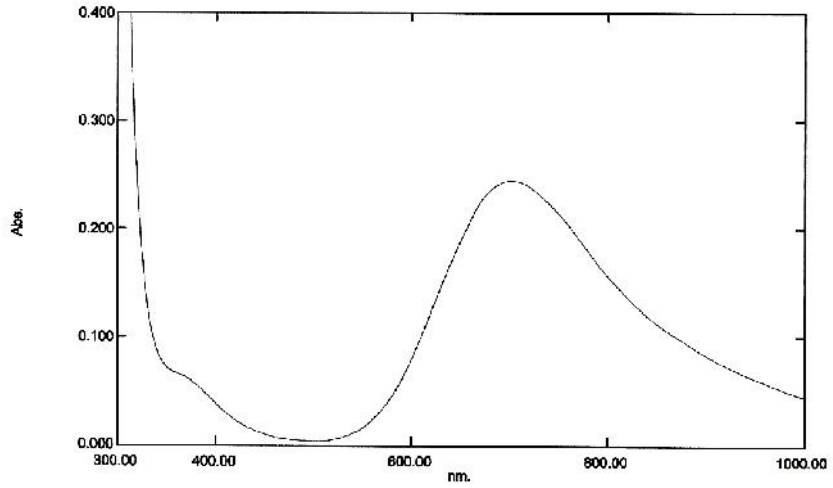

Figure 4.61 UV-vis spectrum of **Complex 6** (solution)

b) Thermal and mesogenic properties

The thermogram **(Figure 4.62)** shows that **Complex 6** (n = 10) is thermally stable up to 207^{o}C, which is lower than **Complex 5** (n = 14; T_{dec} = 241^{o}C). The results seem to suggest that the complex with a shorter chain alkylcarboxylate ligand has a lower thermal stability.

The thermogram also shows a gradual weight loss of 3.1% at about 100^{o}C, assigned to the evaporation of H_2O solvate (expected, 2.1%). The complex then decomposed by a two-stage process with total weight loss of 81.8%, assigned to the decomposition of carboxylate ligands to CO_2 and other volatiles (expected, 83.5%).

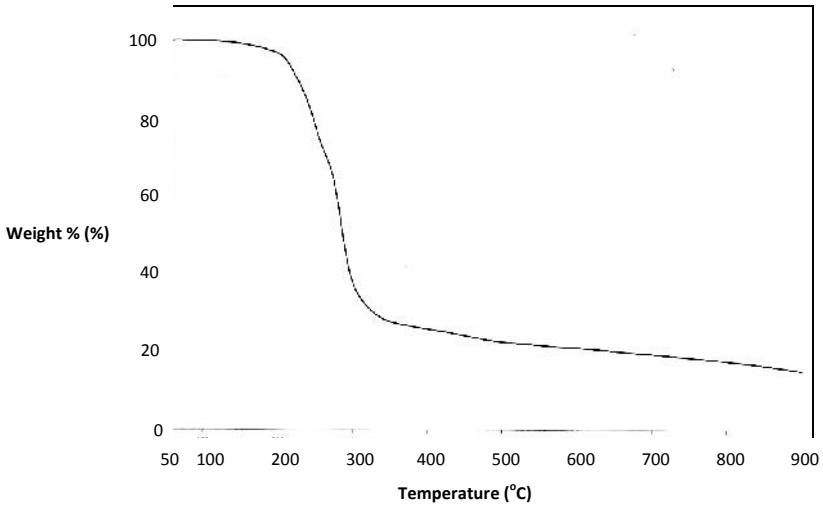

Figure 4.62 Thermogram of **Complex 6**

The amount of residue at temperatures above 800^{o}C cannot be deduced from the thermogram as there is no plateau in the thermogram. Hence, the formula mass of **Complex 6** cannot be estimated as previously done using the gravimetry.

The development of optical structure of **Complex 6** on heating is illustrated by the sequence of OPM photographs as shown in **Figure 4.63.** The complex was a greenish blue powder before heating, and started to melt and clear at about 107^{o}C and 152^{o}C **(Figure 4.63 (a) and (b))** respectively.

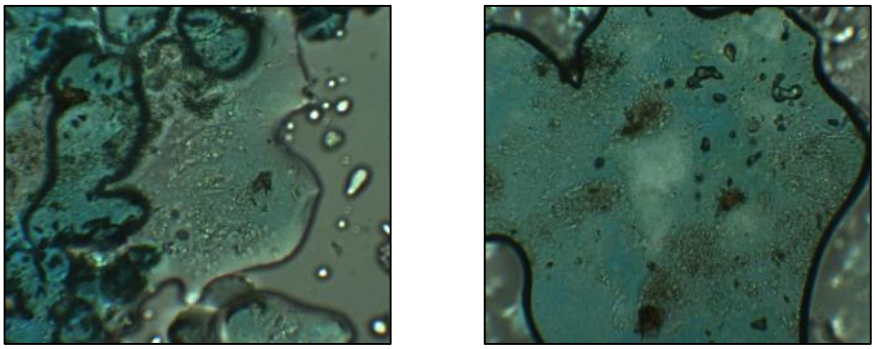

(a) (b)

Figure 4.63 Optical structure of **Complex 6** on heating at (a) 107^{o}C; and (b) 152^{o}C.

On cooling from the isotropic liquid phase, birefringence was observed at 78^{o}C **(Figure 4.64 (b)**. This suggests metallomesogenic properties. However, the type of the mesophase cannot be deduced with certainty from OPM.

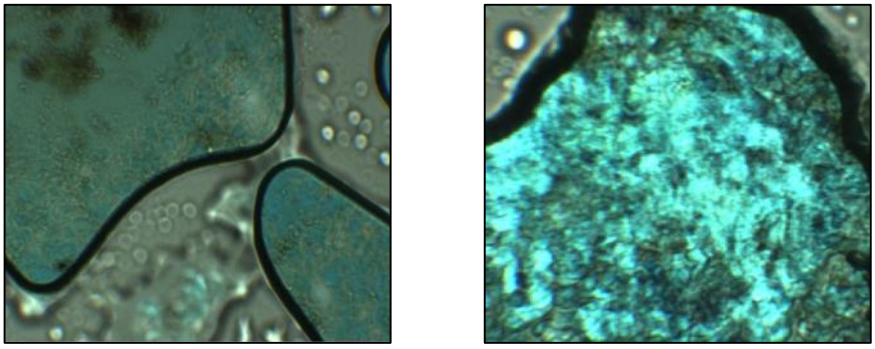

(a) (b)

Figure 4.64 Optical structure of **Complex 6** on cooling at (a) 161^{o}C; and (b) 78^{o}C

The **DSC** (**Figure 4.65)** shows several overlapping endotherms. The assignments of these endotherms are given in **Table 4.14**.

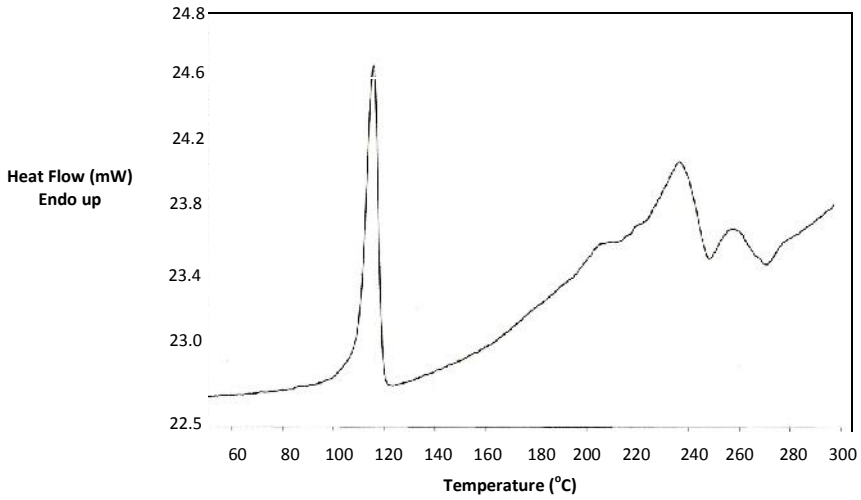

Figure 4.65 DSC curve of **Complex 6**

It is to be noted that **Complex 6** (n = 10) melted at a higher temperature (107^{o}C) compared to **Complex 5** (n = 14; $T_{melting}$ = 96^{o}C).

Table 4.14 DSC data and assignment for **Complex 6**

Temperature (^{o}C)	**ΔH (kJ mol^{-1})**	**Assignment**
115 (peak)	+39	Concurrent evaporation of H_2O solvate and melting
~ 140 (onset)	--	Clearing
200 (onset) 258 (peak)	+28	Decomposition of $CH_3(CH_2)_{10}COO$ and *p*-HOC_6H_4COO ligands #

-- Cannot be determined accurately; * T_{clear} = 152^{o}C from OPM; and #T_{decom} = 207^{o}C from TGA

c) Magnetic properties

The value of μ_{eff} , calculated for **Complex 6** using the tabulated data (**Table 4.15**) as previously discussed, is 2.02 B.M. at 298K. The corresponding -2J value is 294 cm^{-1}. The results indicate strong antiferromagnetic interactions between the two Cu(II) centres.

Table 4.15 The χ values for **Complex 6** used for the calculation of μ_{eff}

χ	value
χ_g	1.56×10^{-6} $cm^3 g^{-1}$
χ_m	137.30×10^{-5} $cm^3 mol^{-1}$
χ_{dia}	-45.61×10^{-5} $cm^3 mol^{-1}$
χ_m^{corr}	182.91×10^{-5} 5 $cm^3 mol^{-1}$

It is noted that **Complex 6** (n = 10) has similar magnetic interaction with that of **Complex 5** (n = 14; μ_{eff} = 1.87 B.M.; -2J = 346 cm^{-1}). From the results, it may be suggested that further reduction in the length of the alkyl chain has insignificant effect on the magnetic properties of such complexes.

d) Redox properties

The cyclic voltammogram for **Complex 6** was similarly recorded as for the other complexes (**Figure 4.66)**. It shows three cathodic peaks at -0.13, -0.26 and -0.84 V, two broad overlapping anodic peaks at +0.16 and +0.22 V, and a small anodic peak at +1.03 V. The electrochemical processes (**Scheme 4.12 ;** ΔE = 1160 mV, 1060 mV and 420 mV) are similar to those of previous complexes, and may be similarly explained.

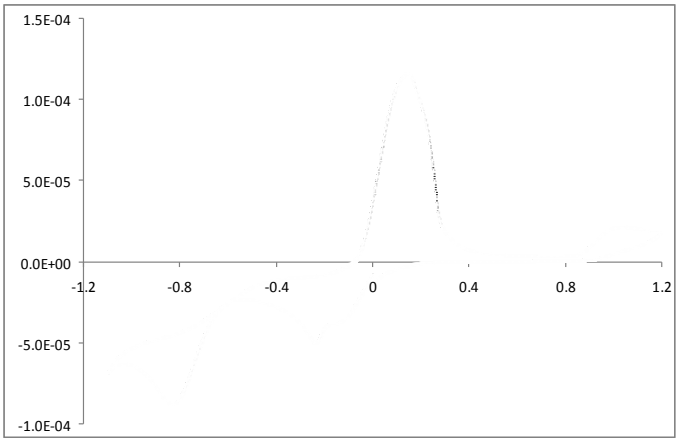

Figure 4.66 Cyclic Voltammogram of **Complex 6**

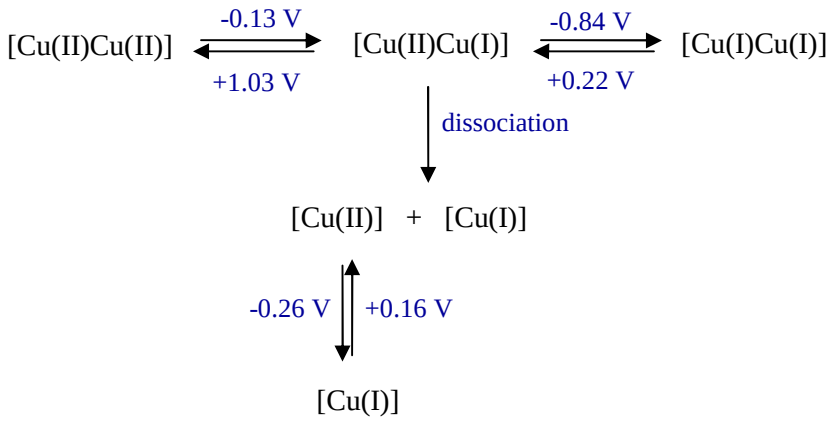

Scheme 4.12 Electrochemical processes for **Complex 6**

It is interesting to note that the initial reduction process of **Complex 6** (n = 10; -0.13 V) occurred at a lower potential compared to that of **Complex 5** (n = 14; -0.26 V). This indicates a more distorted geometry at Cu(II) in the former complex, possibly arising from the weaker $CH_3(CH_2)_{10}COO$-Cu coordinate bond, as suggested from the magnetic result.

4.3.2 [Cu_2(p-HOC_6H_4COO)($CH_3(CH_2)_8COO$)$_3$]

a) Synthesis and structural elucidation

[Cu_2(p-HOC_6H_4COO)($CH_3(CH_2)_8COO$)$_3$] (n = 8; **Complex 7**) was similarly synthesised as for **Complex 6** (n = 10), using [Cu_2(p-HOC_6H_4COO)$_4$] (**Section 4.1.1**) and [$Cu_2(CH_3(CH_2)_8COO)_4$] (formula mass, 812.1 g mol^{-1}; yield 99.3 %).

The structural formula of the latter complex (starting material, greenish blue powder) agrees with the results of **elemental analyses** (found: C, 58.59%; H, 9.69%; calculated for $Cu_2C_{40}H_{76}O_8$: C, 59.16%; H, 9.43%); **FTIR** (**Figure 4.67**; Δ_{OCO} = 157 cm^{-1}), and UV-vis (**Figure 4.68**; λ_{max} = 700 nm, 373 nm (shoulder)).

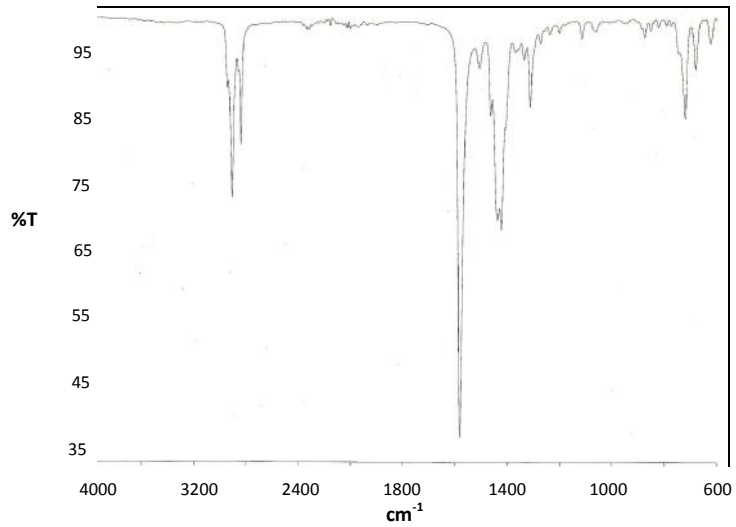

Figure 4.67 FTIR spectrum of $[Cu_2(CH_3(CH_2)_8COO)_4]$

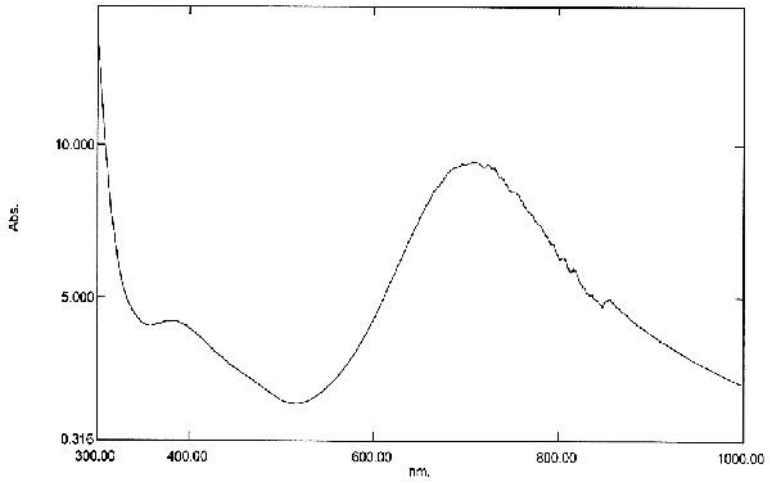

Figure 4.68 UV-visible spectrum of $[Cu_2(CH_3(CH_2)_8COO)_4]$ **(**solid)

Its structure was confirmed when peacock-blue crystals formed in CH_3OH: THF (1:1) after a week standing at room temperature. The crystal with dimensions 0.20 x 0.08 x 0.05 mm) was solved by direct methods and refined by full matrix least square in F^2 in the centrosymmetric space group P-1. The ORTEP presentation and the packing pattern of the crystals is shown in **Figure 4.69** and **4.70** respectively, and the data is shown as **Appendix 7.**

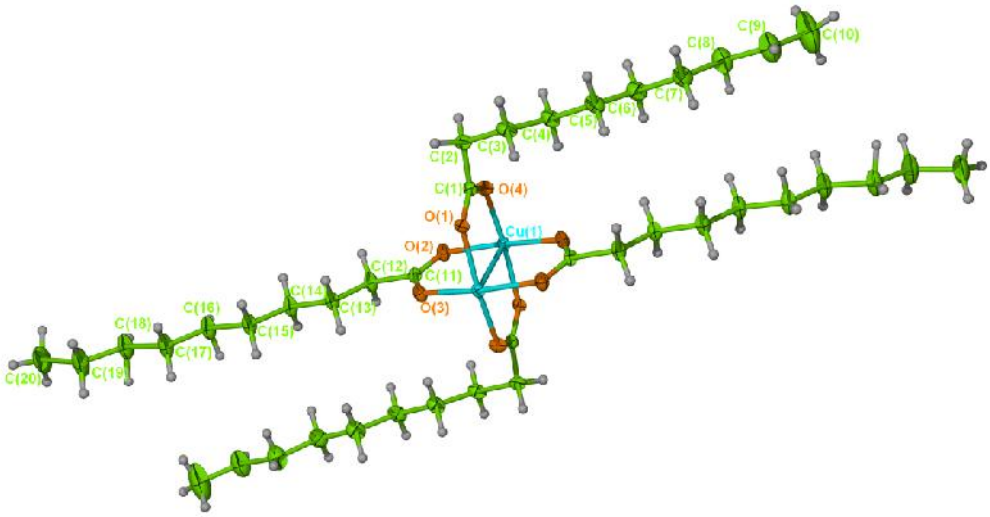

Figure 4.69 An ORTEP presentation of $[Cu_2(CH_3(CH_2)_8COO)_4]$

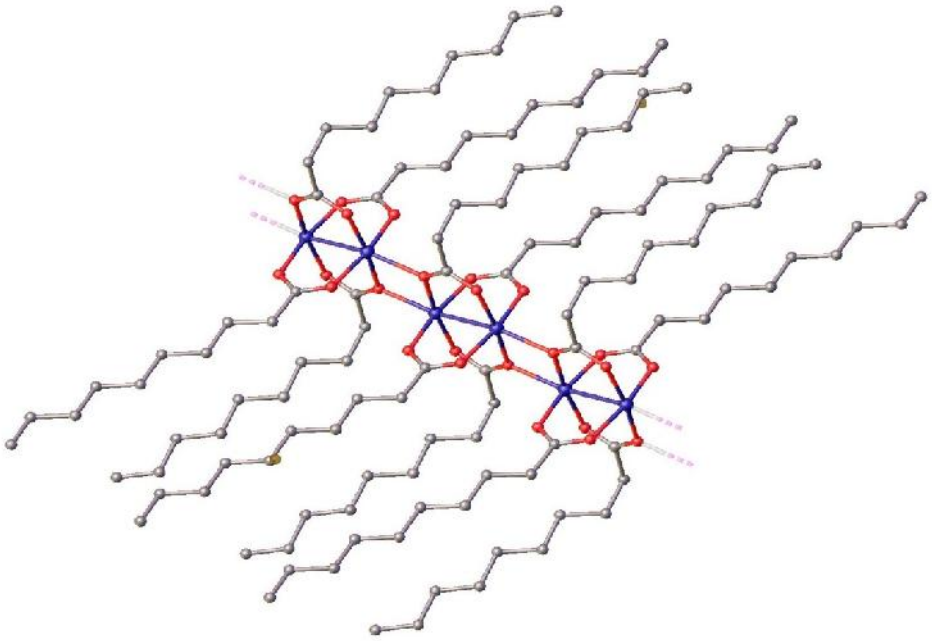

Figure 4.70 The packing pattern of the peacock-blue crystal of $[Cu_2(CH_3(CH_2)_8COO)_4]$

The FTIR spectrum of the crystal (**Figure 4.71)** shows the presence of all of the expected functional groups as previously discussed, and Δ_{OCO} value is 174 cm^{-1}. The spectrum is similar to that of greenish blue powder.

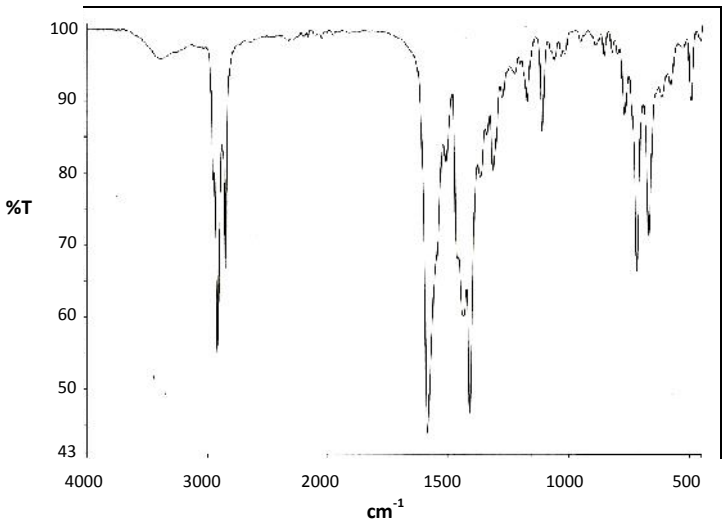

Figure 4.71 FTIR of peacock-blue crystals

The product obtained from the above reaction was a blue powder (**Complex 7**; *n* = 8). Its solubility was similar to that of **Complex 6** (*n* = 10).

Based on the results of **elemental analyses** (found: C, 56.91%; H, 8.63%; calculated for $Cu_2C_{39}H_{68}O_{10}$: C, 56.84%; H, 8.32% H), **FTIR** (**Figure 4.72**; Δ_{OCO} = 167 cm^{-1}), and UV-vis (solid: **Figure 4.73**; λ_{max} = 676 nm, 378 nm (shoulder); solution: **Figure 4.74**; λ_{max} = 700 nm (ε_{max}= 218 M^{-1} cm^{-1}), 363 nm (shoulder; ε = 55 M^{-1} cm^{-1}). Its proposed structural formula, $[Cu_2(p\text{-}HOC_6H_4COO)(CH_3(CH_2)_8COO)_3].CH_3CH_2OH$, (formula mass, 824.0 g mol^{-1}) is very similar to that of **Complex 6** $[Cu_2(p\text{-}HOC_6H_4COO)(CH_3(CH_2)_{10}COO)_3].H_2O$, the only difference being only in the solvate molecules. Thus, its yield was 81.9 %.

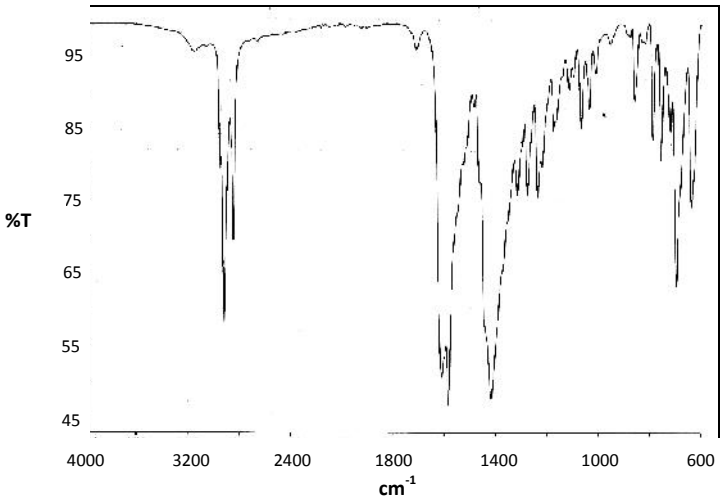

Figure 4.72 FTIR spectrum of **Complex 7**

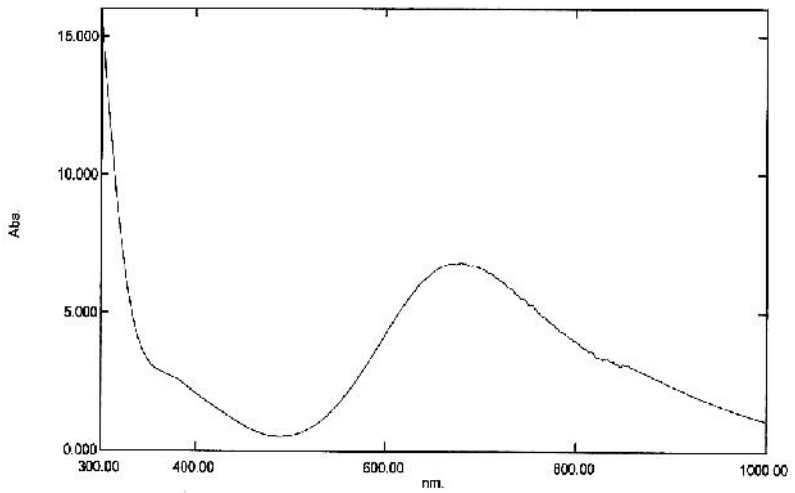

Figure 4.73 UV-vis spectrum of **Complex 7** (solid)

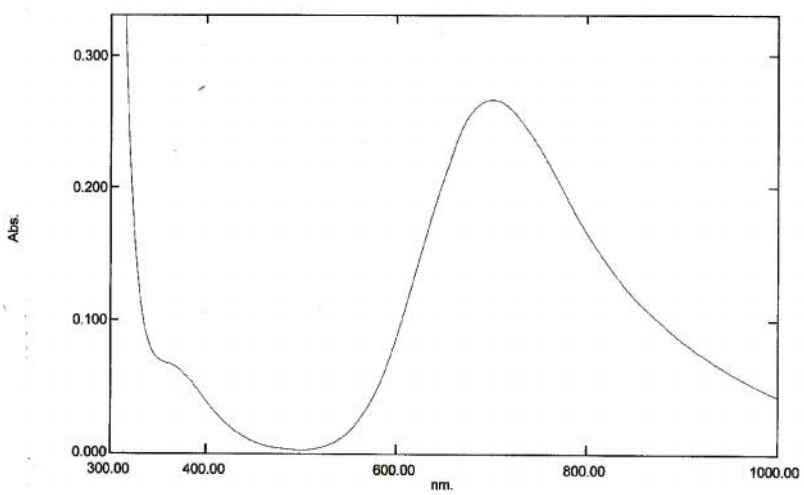

Figure 4.74 UV-vis spectrum of **Complex 7** (solution)

b) Thermal and metallomesogenic properties

The thermogram (**Figure 4.75**) shows that **Complex 7** (n = 8) was thermally stable up to 201^{o}C. This is similar to that of **Complex 6** (n = 10; T_{dec} = 207^{o}C). The results seem to suggest that further reduction in the alkyl chain length has insignificant effect on the thermal stability of such complexes.

The thermogram also shows a weight loss of 5.1% at 80^{o}C, assigned to the evaporation of CH_3CH_2OH molecule (expected 5.6%). The complex then decomposed by a two-stage process, with a total weight loss of 73.4%, assigned to the decomposition of the carboxylate ligands to CO_2 and other volatiles (expected 79.0%).

The amount of residue at temperatures above 600^{o}C is 21.1%. Assuming that it was CuO, the estimated formula mass for the complex, calculated as previously done using the gravimetry concept, is 757 g mol^{-1} (expected, 824 g mol^{-1}). Thus, the results from TGA and elemental analyses are fairly in good agreement, and lend further support for the proposed structural formula.

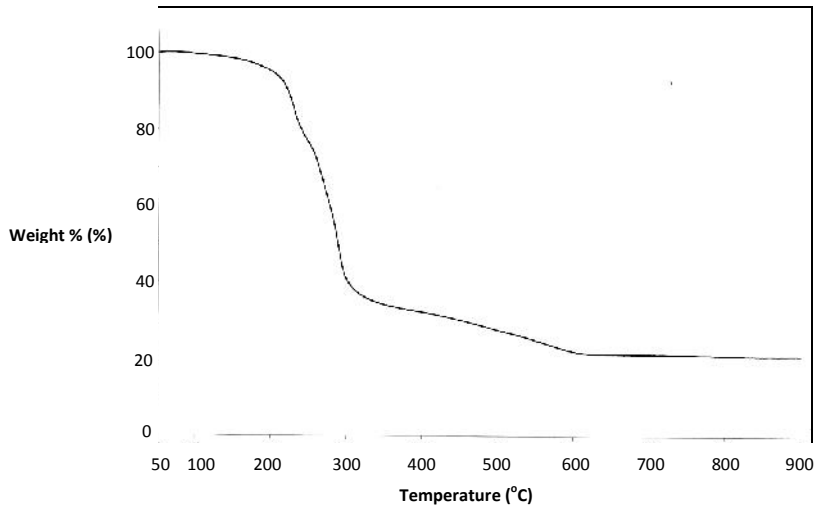

Figure 4.75 Thermogram of **Complex 7**

The development of optical structure of **Complex 7** (n=8) on heating is illustrated by the sequence of photographs shown in **Figure 4.76**. The complex was a bluish green powder before heating, and started to melt and then to clear at around 155^{o}C and 220^{o}C respectively.

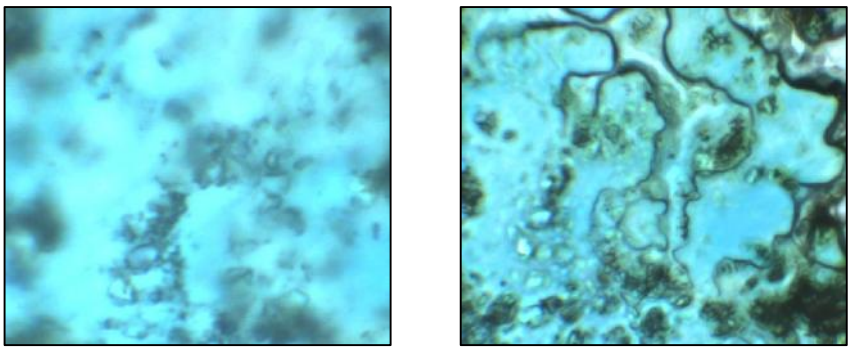

(a) (b)

Figure 4.76 Optical structure of **Complex 6** on heating at (a) 110^{o}C; and (b) 145^{o}C

On cooling from the isotropic liquid phase, birefringence was initially observed at 70^{o}C (**Figure 4.77 (a))** with layered structure**.** Upon further cooling to room temperature, the birefringence became stronger and remain unchanged. This suggests metallomesogenic properties. However, the type of the mesophase cannot be deduced with certainty from OPM.

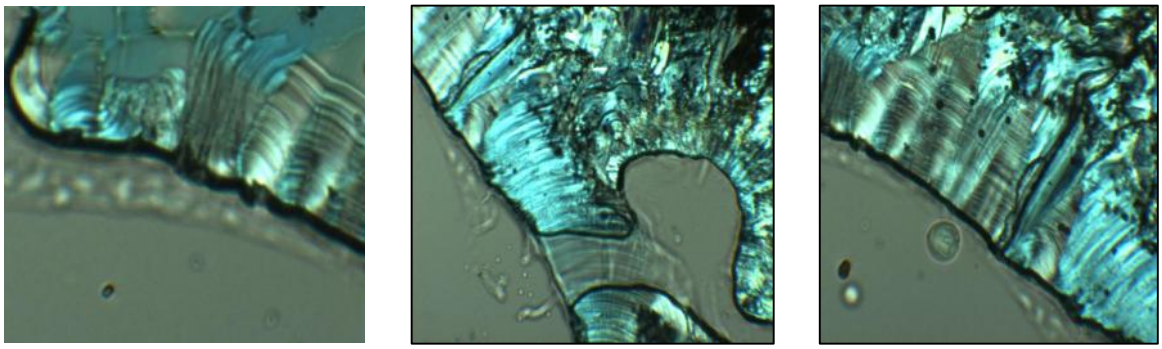

(a) (b) (c)

Figure 4.77 Optical structure of **Complex 7** on cooling at: (a) 70^{o}C; (b) 51^{o}C and (c) 31^{o}C

The **DSC curve** of the complex (**Figure 4.78**) shows several overlapping endotherms. The assignments of these endotherms are given in **Table 4.16**.

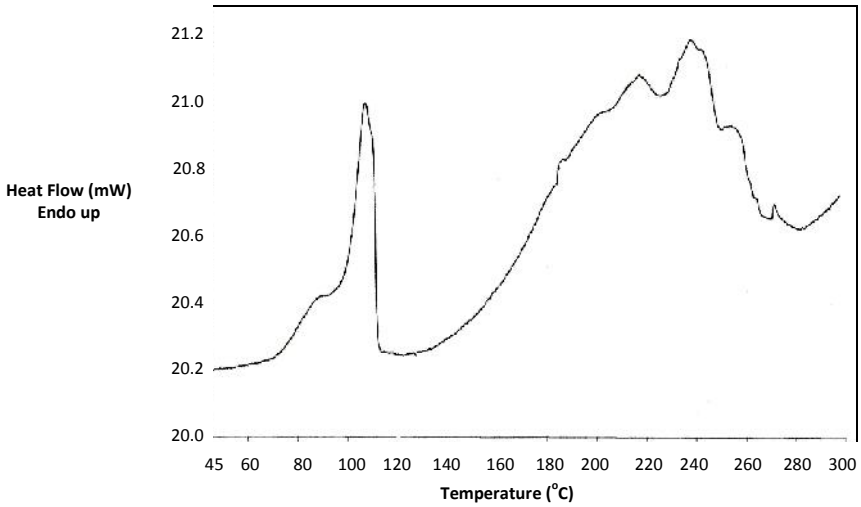

Figure 4.78 DSC curve of **Complex 7**

Table 4.16 DSC data and assignment for **Complex 7**

Temperature (^oC)	**ΔH (kJ mol^{-1})**	**Assignment**
107 (peak)	+33	Concurrent evaporation of CH_3CH_2OH and melting of **Complex 7**
140 (onset)	--	Clearing
216 (peak) 236 (peak)	+28	Decomposition of $CH_3(CH_2)_8COO$ and *p*-HOC_6H_4COO ligands#

-- cannot be determined accurately; * T_{clear} = 145^{o}C from OPM; and $^{\#}T_{dec}$ = 201^{o}C from TGA

It is interesting to note the following trend in the melting temperatures: **Complex 5** (*n* = 14; $T_{melting}$ = 96^{o}C), < **Complex 6** (*n* = 10; $T_{melting}$ = 115^{o}C) > **Complex 7** (*n* = 8; $T_{melting}$ = 107^{o}C) (**Figure 4.79**). As these complexes have almost similar structures, it may be suggested that the turning point in the melting temperatures of such complexes may occur at *n* = 10.

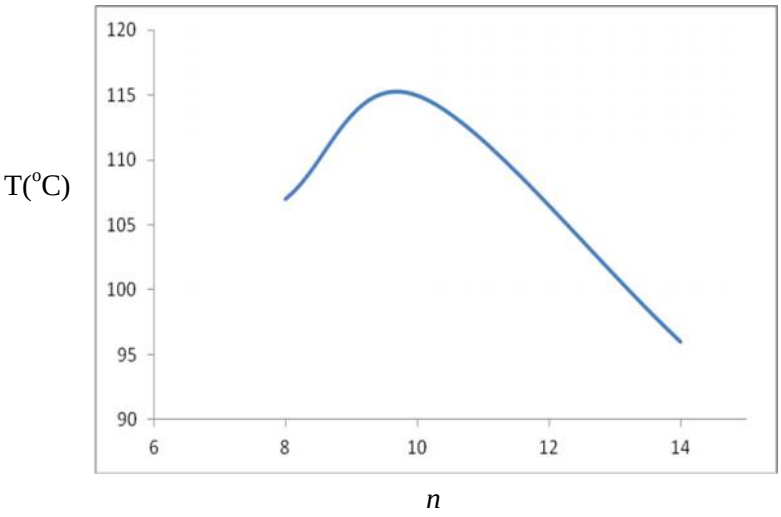

Figure 4.79 Plot of melting temperature *vs*. *n* for $[Cu_2(p\text{-}HOC_6H_4COO)(CH_3(CH_2)_nCOO)_3]$

c) Magnetic property

The value of μ_{eff} for **Complex 7** (*n* = 8)**,** calculated using the tabulated data (**Table 4.17**) as before, is 1.89 B.M. at 298 K, and the corresponding -2J value is 337 cm^{-1}. The results indicate strong antiferromagnetic interactions between the two Cu(II) centres. It

is noted that the magnetic interaction is similar with **Complex 6,** (n = 10; μ_{eff} = 2.02 B.M.; -2J = 294 cm^{-1}), and may be similarly explained. From the results, it may be suggested that further reduction in the length of the alkyl chain has insignificant effect on the magnetic properties of such complexes, as stated previously.

Table 4.17 The χ values used to calculate μ_{eff} for **Complex 7**

χ	**Values**
χ_g	1.48 x 10^{-6} cm^3g^{-1}
χ_m	121.95 x 10^{-5} cm^3mol^{-1}
χ_{dia}	-40.57 x 10^{-5} cm^3mol^{-1}
χ_m^{corr}	162.52 x 10^{-5} cm^3mol^{-1}

c) Redox property

The CV for **Complex 7** was similarly recorded as for the other complexes (**Figure 4.80)**. It shows three cathodic peaks at -0.13, -0.27 and -0.83 V, two broad overlapping anodic peaks at +0.15 and +0.26 V, and a small anodic peak at +1.05 V. The electrochemical processes (**Scheme 4.13 ;** ΔE = 1180 mV, 1090 mV and 420 mV) are similar to those of previous complexes, and may be similarly explained.

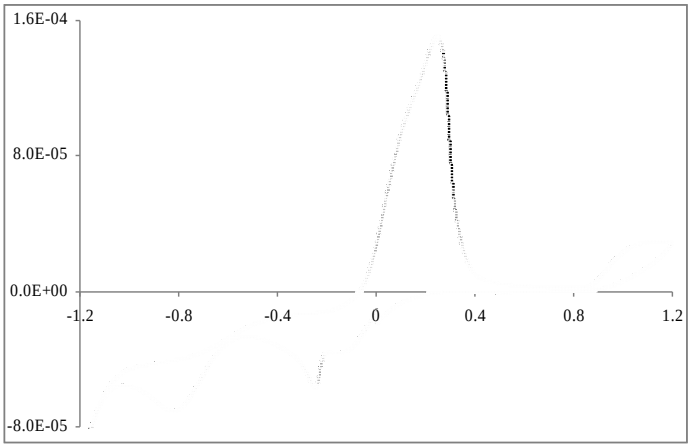

Figure 4.80 Cyclic voltammogram of **Complex 7**

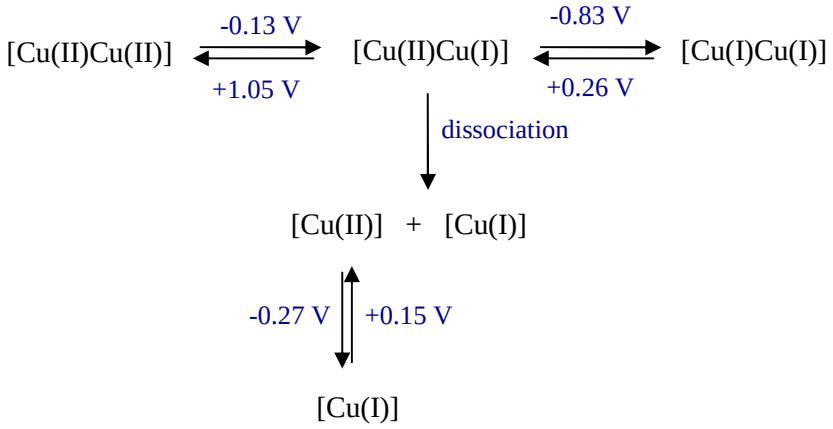

Scheme 4.13 Electrochemical processes for **Complex 7**

It is important to note that the initial reduction process of **Complex 7** (n = 8; -0.13 V) occurs at the same potential as that of **Complex 7** (n = 10; -0.13 V). These further support the similarity in their structures, as suggested above.

4.3.3 [Cu_2(p-HOC_6H_4COO)($CH_3(CH_2)_6COO)_3$]

The complex, [Cu_2(p-HOC_6H_4COO)($CH_3(CH_2)_6COO)_3$] (n = 6; **Complex 8**) was similarly synthesised as for **Complex 7** (n = 8), using [Cu_2(p-$HOC_6H_4COO)_4$] (**Section 4.1.1**) and [$Cu_2(CH_3(CH_2)_6COO)_4(CH_3(CH_2)_6COOH)(CH_3CH_2OH)$] (formula mass 890.2 g mol^{-1}**).** Thus, its percentage yield is 66.7%.

The structural formula of the latter complex (fine blue powder) agrees with the results of **elemental analyses** (found: C, 57.02%; H, 9.24%; calculated for $Cu_2C_{42}H_{82}O_{11}$: (C, 56.67%; H, 9.28%), **FTIR** (**Figure 4.81**; Δ_{OCO} = 169 cm^{-1}), and UV-vis (**Figure 4.82**; λ_{max} = 704 nm (ε_{max}= 255 M^{-1} cm^{-1}); 373 nm (ε = 55 M^{-1} cm^{-1}; shoulder). This is similar to that proposed for [$Cu_2(CH_3(CH_2)_8COO)_4$].CH_3CH_2OH; n = 8; **Section 4.3.2**).

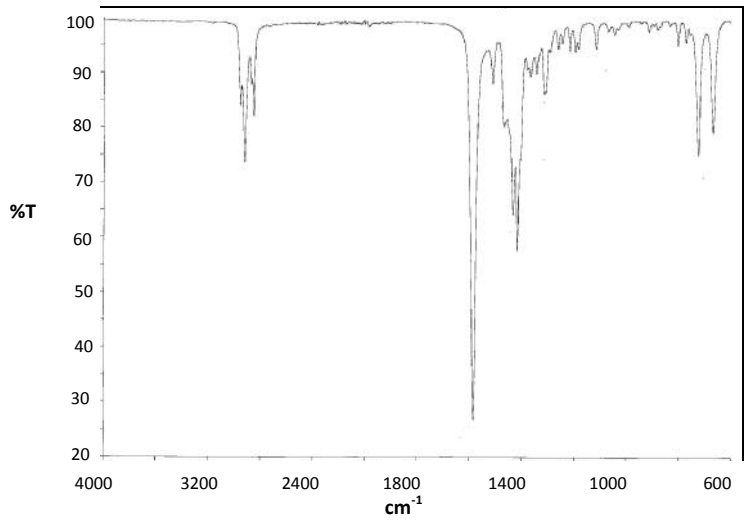

Figure 4.81 FTIR spectrum of $[Cu_2(CH_3(CH_2)_6COO)_4]$

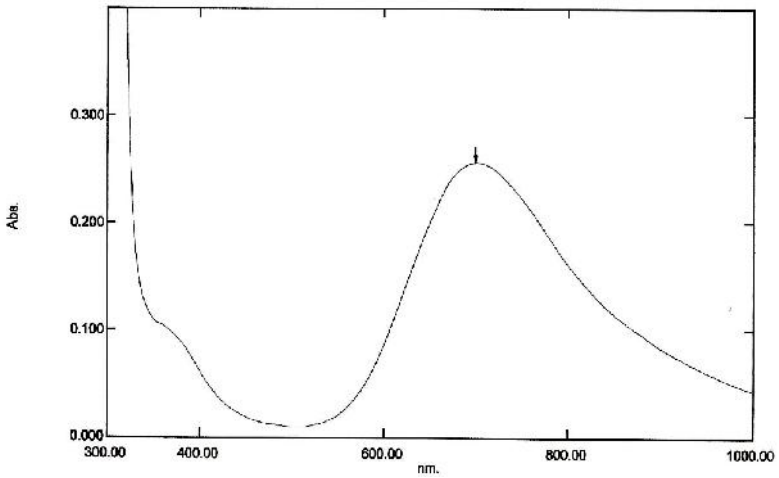

Figure 4.82 UV-visible spectrum of $[Cu_2(CH_3(CH_2)_6COO)_4]$ in solution

Its structure was confirmed when peacock-blue crystals formed in CH_3OH: THF (1:1) after a week standing at room temperature. a crystal with dimensions 0.26 x 0.20 x 0.10 mm) was solved by direct methods and refined by full matrix least square in F^2 in the centrosymmetric space group P-1. The ORTEP presentation and the packing pattern of the crystal is shown in **Figure 4.83** and **4.84** respectively, and the data is shown as **Appendix 8.**

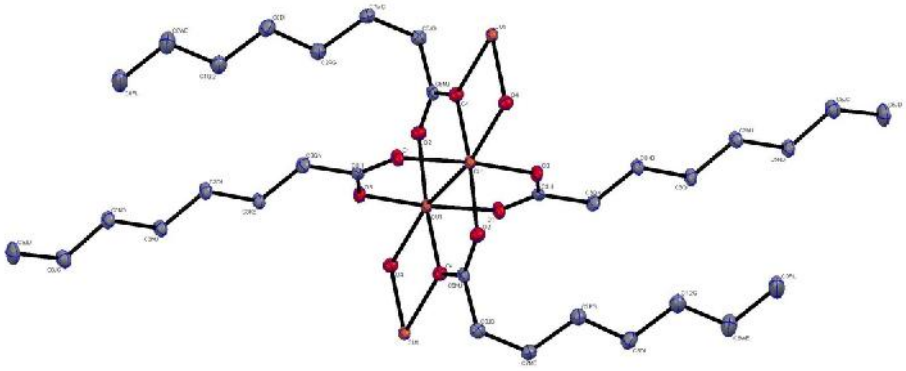

Figure 4.83 An ORTEP presentation of the peacock-blue crystal of $[Cu_2(CH_3(CH_2)_6COO)_4]$

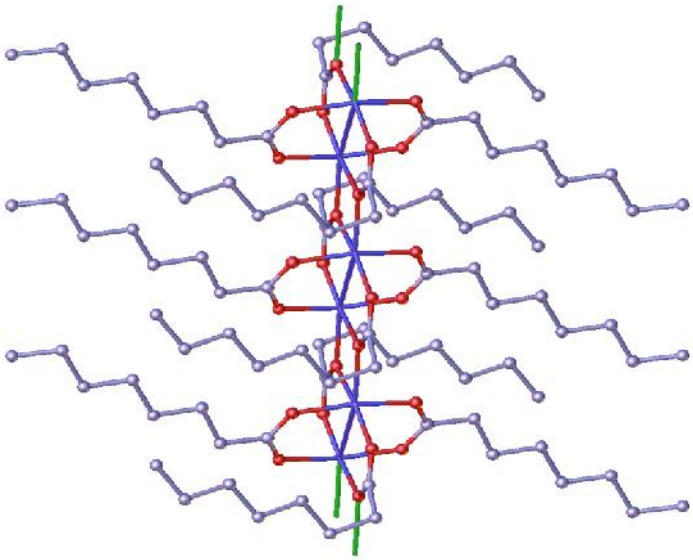

Figure 4.84 The crystal packing of the peacock-blue crystal of $Cu_2(CH_3(CH_2)_6COO)_4]$

The FTIR spectrum of the crystal (**Figure 4.85)** shows the presence of all of the expected functional groups as previously discussed, and Δ_{OCO} value is 174 cm^{-1}. The spectrum is similar to that of greenish blue powder.

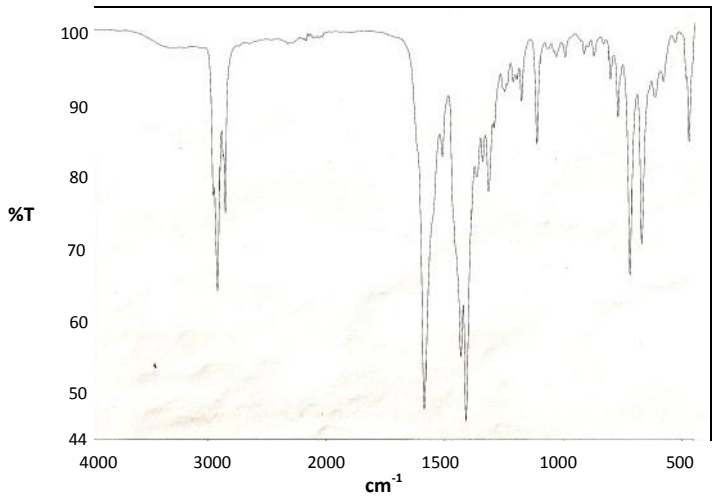

Figure 4.85 FTIR spectrum of single crystal of $[Cu_2(CH_3(CH_2)_6COO)_4]$

The product obtained from the above reaction was a greenish sticky solid (**Complex 8**; $n = 6$). Its solubility was similar to that of **Complex 7** ($n = 8$).

From the results of **elemental analyses** (found: C, 54.06%; H, 9.15%; calculated for $Cu_2C_{41}H_{74}O_{13}$: C, 54.61%; H, 8.21%), **FTIR** spectroscopy (**Figure 4.86**; $\Delta = 175$ cm^{-1}), and **UV-vis** spectroscopy (**Figure 4.87**; 700 nm (ε_{max}= 228 M^{-1} cm^{-1}), 378 nm (ε = 40 $M^{-1}cm^{-1}$), it is proposed that the structural formula for **Complex 8** is $[Cu_2(p\text{-}HOC_6H_4COO)(CH_3(CH_2)_6COO)_3(CH_3(CH_2)_6COOH)(CH_3CH_2OH)].H_2O$ (formula mass, 902.1 $gmol^{-1}$), which is similar to that of **Complex 6** ($[Cu_2(p\text{-}HOC_6H_4COO)(CH_3(CH_2)_{10}COO)_3].H_2O$, the only difference being only in the coordinated and solvated molecules. Thus, its yield was 75.8 %.

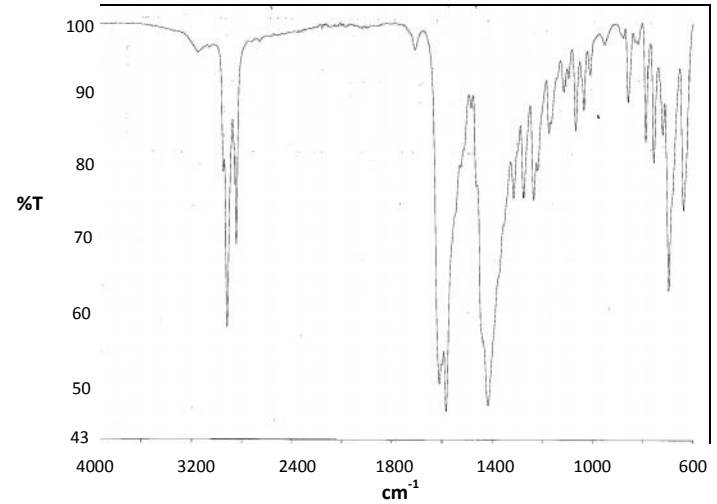

Figure 4.86 FTIR spectrum of **Complex 8**

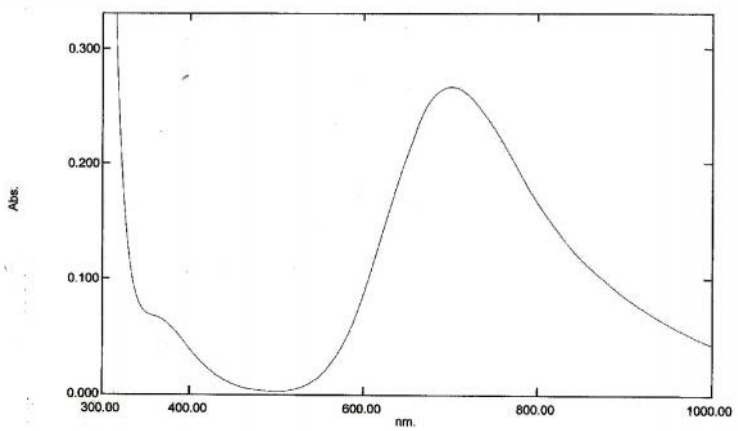

Figure 4.87 UV-vis spectrum of **Complex 8** (solution)

c) Thermal and metallomesogenic properties

The thermogram of **(Figure 4.88)** shows that **Complex 8** is thermally stable up to around 200^{o}C. It also shows a gradual initial weight loss of 6.9% which corresponds to the evaporation of ethanol and water molecules (expected 7.1%). The complex then decomposed by a two-stage process with total weight loss of 75.0% assigned to the decomposition of the carboxylate ligands to CO_2 and other volatiles (expected 78.8%).

The amount of residue at temperatures above 600^{o}C is 18.1%. Assuming that it was CuO, the estimated formula mass of **Complex 8**, calculated as previously done using the gravimetry concept, is 879.5 g mol^{-1} (expected 902.1 g mol^{-1}). Thus, the results from TGA and elemental analyses are in good agreement, and lend further support for the proposed structural formula.

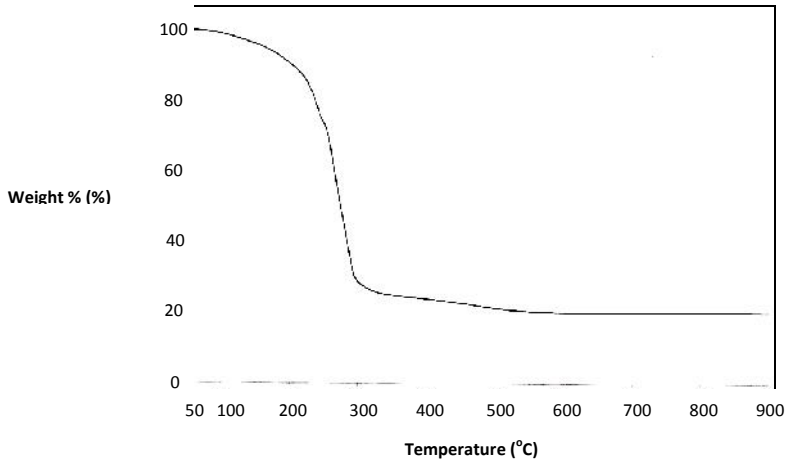

Figure 4.88 Thermogram of **Complex 8**

The development of optical structure of **Complex 8** on heating is illustrated by the sequence of photographs (**Figure 4.89)**. The complex was a greenish sticky solid and was already melted at room temperature. Upon heating, it started to clear to the isotropic liquid phase, at around 50^{o}C.

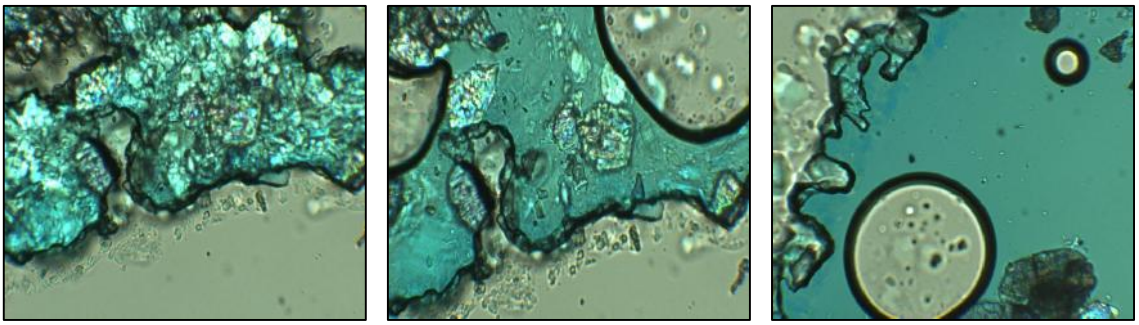

(a) (b) (c)

Figure 4.89 OPM of **Complex 8** on heating: (a) 27^{o}C; (b) 50^{o}C and (c) 101^{o}C

On cooling from an isotropic liquid phase to room temperature, it was observed that a mesophase began to developed at 148^{o}C **(Figure 4.90(a)).** It is observed that on further cooling to room temperature, the mesophase developed into a more ordered mesophase, which accounts for the brighter birefringence **(Figure 4.90 (b) - (d)).** From the optical texture **(Figure 4.90(d))**, the mesophase of the complex may be said to be smectic.

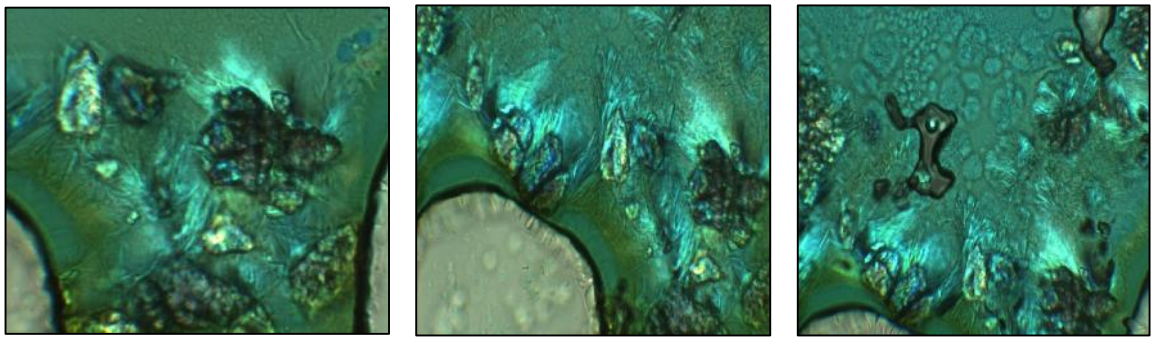

(a) (b) (c)

Figure 4.90 OPM of **Complex 8** on cooling: (a) 148^{o}C; (b) 145^{o}C; (c) 80^{o}C; and (d) 32^{o}C

The **DSC curve** of the complex (**Figure 4.91**) shows several overlapping endotherms. The assignments of these endotherms are given in **Table 4.18.**

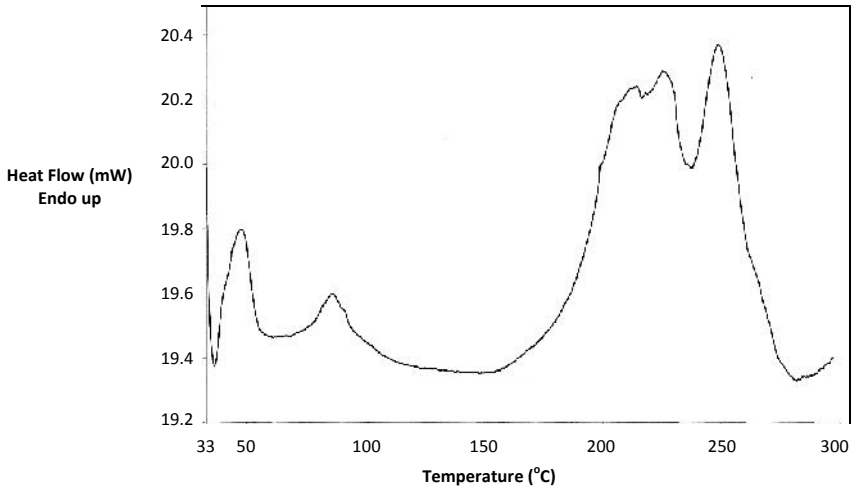

Figure 4.91 DSC curve of **Complex 8**

Table 4.18 DSC data and assignment for **Complex 8**

Peak temperature (°C)	**ΔH (kJ mol^{-1})**	**Assignment**
48	+10	Clearing*
86	+7	Evaporation of CH_3CH_2OH molecules
200 224	--	Decomposition of $CH_3(CH_2)_8COO$ and *p*-HOC_6H_4COO ligands[#]
249	--	Boiling point of $CH_3(CH_2)_6COOH$

-- cannot be determined accurately; * T_{clear} = 50°C (from OPM); and $^{\#}T_{decompose}$ = 200°C from TGA).

However, the melting temperature for **Complex 8** cannot be determine from DSC as it is assumed to be lower than the temperature range of the DSC instrument used. The assumption is justified since the complex was a sticky solid at room temperature (about 27°C).

d) Magnetic properties

Magnetic susceptibility measurement could not be determined as the sample was a semi-solid at room temperature, and thus could not be packed into the tube of the Gouy balance.

e) Redox properties

The CV for **Complex 8** (**Figure 4.92)** was similarly recorded as for the other complexes. It shows three cathodic peaks at -0.12, -0.26 and -0.84 V, two broad overlapping anodic peaks at +0.10 and +0.22 V, and a small anodic peak at +1.05 V. The electrochemical processes (**Scheme 4.14 ;** ΔE = 1170 mV, 1060 mV and 360 mV) are similar to those of previous complexes, and may be similarly explained.

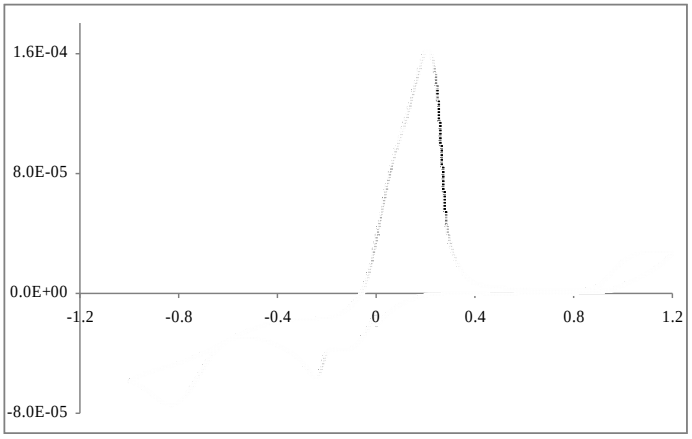

Figure 4.92 Cyclic voltammogram of **Complex 8**

It is important to note that the initial reduction process of **Complex 8** (*n* = 6; -0.12 V) occurs at the same potential as that of **Complex 7** (*n* = 8; -0.13 V). These further support the similarity in their structures, as suggested above.

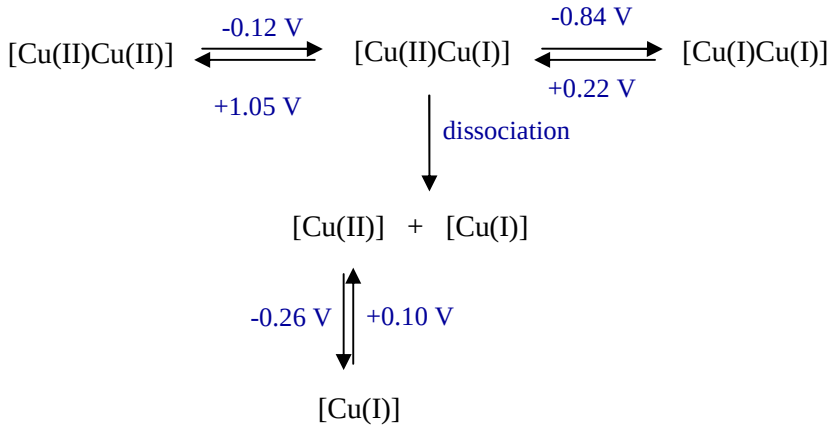

Scheme 4.14 Electrochemical processes for **Complex 8**

4.4 CONVERSION TO IONIC COMPLEX

The final step of the ligand-exchange reaction is the ionisation of the prepared complexes, $[Cu_2(p\text{-}HOC_6H_4COO)_2(CH_3(CH_2)_nCOO)_3]$; where n =14, 10, 8 and 6, to the corresponding ionic complexes, $K[Cu_2(p\text{-}OC_6H_4COO)_2(CH_3(CH_2)_nCOO)_3]$, using one mole equivalent of KOH. The ionisation reaction is expected to proceed according to **Scheme 4.15.**

$$[Cu_2(p\text{-}HOC_6H_4COO)(CH_3(CH_2)_nCOO)_3] \xrightarrow[EtOH,\,\Delta]{KOH} K[Cu_2(p\text{-}OC_6H_4COO)(CH_3(CH_2)_nCOO)_3]$$

Scheme 4.15 Ionisation of $[Cu_2(p\text{-}HOC_6H_4COO)(CH_3(CH_2)_nCOO)_3]$

4.4.1 $K[Cu_2(p\text{-}OC_6H_4COO)(CH_3(CH_2)_{14}COO)_3]$

a) Synthesis and Structural Elucidation

Reaction between $[Cu_2(p\text{-}HOC_6H_4COO)(CH_3(CH_2)_{14}COO)_3]$ (**Complex 5**) and KOH gave a fine grey powder (**Complex 9**). Its solubility is similar to the previously-discussed complexes.

Based on the following analytical results, it is proposed that the chemical formula of the product is $[Cu_2(CH_3(CH_2)_{14}COO)_2(OH)_2(H_2O)_4].2C_2H_5OH$ (formula mass, 836.1 g mol^{-1}; yield 50.7 %). Hence, it was not the intended ionic complex, $K[Cu_2(p\text{-}OC_6H_4COO)(CH_3(CH_2)_{14}COO)_3]$.

The results of CHN **elemental analyses** (C, 51.31%; H, 9.94%) are in good agreement with the calculated values for $Cu_2C_{36}H_{84}O_{12}$ (C, 51.71%; H, 10.13%)

Its **FTIR spectrum** (**Figure 4.93)** is distinctly different from its starting complex **(Figure 4.19)**, indicating a reaction occurred between **Complex 5** and KOH. It shows a very broad peak at 3431 cm^{-1} and two sharp peaks at 2921 cm^{-1} and 2851 cm^{-1}, assigned to the –OH group and the long alkyl chain, respectively. The peak for the aromatic ring, expected at about 1600 cm^{-1}, is not obvious from the spectrum. The peaks for $\nu_{asym}COO$ is at 1561 cm^{-1} and for $\nu_{sym}COO$ are at 1545 cm^{-1} and 1405 cm^{-1}. Hence, Δ values = 156 cm^{-1} and 140 cm^{-1}, suggesting bridging and/or chelating carboxylate groups, and thus a binuclear complex. The simple spectrum further suggests a symmetrical complex (*trans*- isomer).

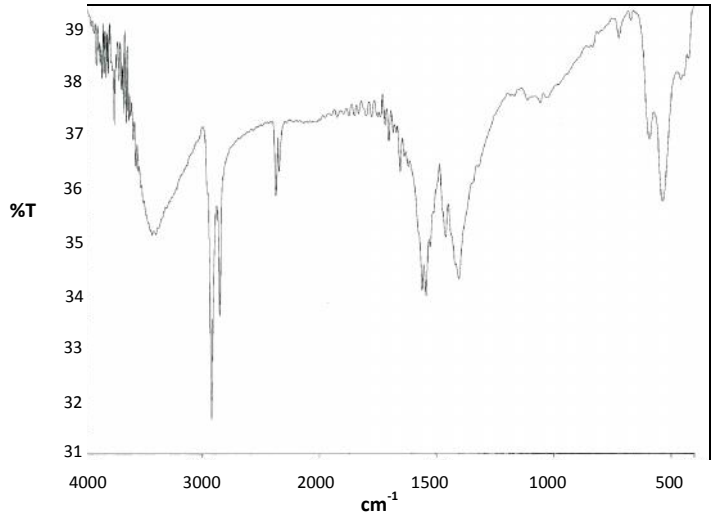

Figure 4.93 FTIR spectrum of **Complex 9**

The **UV-vis spectrum** of the complex in solution (**Figure 4.94)** shows a broad *d-d* band at 703 nm (ε_{max}= 146 M^{-1} cm^{-1}) and a distinct shoulder on the charge-transfer band at 360 nm (ε = 74 M^{-1} cm^{-1}). This suggests a binuclear complex with square pyramidal geometry at Cu(II) centres.

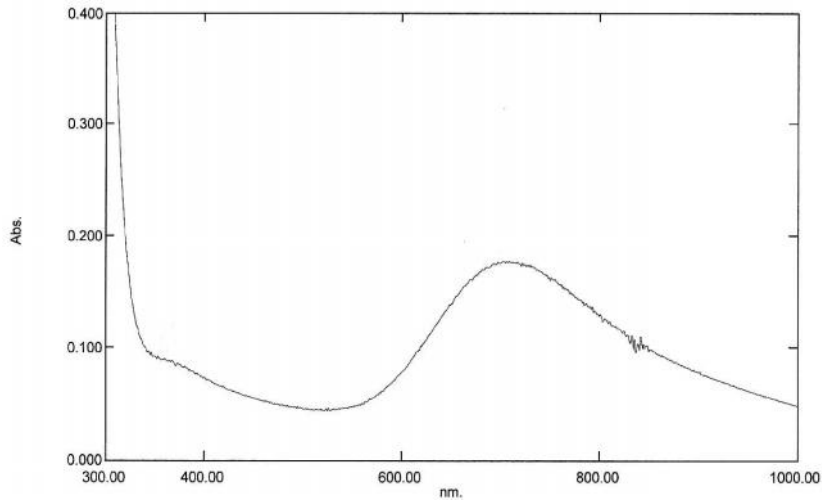

Figure 4.94 UV-vis spectrum of **Complex 9** (solution)

A proposed structural formula of **Complex 9** is shown in **Figure 4.95**. It is consistent with the chemical formula $Cu_2C_{36}H_{84}O_{12}$ as suggested by the elemental analyses, bridging carboxylate ligands as suggested from FTIR, and square pyramidal geometry at Cu(II) as suggested from UV-vis spectroscopy.

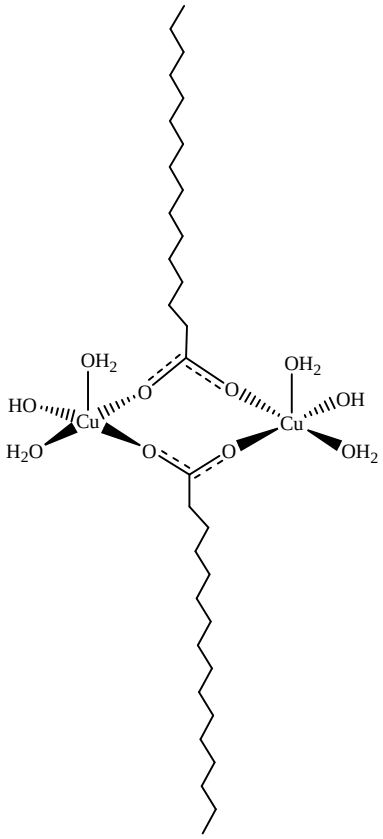

Figure 4.95 Proposed structure of **Complex 9**; solvated C_2H_5OH molecules are not shown

b) Thermal Properties

The thermogram (**Figure 4.96)** shows that **Complex 9** initially suffered a gradual initial weight loss of 8.8%, assigned to the evaporation of two C_2H_5OH solvates (expected, 11.0%). The complex then decomposed at 240^oC in several steps with a total weight loss of 63.0%, assigned to the loss of four H_2O molecules and two $CH_3(CH_2)_{14}COO$ ligands (expected, 69.6%). The amount of residue at temperatures above 750^oC is 28.2% (expected 19.0%, assuming that it is purely CuO), indicating the presence of other involatile compound(s).

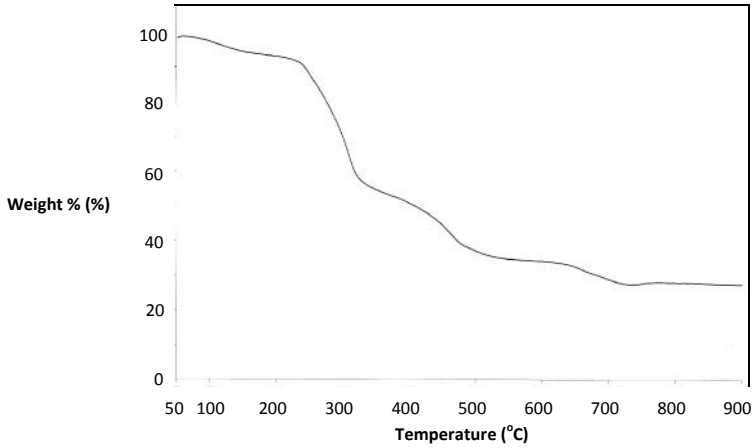

Figure 4.96 Thermogram of **Complex 9**

The development of optical structure of **Complex 9** on heating is illustrated by the sequence of photographs (**Figure 4.97)**. The complex was a grey fine powder at room temperature and was observed as fine needles under the microscope. Upon heating, it started to melt and then to clear at around 162^oC and 175^oC respectively.

(a) (b) (c)

Figure 4.97 Optical structure of **Complex 9** on heating at (a) 30^oC; (b) 162^oC; and (c) 175^oC

On cooling from an isotropic liquid phase to room temperature, it was observed that a fan-shaped mesophase, which may assigned as Smectic A, began to developed, at 105^{o}C **(Figure 4.98(a)).** On further cooling to room temperature, the tecture developed into Smectic C **(Figure 4.98 (b) - (d))**. The results support the rod-like structure, as shown in **Figure 4.95**.

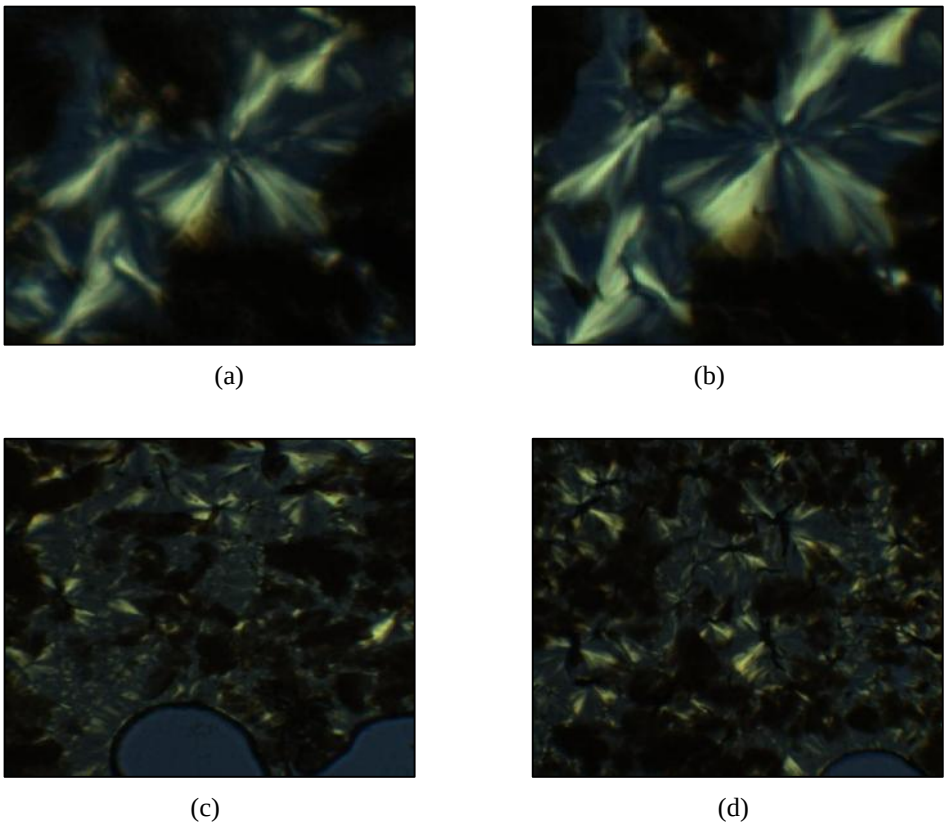

(a) (b)

(c) (d)

Figure 4.98 Optical structures of **Complex 9** on cooling at (a) 105^{o}C; and (b) 96^{o}C; (c) 25^{o}C and (d) 24^{o}C

The DSC curve for **Complex 10** (**Figure 4.99**) shows several endotherms. The assignments of these endotherms are given in **Table 4.19.**

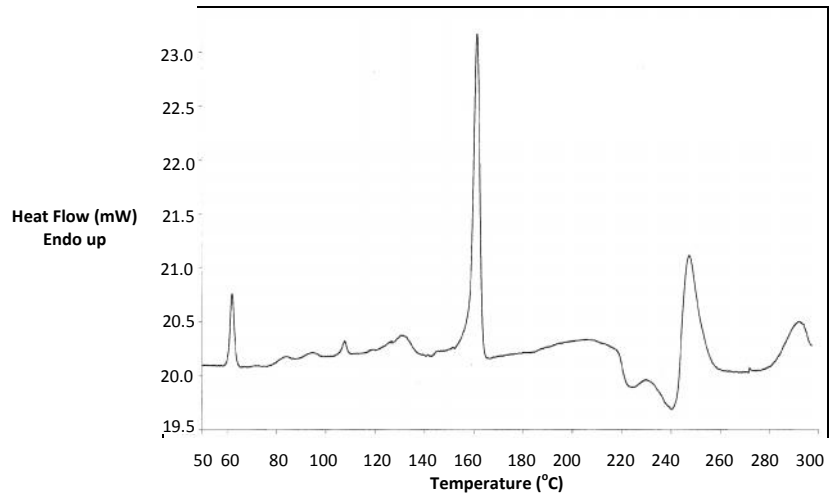

Figure 4.99 DSC curve of **Complex 9**

Table 4.19 DSC data and assignment for **Complex 9**

Temperature (^{o}C)	ΔH/ kJ mol^{-1}	Assignment
64 (peak)	+ 5	Breaking of H-bonded C_2H_5OH molecules
84 (peak) 95 (peak) 108 (peak) 131(peak)	--	Evaporation of C_2H_5OH and H_2O molecules, crystal-crystal phase transitions
162 (peak)	+32	Melting of the complex
180 (onset)	+25	Clearing of the complex
247 (peak)	+33	Decomposition of the complex

-- cannot be determined accurately; * T_{clear} = 175^{o}C from OPM; and $^{\#}T_{dec}$ = 240^{o}C from TGA

4.4.2 K[Cu$_2$(p-OC$_6$H$_4$COO)(CH$_3$(CH$_2$)$_{10}$COO)$_3$]

a) Synthesis and Structural Elucidation

The reaction between [Cu$_2$(*p*-HOC$_6$H$_4$COO)(CH$_3$(CH$_2$)$_{10}$COO)$_3$] **(Complex 6)** and KOH produced a dark green powder **(Complex 10; *n* =10)** with similar solubility to that of **Complex 9**; *n* = 14). Based on the following analytical results, it is proposed that its chemical formula is K$_2$[Cu$_2$(CH$_3$(CH$_2$)$_{10}$COO)$_2$(OH)$_4$] (formula mass 671.9 g mol^{-1}; yield 33.9%). Hence, it is not the intended ionic complex, K[Cu$_2$(*p*-OC$_6$H$_4$COO)(CH$_3$(CH$_2$)$_{10}$COO)$_3$].

The results of **elemental analyses** (found: C, 43.19% and H, 7.43%; calculated for $K_2Cu_2C_{24}H_{50}O_8$: C, 42.90%; H, 7.50% H); **FTIR** (**Figure 4.100,** Δ_{OCO} = 135 cm^{-1}), and UV-vis (**Figure 4.101**; λ_{max} = 701 nm (ε_{max} = 372 M^{-1} cm^{-1}), shoulder, 365 nm (ε_{max} = 148 $M^{-1}cm^{-1}$), and 306 nm (ε_{max} = 875 $M^{-1}cm^{-1}$).

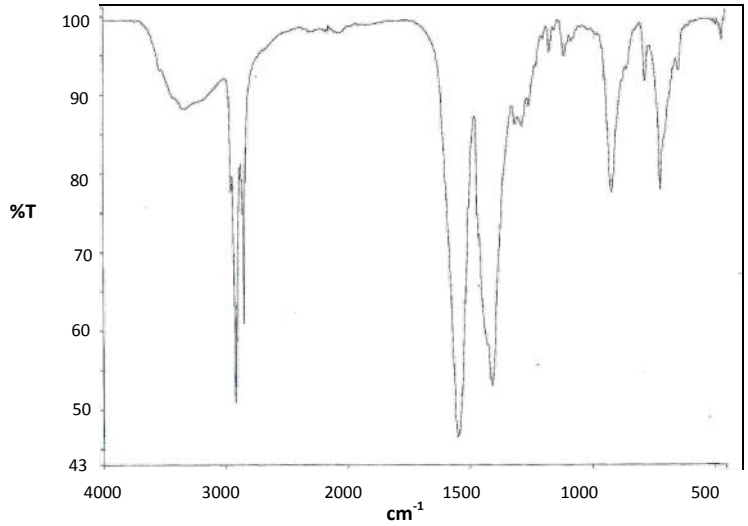

Figure 4.100 FTIR spectrum of **Complex 10**

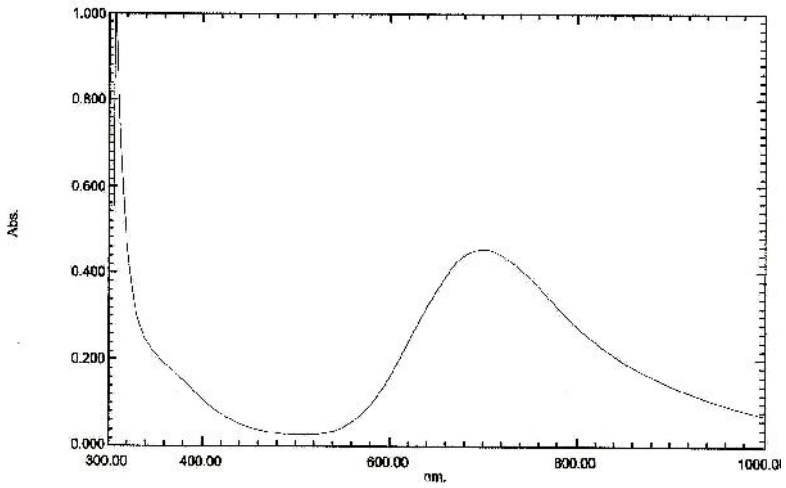

Figure 4.101 UV-vis spectrum of **Complex 10**

Its proposed structural formula **(Figure 4.102)** is similar to that of **Complex 10**.

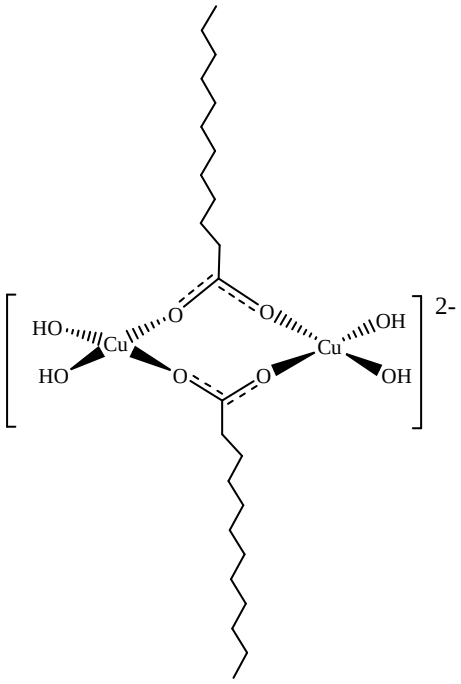

Figure 4.102 Proposed structure of **Complex 10** (K^+ is not shown)

b) Thermal properties

The thermogram (**Figure 4.103)** shows that **Complex 10** initially suffered a gradual initial weight loss of 7.1%, assigned to the loss of two H_2O, formed from four -OH ligands (expected, 10.1%). The complex then decomposed at 255^oC with a total weight loss of 58.1%, assigned to the loss of two $CH_3(CH_2)_{10}COO$ ligands (expected, 59.2%).

The amount of residue at temperatures above 550^oC to 900^oC is 36.8%. Assuming that it is K_2O and CuO, the estimated formula mass of **Complex 10**, calculated, using the gravimetry concept, is 689.7 g mol^{-1} (expected 671.9 g mol^{-1}). Thus, the results from TGA and elemental analyses are in good agreement, and lend further support for the proposed structural formula.

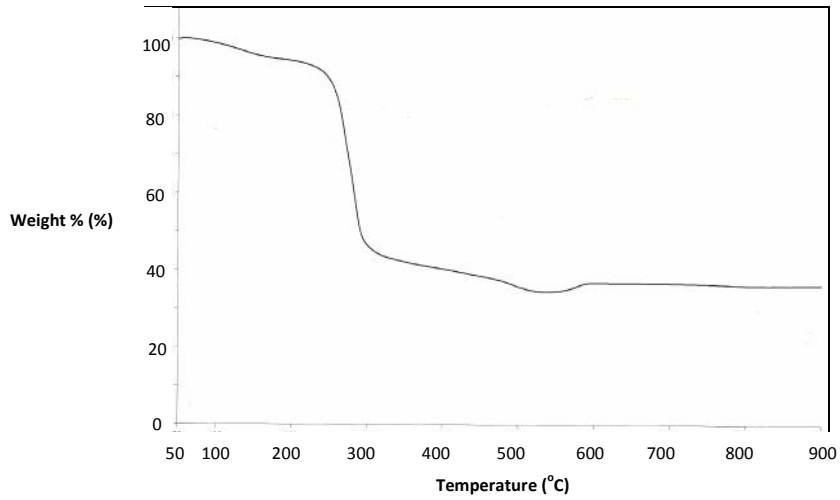

Figure 4.103 Thermogram of **Complex 10**

The DSC curve for **Complex 10** (**Figure 4.104**) shows two very weak and broad endotherms centered at 100°C (ΔH cannot be determined) and 204°C (ΔH = +14 kJ mol^{-1}) correspond to the loss of two H_2O. It is followed by an overlapping broad endotherm at 250°C ($\Delta H_{combined}$ = 70 kJ mol^{-1}), which may be assigned to the decomposition of **Complex 10** (from TGA, T_{dec} = 255°C). The DSC curve did not show peaks for the melting and clearing processes prior to decomposition.

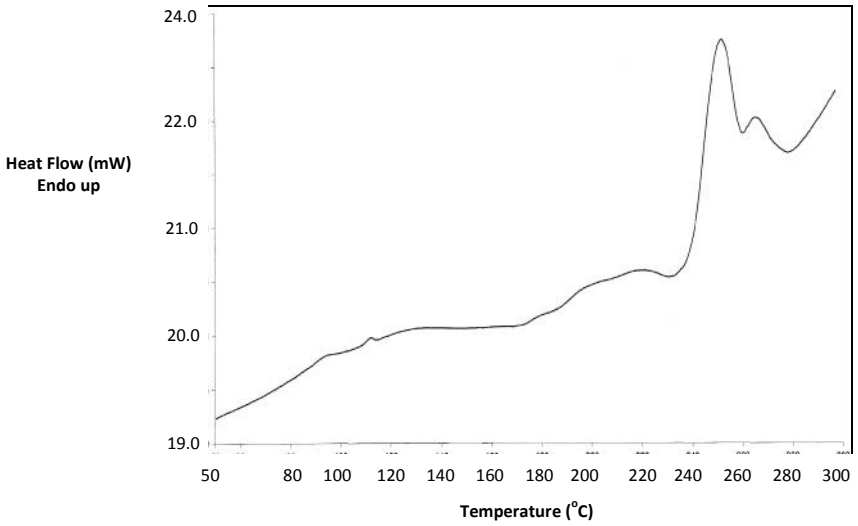

Figure 4.104 DSC curve of **Complex 10**

4.4.3 K[Cu_2(p-OC_6H_4COO)($CH_3(CH_2)_8COO)_3$]

a) Synthesis and Structural Elucidation

[Cu_2(*p*-HOC_6H_4COO)($CH_3(CH_2)_8COO)_3$] (**Complex 7)** was similarly ionized as done for **Complex 6** and **Complex 5** (**Section 4.4.1** and **4.42**).

Based on the following analytical results, it is proposed that the chemical formula of the fine black powder obtained (**Complex 11**) is $K_2[Cu_2(CH_3(CH_2)_8COO)_2(OH)_4]$ (formula mass 615.8 g mol^{-1}; yield 72.5 %). Hence, it is also not the intended ionic complex, K[Cu_2(*p*-OC_6H_4COO)($CH_3(CH_2)_8COO)_3$].

The structural formula of the complex, agrees with the results of **elemental analyses** (found: C, 39.82% and H, 6.29%; calculated for $K_2Cu_2C_{20}H_{42}O_8$: C, 39.01%; H, 6.87%; **FTIR** (**Figure 4.105**), Δ_{OCO} = 133 cm^{-1}; UV-vis (solution) (**Figure 4.106),** λ_{max} = 697 nm (ε_{max} = 662 M^{-1} cm^{-1}), shoulder, 360 nm (ε = 176 $M^{-1}cm^{-1}$) and 307 nm (ε_{max} = 1184 $M^{-1}cm^{-1}$). Its proposed structural formula is very similar to the complexes previously ionized.

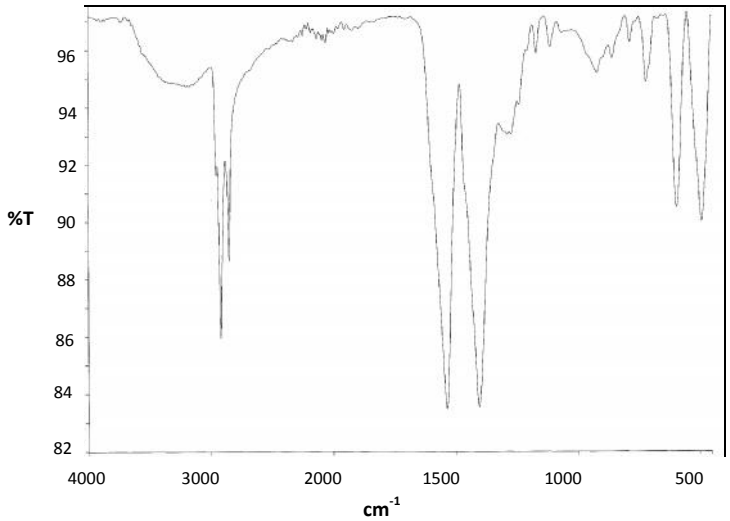

Figure 4.105 FTIR spectrum of **Complex 11** (n = 8)

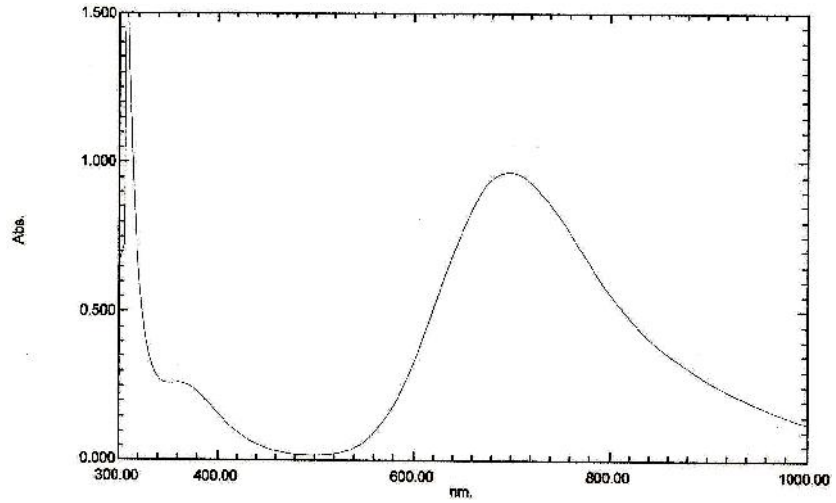

Figure 4.106 UV-vis spectrum of **Complex 11** (n = 8)

b) Thermal properties

The thermogram (**Figure 4.107)** shows that **Complex 11** initially suffered a gradual initial weight loss of 5.0%, assigned to the loss of two H_2O (expected, 5.8%). The complex then decomposed at 230^oC with a total weight loss of 37.0%, assigned to the loss of two $CH_3(CH_2)_8COO$ ligands (expected, 55.5%). There is an increased of weight at around 475^oC, may be due to the formation of other volatiles.

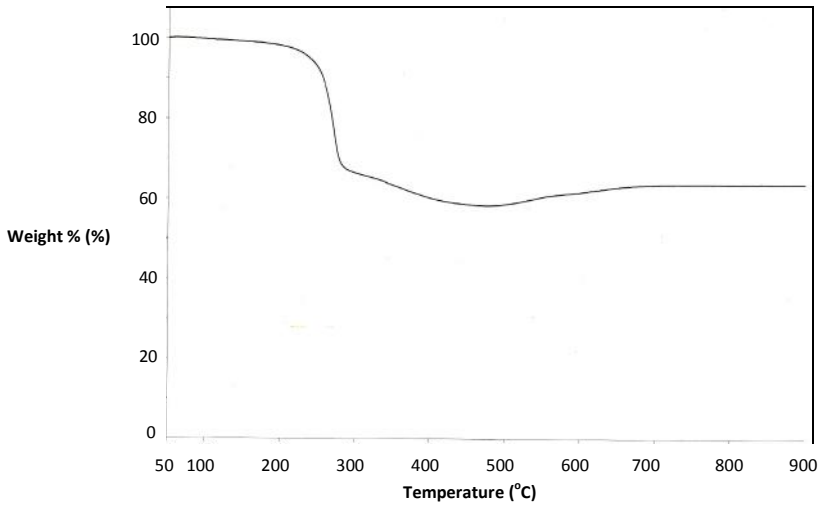

Figure 4.107 Thermogram of **Complex 11** (n = 8)

The amount of residue at temperatures below 700^oC is 63.7%. The expected amount, assuming that the complex decomposed completely to K_2O and CuO, is 41.1%

(Appendix 1). This suggests that the organic ligands of the complex did not decompose completely below this temperature.

The DSC curve for **Complex 11** (**Figure 4.108**) shows a very weak endotherms centered at 80^{o}C (ΔH cannot be determined) which is correspond to the loss of water molecules (formed from the four –OH). It is followed by a broad endotherm at 226^{o}C (ΔH = 70 kJ mol^{-1}), which may be assigned to the decomposition of **Complex 11.** No melting and clearing peaks were observed prior to decomposition.

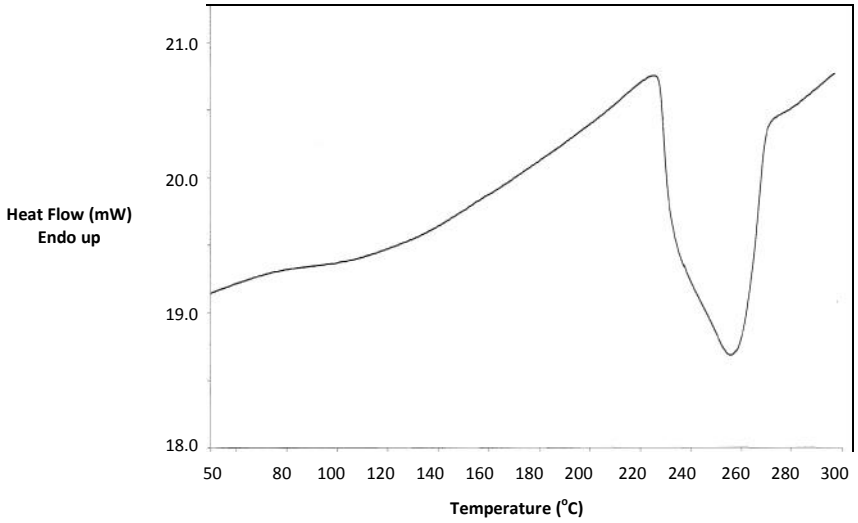

Figure 4.108 DSC curve of **Complex 11** (n = 8)

4.4.4 K[Cu$_2$(p-OC$_6$H$_4$COO)(CH$_3$(CH$_2$)$_6$COO)$_3$]

[Cu$_2$(*p*-HOC$_6$H$_4$COO)(CH$_3$(CH$_2$)$_6$COO)$_3$] (**Complex 8)** was similarly ionized as for the earlier complexes (**Section 4.4.1, 4.42** and **4.43**).

The structural formula of the fine black powder obtained (**Complex 12**; n = 6) agrees with the results of **elemental analyses** (found: C, 34.83% and H, 5.67%; calculated for $K_2Cu_2C_{16}H_{34}O_8$: C, 34.33%; H, 6.12%; chemical formula $K_2[Cu_2(CH_3(CH_2)_6COO)_2(OH)_4]$, (formula weight 559.7 g mol^{-1}; yield 25.0 %); **FTIR** (**Figure 4.109**; Δ_{OCO} = 134 cm^{-1}) and UV-vis (solution), (**Figure 4.110**; λ_{max} = 696 nm, ε_{max} = 626 M^{-1} cm^{-1}); 360 nm (ε = 168 M^{-1}cm^{-1}) and 307 nm (ε = 1090 M^{-1}cm^{-1}).

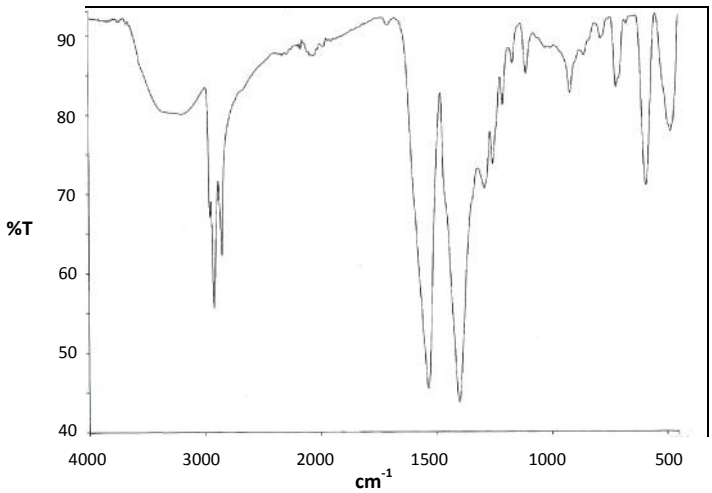

Figure 4.109 FTIR spectrum of **Complex 12**

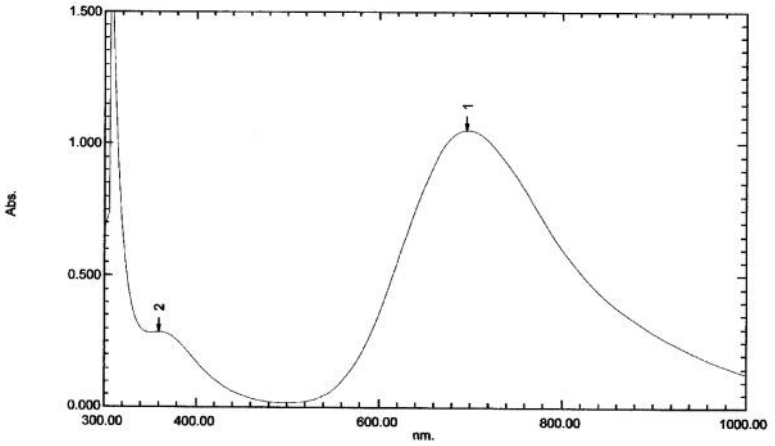

Figure 4.110 UV-vis spectrum of **Complex 12**

The proposed structural formula of **Complex 12** is similar to the previous ionized complexes. Its thermogram **Figure 4.112** and the DSC curve **(Figure 4.113)** are very similar to **Complex 11** and can be similarly explained.

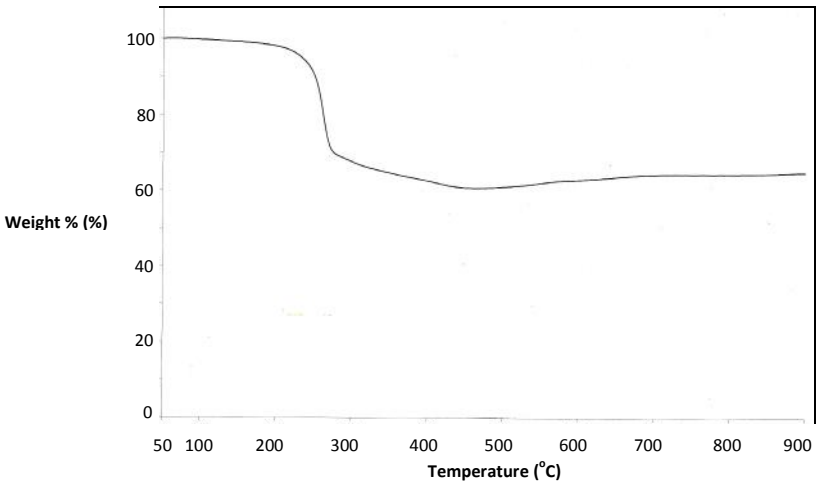

Figure 4.111 Thermogram of **Complex 12**

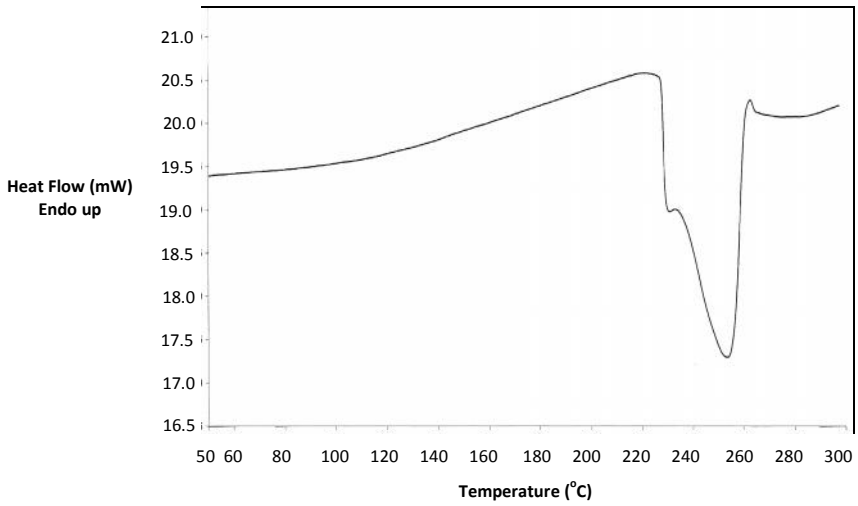

Figure 4.112 DSC curve of **Complex 12**

4.5 THE C-C BOND FORMING REACTION

Complex 1 ($K_2[Cu_2(p\text{-}OC_6H_4COO)_2(CH_3(CH_2)_{14}COO)_2(p\text{-}HOC_6H_4COOH)_2].2H_2O$) and **Complex 4** ($K[Cu_2(p\text{-}OC_6H_4COO)(CH_3(CH_2)_{14}COO)_3]$) were selected for the carbon-carbon bond-forming reaction of a methyl ketone, namely 3,3-dimethyl-2-butanone ($(CH_3)_3C\text{-}CO\text{-}CH_3$). The complexes were chosen as both are ionic with the paddle wheel structure, while the ketone was chosen as it has only one CH_3 group bonded to the carbonyl group, and hence should simplify the anticipated C-C bond reaction.

The reaction involves refluxing the complexes with the ketone in the presence of concentrated HCl for four hours. The colour of the reaction mixture change from dark brown to orange brown after this time. The unreacted ketone (clear solution) was distilled off from mixture, and the reaction products were collected and analyzed by GCMS.

4.5.1 Complex 1

The products obtained from the above reaction were a dark brown (**A1**; 1.71 g) and yellow (**A2**; 6.04 g) liquids, collected at 90^{o}C and 105^{o}C respectively.

The chromatograms of **A1** (**Figure 4.113)** and **A2** (**Figure 4.114**) show many peaks. However, the peaks for compounds presence in significant amounts in both **A1** and **A2** are shown in **Table 4.20**, and the corresponding mass spectra are shown in **Figure 4.115**.

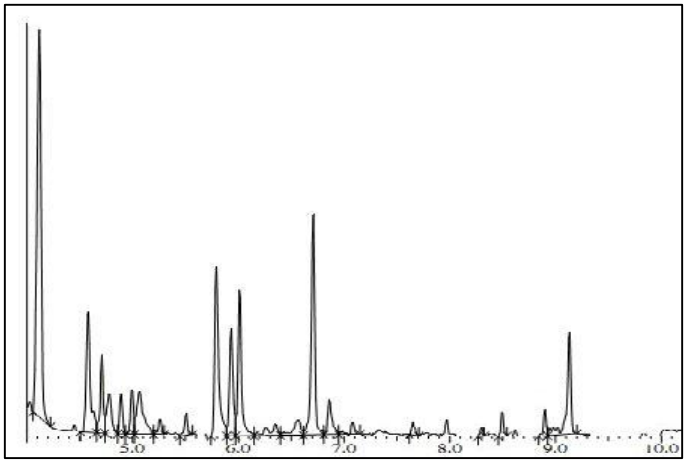

Figure 4.113 Chromatogram of dark brown liquid (**A1)**

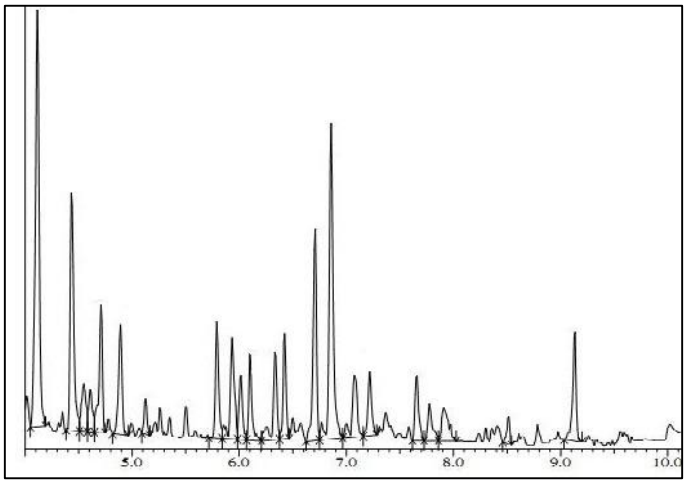

Figure 4.114 Chromatogram of yellow liquid (**A2)**

Table 4.20 GC data of main components in **A1** and **A2**

R_t (min)	Amount (%)	
	A1	**A2**
4.1	19.5	15.6
4.4	-	8.8
5.8	8.5	-
6.7	10.9	7.8
6.9	-	11.7

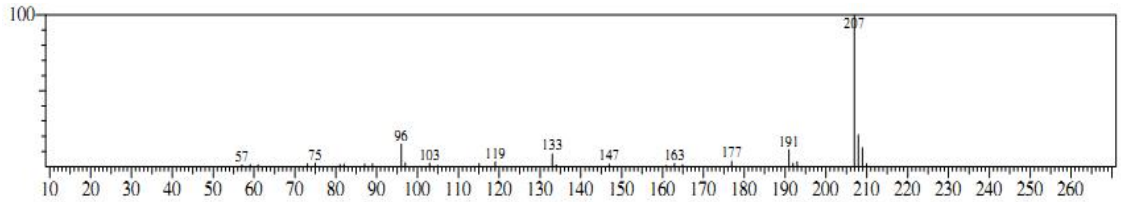

(a)

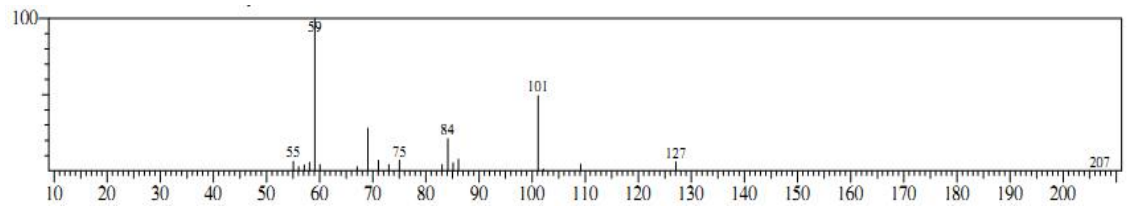

(b)

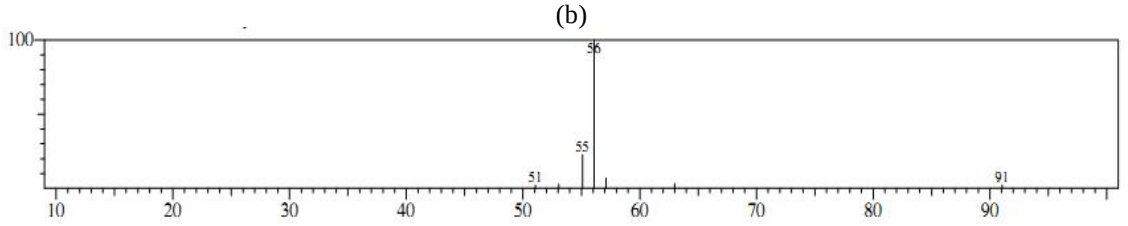

(c)

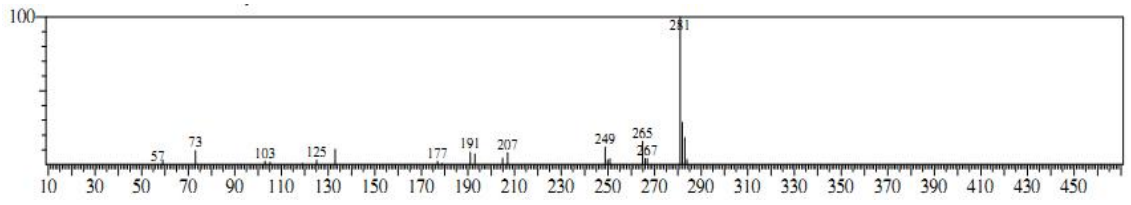

(d)

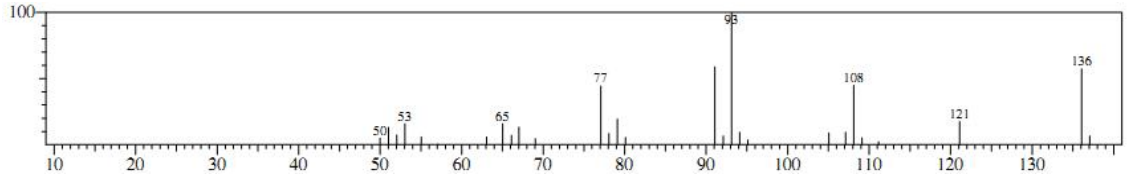

(e)

Figure 4.115 Mass spectrum of molecules at R_t (min): (a) 4.1, (b) 4.4, (c) 5.8, (d) 6.7, and (e) 6.9

The peak at retention time, R_t = 5.8 min (m/z = 91) may be assigned to the unreacted ketone, while the peaks common in both fractions are at retention times, R_t = 4.1 min (m/z = 207), assigned to product formed from the condensation of two ketone molecules, and R_t = 6.7 min (m/z = 281), tentatively assigned to the product formed from the condensation of three ketone molecules (**Figure 4.116**).

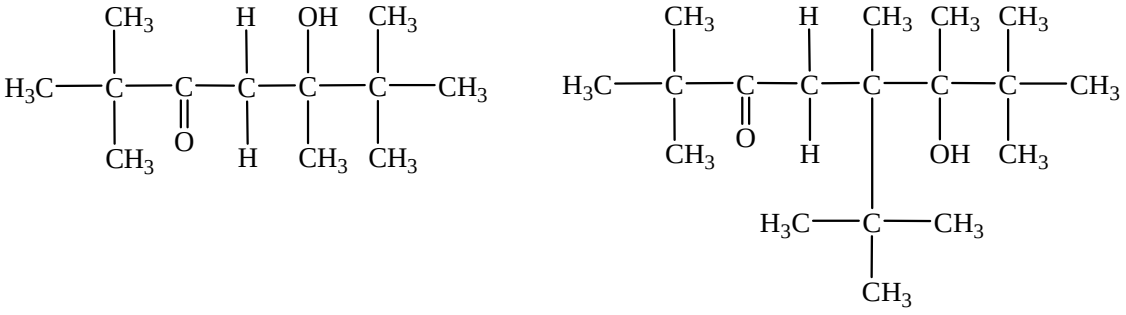

(a) (b)

Figure 4.116 Structural formulas of the molecules eluated at R_t (a) 4.1 min and (b) 6.7 min

Two peaks found only in **A2** are at R_t = 4.4 min (m/z = 207) and R_t = 6.9 min (m/z = 136). These are assigned to enol form of the above condensation product of two ketone molecules, and to *p*-hydroxybenzoic acid, respectively (**Figure 4.117**).

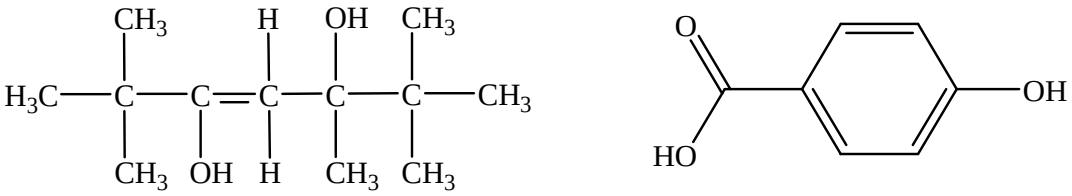

(a) (b)

Figure 4.117 Structural formulas of the molecules eluated at R_t (a) 4.4 min, and (b) 6.9 min

The mechanism proposed to explain the formation of the product formed from the condensation of two ketone molecules is shown in **Scheme 4.17** [40].

***Step 1**: Axial ligation by 3,3-dimethyl-2-butanone, one electron reduction of Cu(II), breaking of Cu-$OOCC_6H_5$ equatorial bond and formation of enone.*

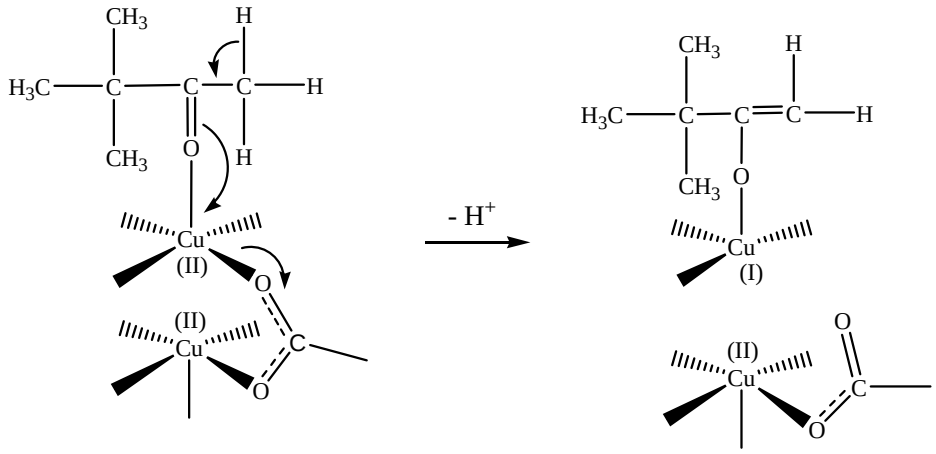

***Step 2**: Protonation of 3,3-dimethyl-2-butanone to form a carbocation (an enophile)*

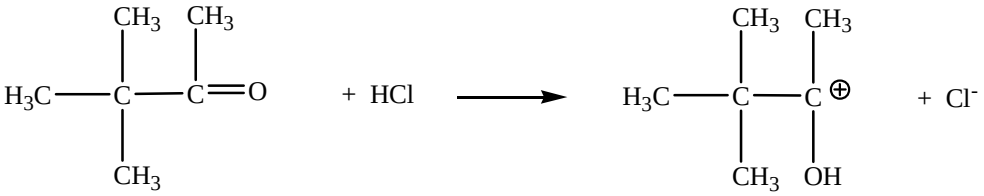

***Step 3:** The C-C bond forming reaction between the enone and the enophile*

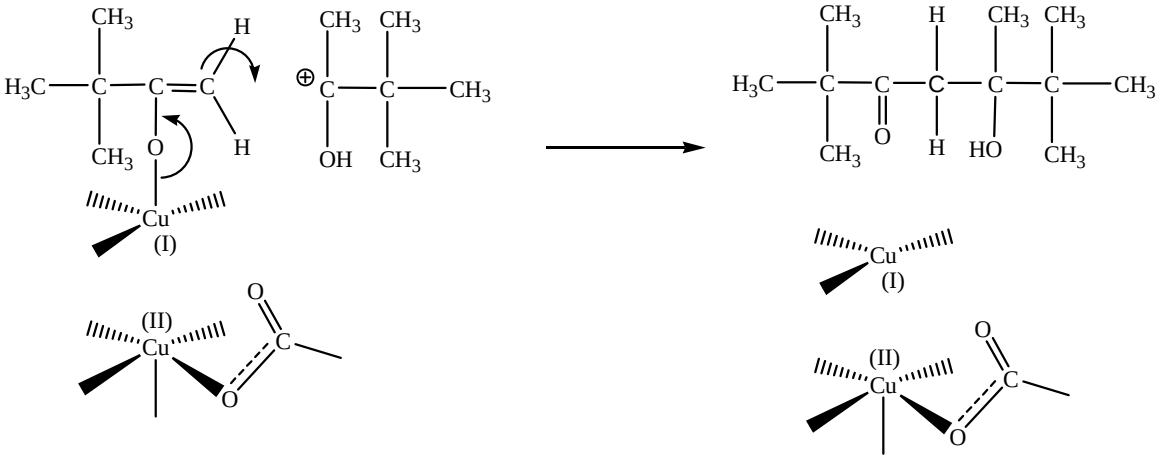

Scheme 4.17 Proposed mechanism for the C-C bond-forming reaction of **Complex 1** with 3,3-dimethyl-2-butanone

4.5.2 Complex 4

The products obtained from the above reaction were a dark brown liquid (**B1**; 0.66 g) and a yellow liquid (**B2**; 2.29 g) solution, collected at 90^{o}C and 105^{o}C respectively.

Compared to the GC from the reaction involving **Complex 1**, the GC from the reaction involving **Complex 4** is cleaner, showing three main peaks for both **B1** (**Figure 4.118)** and **B2** (**Figure 4.119**). The results are collected in **Table 4.21**.

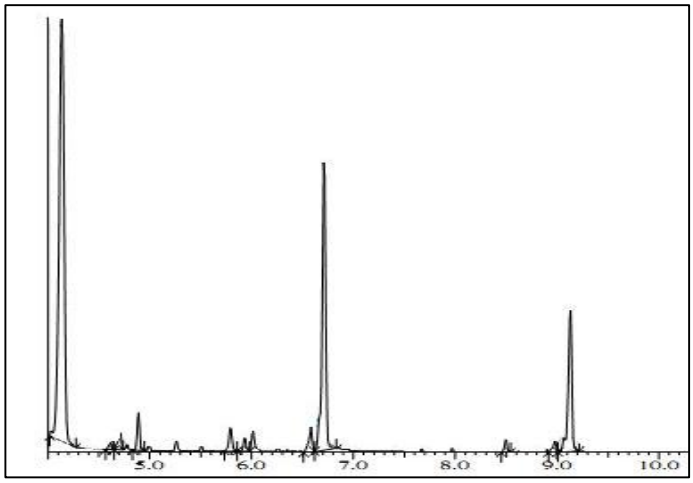

Figure 4.118 Chromatogram of dark brown liquid (**B1**)

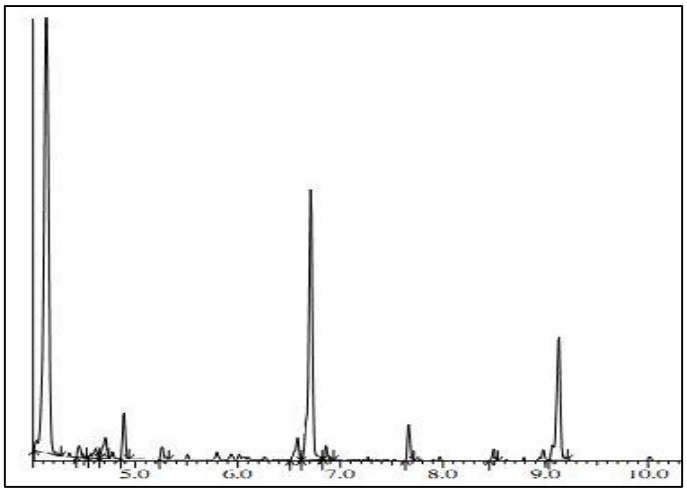

Figure 4.119 Chromatogram of yellow liquid (**B2**)

Table 4.21 GC data of main components in **B1** and **B2**

R_t (min)	Amount (%)	
	B1	**B2**
4.1	38.6	40.2
6.7	26.2	24.9
9.1	12.9	11.3

It is noted that the first two peaks are at the same R_t and have the same m/z values as those obtained from the reaction involving **Complex 1**, and hence may be similarly assigned. Next, it is tempting to assign the peak at R_t = 9.1 min (m/z = 355; **Figure 4.120**) to the H-bonded adduct formed between $CH_3(CH_2)_{14}COOH$ and $(CH_3)_3C\text{-}CO\text{-}CH_3$ (m/z = 356).

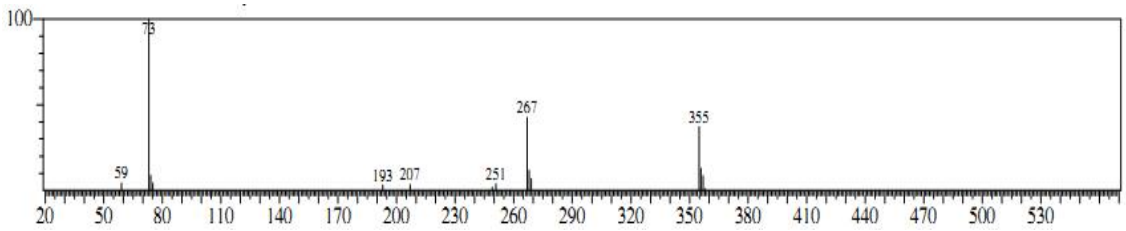

Figure 4.120 Mass spectrum of the product at R_t = 9.1 min

To summarise, both **Complex 1** and **Complex 4** assisted the formation of C-C bond-forming products from the reaction of $(CH_3)_3C\text{-}CO\text{-}CH_3$. These products were obtained in higher yields from the reaction involving **Complex 4** compared to that of **Complex 1.** This may be due to the difference in structure of both complexes**. Complex 1** was a square pyramidal while **Complex 4** was a square planar. As such, one of the axial positions of **Complex 1** was unavailable to form bond with the ketone compare to **Complex 4.**

References

[1] Tom Welton (Eds.), *Coordination Chemistry Review* 248, 2459-2477 (2004).

[2] N. Abdullah and M. H. Chisholm, *Role of $Cu_2(XC_6H_4COO)_4$ in facile C-C bond forming reaction of carbonyls*, International Conference on Molecular Chemistry, 54 (2008).

[3] G. S. Attard and P. R. Cullum, *Liquid Crystals*, Vol. 8, No. 3, 299-309 (1990).

[4] P. Espinet, *Inorganica Chimica Acta* 361, 2270-2278 (2008)

[5] R. Paschke, D. Balkow, and E. Sinni, *Inorganic Chemistry* (published on the web) (2001)

[6] J. Lewis and F. Mabbs, *Notes*, 3894-3897 (1965)

[7] W. E. Hatfield, C. S. Fountain, and R. Whyman, *Inorganic Chemistry*, Vol. 5, No. 11, 1855-1858 (1966).

[8] F. Cariati, L. Erre, G. Micera, A. Panzanelli, and P. Piu, *Thermochimica Acta*, 66, 1-10 (1983).

[9] M. Inoue, M. Kishita, and M. Kubo, *Inorganic Chemistry*, Vol. 3, No. 2, 239-242 (1964)

[10] F. Cariati, L. Erre, G. Micera, A. Panzanelli, G. Ciani, and A. Sironi, *Inorganica Chimica Acta*, 80, 57-65 (1983).

[11] L. Strinna Erre, G. Micera, P. Piu, F. Cariati, and G. Ciani, *Inorg. Chem*., 24, 2291-2300 (1985).

[12] L. S. Erre and G. Micera, *Polyhedron* Vol. 6, No. 10, pp 1869-1874 (1987).

[13] S.P. Perlepes, E.Libby, W. E. Streib, K. Folting and G. Christou, *Polyhedron* Vol. 11, No. 8, pp 923-936, (1992)

[14] W. Zhang, S. Liu, C. Ma and D. Jiang, *Polyhedron* Vol. 17, No. 22, pp. 3835-3839, (1998)

[15] Y. Rodriguez-Martin, J. Sanchiz, C. Ruiz-Perez*, F. Lloret, M. Julve*, *Inorganica Chimica Acta* 326, 20-26 (2001).

[16] D. Choquesillo-Lazarte, B. Covelo, J. M. González-Pérez, A. Castiñeiras, and J. Niclós-Gutiérrez, *Polyhedron* 21, 1485-1495 (2002).

[17] T. Kawata, H. Uekusa, S. Ohba, T. Furukawa, T. Tokii, Y. Muto, and M. Kato, *Acta. Cryst*., B48, 253-261 (1992).

[18] M. Devereux, D. O'Shea, M. O'Connor, H. Grehan, G. Connor, M. McCann, G. osair, F. Lyng, A. Kellett, M. Walsh, D. Egan and B. Thati, *Polyhedron* 26, 4073-4084 (2007).

[19] G. C. Campbell and J. F. Haw, *Inorg. Chem.*, 27, 3706-3709 (1988).

[20] M. Melnik, M. Dunaj-Jurco, and M. Handlovic, *Inorganica Chimica Acta*, 86, 185-190 (1984).

[21] M. Kato and Y. Muto, Elseveir Science Publishers B.V. (1988).

[22] M. Yamanaka, H. Uekusa, S. Ohba, Y. Saito, S. Iwata, M. Kato, T. Tokii, Y. Muto, and O. W. Steward, *Acta Cryst*., B47, 344-355 (1991).

[23] Deacon GB, Philips RJ, *Coord. Chem. Rev*., 33, 227 (1980).

[24] J. E. Wedder, T. W. Hambley, B. J. Kennedy, P. A. Lay, D. MacLachlan, R. Bramley, C. D. Delfs, K. S. Murray, B. Moubaraki, B. Warwick, J. R. Biffin, J. R. and H. L. Regtop, *Inorg. Chem.*, 38, 1736 (1999).

[25] M. Kato and Y. Muto, Y., Coord. Chem. Rev., 92, 45 (1988).

[26] C. Dendrinou-Samara, P. D. Jannakoudakis, D. P. Kessissoglou, G. E. Manoussakis, D. Mentzafos and A. Terzis, *J. Chem. Soc.*, Dalton Trans., 3259 (1992).

[27] M. Pajtasova, D. Ondrusova, E. Jona, S. C. Mojumdar, S. L'alikova, T. Bazylakova, M. Gregor, *J. Therm. Anal. Calorim.*, 100, 769-777 (2010).

[28] S Karthikeyan, T M Rajendiran, R Kannappan, R Mahalakshmy, R Venkatesan and P Sambasiva Rao, *Proc. Indian Acad. Sci. (Chem. Sci.),* Vol. 113, No. 4, August, pp 245-256 (2001).

[29] A. M. Godquin-Giroud, J. C. Marchon, *J. Physique Lett.*, 45, L-681-L-684. (1984)

[30] M. Petric, I. Leban and P. Segedin, *Polyhedron* Vol. 14, No. 8, pp. 983-989 (1995).

[31] M. I. Mohamadin, N. Abdullah, Cent. Eur. J. Chem. 8, 1090 (2010).

[32] Kamaliah Mahmood, Norbani Abdullah, *A first course in Organic Chemistry* (2009).

[33] B. Bleaney, K.D. Bowers, Proc. R. Soc. London, Ser. A, 214, 451 (1952).

[34] M. Kato, H. B. Jonassen, J. C. Fanning, Chem. Rev., 64-99 (1964).

[35] Ayhan Elmali, Turk. J. Phy., 24, 667-672 (2000).

[36] P. Kogerler, P. A. M. Williams, B. S. Parajon-Costa, E. J. Baran, L. Lezama, T. Rojo, A. Muller, Inorg. Chim. Acta 268, 239 (1998).

[37] J. A. R. Cheda, M. V. Garcia, M. I. Redondo, S. Gargani and P. Ferloni, Liquid Crystals, Vol., No., 1, 1-14. January 2004.

[38] Fatmir Hamza and Guido Kickelbick, Macromolecules, 42, 7762-7771 (2009).

[39] I. Toledo, M. Aranbica, C. Andrade and I. Crivelli, Polyhedron, Vol. 17, No. 1, pp. 173-178 (1998).

[40] Mohammad Isa Mohamadin, *Copper(II) Arylcarboxylates : Substituent Effects on Structure, Thermal, Magnetic and Carbon-carbon Bond Forming Reaction of Carbonyls*. Thesis submitted for degree of Doctor of Phylosophy (2011).